CLAASSEN R

MICROBIOLOGICAL OXIDATION OF SULPHIDE MINERALS FROM AGNES, NEW CONSORT AND SHEBA GOLDMINES

MSc UP 1991

MICROBIOLOGICAL OXIDATION OF SULPHIDE MINERALS FROM AGNES, NEW CONSORT AND SHEBA GOLDMINES

by

Ronelle Claassen

Thesis submitted in partial fulfilment of the requirements
for the degree MAGISTER SCIENTIAE,
in the Faculty of Science,
University of Pretoria

Promoter: Prof CP Snyman
Co-promoter: Dr CT Logan

July 1991

Based on nature's own workings, on controlled laboratory studies done by many workers and on current applications in the field, it is clear that microorganisms and their versatile activities will help man to lay claim to mineral wealth buried deep in the ground or available in amounts not economically feasible to recover at present. These small servants of man promise to help in cleaning the air and water while retrieving valuable metal resources.

- *Corale L. Brierley*

SYNOPSIS

Microbiological oxidation of sulphide mineral from Agnes, New Consort and Sheba goldmines

Ronelle Claassen

Promoter: Prof CP Snyman; Co-promoter: Dr CT Logan
Geology Department
M.Sc. - Degree

Recently the gold mining industry has been forced to treat leaner and more refractory gold ores. Pre-treatment by bacterial oxidation is one of the most promising alternative methods of recovering refractory gold. The bacterial oxidation process occurs at moderate temperature and ambient pressure. Under these conditions, oxidation kinetics are comparatively slow, and the effect of mineralogical characteristics on sulphide oxidation and gold recovery relationships assumes greater importance.

Ore samples from the Sheba, Agnes and New Consort goldmines from the Barberton Mountainland were studied. Sulphides were liberated and concentrated from whole rock samples. Polished sections were prepared from selected crystals and were studied mineralogically. Bacterial oxidation testwork was conducted in air-stirred puchucas. Polished sections were suspended and submerged in the bacterial leach pulp (containing an arsenopyrite-pyrite flotation concentrate and *Thiobacillus ferrooxidans* bacteria) for various periods of time. The effect of oxidation was monitored by observations of the leached sections using an optical microscope and a Scanning Electron Microscope (SEM).

The Sheba ore comprises a S-rich mineral assemblage consisting mainly of arsenopyrite and pyrite. These sulphides are chemically zoned, with respect to As-content. Both the arsenopyrite and pyrite host submicroscopic gold (up to 0.7 wt% and 0.1 wt% respectively) in the relatively As-rich zones. Particulate gold occurs mostly at the contacts of different zones in arsenopyrite. More than one generation are present in the Agnes pyrite. The core generation is compositionally zoned, with respect to As-content. The As-rich zones contain the highest amount of submicroscopic gold. A second generation of pyrite (As-poor) developed after a period of resorption. The New Consort ore consists of As-rich arsenopyrite (unzoned) and loellingite, with particulate gold being the dominant gold-type in these minerals.

During bacterial oxidation of the Sheba sulphides the arsenopyrite was more rapidly oxidized than the pyrite. Preferential oxidation of the As-rich zones in the arsenopyrite took place. During the initial bacterial oxidation period of both Sheba and Agnes pyrite, dissolution channels developed along grain boundaries, zone and generation contacts and along pre-existing cracks. Square, rectangular, elongated and hexagonal shaped dissolution pits developed at different rates of pyrite oxidation. The loellingite inclusions within the New Consort arsenopyrite were oxidized extremely rapidly. This is due to the reactive nature of loellingite towards ferric sulphate. The oxidation of arsenopyrite was, however, slow.

It can be concluded that knowledge of the mineralogical characteristics of gold-bearing sulphides (such as the modes of occurrence and distribution of gold, compositional zoning and generational differences), can aid in the understanding of gold recovery-sulphide oxidation curves. Furthermore, the sites of preferential bacterial attack are in most cases determined by the presence of defects in crystal structures (chemical deviations as reflected by zoning and generations or mechanical deviations such as zone contacts, grain boundaries, etc.). Detailed mineralogical information can thus provide an understanding of the behaviour of different ore types during the bacterial leaching process.

SAMEVATTING

Mikrobiologiese oksidasie van sulfied minerale vanaf Agnes, New Consort en Sheba goudmyne
Ronelle Claassen
Leier: Prof CP Snyman; Mede-leier: Dr CT Logan
Geologie Departement
M.Sc. - Graad

Die goudmyn bedryf is onlangs genoop om armer en meer reduksievaste gouderts te verwerk. Die pre-oksidasie van hierdie erts deur middel van bakteriese loging is een van die mees belowend metodes van reduksietrae goudherwinning. Die bakteriese oksidasie proses vind plaas by matige temperature en atmosferiese druk. Onder hierdie omstandighede is die oksidasie tempo stadig en neem die invloed van die mineralogiese eienskappe op die verhouding tussen sulfiedoksidasie en goudherwinning groter belangrikheid aan.

Ertsmonsters vanaf Sheba, Agnes en New Consort goudmyne van die Barbertonse Bergland is bestudeer. Sulfiedes is bevry uit heel rots monsters en gekonsentreer. Uitgesoekte kristalle is gemonteer in poleerstukke. Hierdie kristalle is eers mineralogies bestudeer, waarna bakteriese oksidasie eksperimente in luggeroerde houers uitgevoer is. Poleerstukke is vir verskillende tydperke in 'n bakteriese loogpulp, bestaande uit 'n arseenpiriet-piriet flotasie-konsentraat en *Thiobacillus ferrooxidans* bakterië, gedompel. Die uitwerking van die oksidasieproses is bestudeer deur die geloogde stukke onder sowel 'n optiese mikroskoop as 'n aftaselektronmikroskoop (AEM) te ondersoek.

Die sulfiedes vanaf Sheba is swaelryk in samestelling en hoofsaaklik piriet en arseenpiriet word aangetref. Hierdie sulfiedes is chemies gesoneerd na gelang van hulle arseeninhoud. Partikulêre goud kom voor as insluitsels, hoofsaaklik op die kontakte tussen die verskillende sones. Verder is beide arseenpiriet en piriet ook draers van submikroskopiese goud (van 0.7 tot 0.1 gewigspersentasie onderskeidelik). Meer as een generasie van Agnes piriet word aangetref. Die eerste generasie vorm die kern en is gesoneerd met afwisselende verryking en verarming in arseeninhoud. 'n Tweede arseenarm generasie het gevorm na 'n periode van heroplossing. Gouderts van New Consort bestaan uit arseenryke arseenpiriete en loelingiet. Partikulêre goud is die oorheersende goudtipe in hierdie erts.

Tydens die bakteriese loging van die Sheba erts is gevind dat arseenpiriet vinniger loog as piriet. Die arseenryke sones in die arseenpiriet is by voorkeur geoksideer. Gedurende die aanvanklike periode van pirietoksidasie het logingsgroewe ontwikkel langs korrelgrense, langs kontakte tussen verskillende sones en generasies, en langs bestaande krake. Vierkantige, reghoekige, verlengde en heksagonale logingsgaatjies het tydens verskillende periodes van pirietoksidasie gevorm. Die loellingiet insluitsels in die New Consort arseenpiriet is vinnig geoksideer. Dit is te wyte aan die reaktiewe geaardheid van loellingiet met betrekking tot yster III-sulfaat (wat aanwesig is in die bakteriese loogpulp). Die loging van die arseenryke arseenpiriet was egter stadig.

Die resultate verkry in hierdie studie dui aan dat die plekke van voorkeuroksidasie in die meeste gevalle bepaal word deur strukturele afwykings in die sulfiedrooster (hetsy meganies of chemies). Verder is getoon dat kennis oor die mineralogiese eienskappe van gouddraende sulfiedes (soos die voorkomswyse van goud, die verspreiding van verskillende goudtipes, chemiese sonering en generasieverskille) noodsaaklik is om die goudherwinning-sulfiedoksidasie kurwes van ertse te interpreteer.

TABLE OF CONTENTS

TABLE OF FIGURES

TABLE OF TABLES

1 INTRODUCTION

Gold, the noblest of metals, has influenced the history of man since the dawn of civilization some 5 000 years ago. Gold turned men into explorers and lured them across oceans and continents. Until today man has retained his curious infatuation with this king of metals, its great natural beauty and it durability.

Yet, the early method of mining gold placers by simple gravity treatment is gone forever. Since those days impressive advances were made in gold recovery techniques. Recently, however, the mining world has been burdened by a low gold price and the depletion of high grade gold reserves. This has forced the mining companies to treat leaner and more refractory gold ores, leading to higher working and capital costs and thus lower profit margins. With environmental standards and pollution-control regulations to stiffen in the years to come, the additional processing costs involved in converting toxic waste to environmentally acceptable products, will increase. These factors have led to attempts to develop techniques that offer cost-effective alternatives to present methods of mining and treating low grade and refractory ores.

Mineralogical investigations have established a variety of different types of refractory gold (Schweigart and Liebenberg, 1966; Boyle, 1979; and Petruk, 1989). One of the most important forms of refractory gold is submicroscopic gold occurring mainly in arsenopyrite and pyrite. It is this type of gold which is the subject of this study.

This submicroscopic gold is present in significant amounts in the majority of gold ores (Cook and Chryssoulis, 1990). The mode of occurrence of this type of refractory gold, also termed "*invisible*" gold, is either as small inclusions ($<0.1\mu m$,) or in solid solution within sulphides (Chryssoulis and Cabri, 1990). However, this invisible refractory gold cannot be recovered by conventional processing techniques, and some form of pre-treatment of the ore is required to enhance the liberation of this gold and render it amenable to the cyanidation process.

Several pre-treatment techniques for the recovery of refractory gold ores exist in the mining industry, such as oxidative roasting, pressure oxidation, nitric acid oxidation, chlorination, ultrafine-milling and alkaline leaching (Foo, *et al.*, 1989; Komnitsas and Pooley, 1989; Carter, 1991). Many of these processes involve oxidation of the sulphide minerals.

One of the most promising and certainly the most revolutionary pre-treatment method is microbiological oxidation. Bacterial oxidation is a hydrometallurgical process in which bacteria are used to promote the oxidation of sulphide minerals by oxygen at moderate temperatures and ambient pressures.

Interest in bacterial oxidation has greatly increased over the last couple of years, mainly for the following reasons. The gaseous and liquid effluents produced by the process are environmentally acceptable (Komnitsas and Pooley, 1990). Furthermore, it holds the promise of lower capital and operating costs, due to lower operating temperatures and pressures than the alternative methods. It offers the flexibility to

treat both large and small tonnages. A further advantage is the simplicity of the process, by comparison to alternative methods (Gibbs, *et al.,* 1985). This method can be a breakthrough for developing nations, because it requires low energy inputs and an unsophisticated treatment plant (Agate, 1988).

Several reviews of microbiological oxidation confirm that it is a viable and efficient pre-treatment method for arsenopyrite- and pyrite-bearing auriferous refractory ores (Lawrence and Bruynesteyn, 1983; Livesey-Goldblatt, 1986; Spisak, 1986; Komnitsas and Pooley, 1989). Bruynesteyn (1988) summarises the general opinion on bacterial leaching as a pre-treatment method: "*... an economically viable process which is capable of treating refractory ores, liberating precious metals held captive and at the same time converting any arsenic or antimony into environmentally acceptable products*".

2 BACTERIAL OXIDATION PROCESS

Bioleaching was practised empirically at least as far back as the times of the Phoenicians and Romans (Nicolaides, 1987). But it was only in 1947 that Colmer and Hinkle first isolated the microorganism responsible for the oxidation of sulphide minerals, and identified it as *Thiobacillus ferrooxidans*.

The *Thiobacilli* microorganisms belong to a group known as chemosynthetic autotrophs (Corrans, *et al.,* 1972). *T. ferrooxidans* is a rod-shaped bacterium with dimensions of 0.3-0.4 x 0.7-1.7 μm (Kutznetsov, *et al.*, 1963). This microorganism is able (as the name implies) to derive energy from the oxidation of sulphur compounds to sulphuric acid and from the oxidation of ferrous iron (Fe^{2+}) to ferric iron (Fe^{3+}) (Ingledew, 1986). Furthermore, it also utilizes carbon dioxide as a source of carbon and requires a source of nitrogen and phosphates and trace amounts of calcium, magnesium and potassium for chemosynthesis and growth (Pooley, 1987). Generally it operates at temperatures between 25 °C to 40 °C. It is active over a pH range of 1 - 5, with an optimum pH for growth of 2.

Under these conditions, oxidation kinetics are comparatively slow, and the effect of mineralogical characteristics on sulphide oxidation and gold recovery relationships assumes greater importance.

The main reactions that take place during the bacterial oxidation of arsenopyrite and pyrite are the following (Komnitsas and Pooley, 1989; Karavaiko, *et al.,* 1977; Hutchins, *et al.,* 1988):

for the oxidation of arsenopyrite:

The bacteria directly attack the arsenopyrite to produce ferrous sulphate and arsenic acid by the following reaction:

$$2FeAsS + \frac{13}{2}O_2 + 3H_2O \xrightarrow{bacteria} 2H_3AsO_4 + 2FeSO_4 \qquad [1]$$

The ferrous sulphate produced is oxidized bacterially to ferric sulphate, according to reaction [2].

$$2FeSO_4 + H_2SO_4 + \frac{1}{2}O_2 \xrightarrow{bacteria} Fe_2(SO_4)_3 + H_2O \qquad [2]$$

In addition to the attack of bacteria on arsenopyrite according to reaction [1], arsenopyrite can also be oxidized by the ferric sulphate produced in reaction [2]. Reaction [1] is therefore supplemented by the ferric sulphate produced which reacts with arsenopyrite in the following manner:

$$2FeAsS + Fe_2(SO_4)_3 + 3H_2O + \frac{9}{2}O_2 \xrightarrow{chemical} 2H_3AsO_4 + 4FeSO_4 + S \qquad [3]$$

The elemental sulphur produced in reaction [3], is converted to sulphuric acid through further bacterial oxidation:

$$S + \frac{3}{2}O_2 + H_2O \xrightarrow{bacteria} H_2SO_4 \qquad [4]$$

The arsenic acid produced in reaction [1] may also react with ferric sulphate to produce ferric arsenate ($FeAsO_4$) precipitate, which is environmentally acceptable:

$$2H_3AsO_4 + Fe_2(SO_4)_3 \xrightarrow{chemical} 2FeAsO_4 + 3H_2SO_4 \qquad [5]$$

Thus, the overall reaction that takes place during bacterial leaching of arsenopyrite is as follows:

$$FeAsS + \frac{7}{2}O_2 + H_2O \xrightarrow{bacteria} FeAsO_4 + H_2SO_4 \qquad [6]$$

for the oxidation of pyrite:

The oxidation of pyrite by oxygen in the presence of bacteria can be expressed as:

$$FeS_2 + \frac{7}{2}O_2 + H_2O \xrightarrow{bacteria} FeSO_4 + H_2SO_4 \qquad [7]$$

The bacterium catalyse the oxidation of ferrous iron to ferric iron according to reaction [2].

Through this reaction [2] the bacteria maintain a high Fe(III) : Fe(II) ratio in the leach liquor. This ferric iron can thus promote chemical oxidation of pyrite by the reaction:

$$FeS_2 + Fe_2(SO_4)_3 \xrightarrow{chemical} 3FeSO_4 + 2S \quad [8]$$

The bacteria can directly catalyse the oxidation of elemental sulphur, via reaction [4].

The overall reaction of pyrite during bacterial oxidation is therefore as follows:

$$FeS_2 + \frac{7}{2}O_2 + H_2O \xrightarrow{bacteria} FeSO_4 + H_2SO_4 \quad [9]$$

The overall oxidation process is complex, but is thought to be a product of both indirect and direct bacterial activity (Atkins, 1989). Dissolution, proceeding via a *direct* contact mechanism (reactions [1] and [7]), although poorly understood, involves bacterial attachment to the sulphide mineral surface. This attack may be by a bacterial enzyme (Ehrlich, 1988).

During the *indirect* bacterial leaching mechanism ferrous iron is metabolized to ferric iron (reaction [2]) and sulphur is oxidized to sulphuric acid (reaction [4]). In dilute acid and at ambient temperatures, without any bacteria present, the conversion of ferrous to ferric iron (reaction [2]) is minimal. Lacey and Lawson (1970) have established that the rate of reaction [2], in the presence of bacteria, is approximately 10^6 times faster than the same reaction without any bacterium present. The high availability of reactive ferric sulphate has been suggested by Karavaiko *et al.* (1977), Bennet and Tributsch (1978) and others to promote a chemical attack on the sulphides according to reactions [3] and [8]). However, it appears that the extent of this dissolution of sulphides by ferric sulphate present in the bacterial solution is still uncertain.

The growing economic importance and interest in this pre-treatment process, have resulted in considerable research efforts to establish the factors that influence the bio-oxidation process.

3 PREVIOUS INVESTIGATIONS

The mineralogical controls of bacterial oxidation on sulphides were initially studied by Silverman and Ehrlich (1964) who suggested that poorly ordered crystal lattices are more susceptible to bacterial corrosion than well-ordered crystal structures. Duncan and Drummond (1973) observed extremely irregular grooves and pits on the surface of leached individual pyrite grains. They suggested that "*leaching has not occurred solely along crystallographic directions, nor has it been guided completely by minute fractures*". In 1976 Tributsch suggested that the crystalline imperfections (dislocations) can influence bacterial activity. Berry and Murr (1978) observed that bacteria attached to mineral surfaces were arranged in arrays, resembling grain boundaries or sub-grain boundaries.

In 1978 Bennett and Tributsch observed dissolution pits with different modes of occurrence in pyrite, ranging from individually distributed pits, to groups and chains. They concluded that the bacterial oxidation is critically dependent on the crystal structure and on deviations in the crystal order (fracture lines, dislocations).

This point of view is shared by Southwood and Southwood (1985) who observed the development of cylindrical pores, parallel to certain crystallographic directions in the sulphide particles, during bacterial oxidation. They concluded that pores developed along dislocations and that dissolution was confined to the leading end of the pores, and thus no oxidation of pore walls took place. Their propagating-pore model for the bio-oxidation of sulphides developed from these conclusions. However, Hiltunen *et al.* (1981) also studied the surfaces of leached sulphide grains, but they observed only an irregular distribution of dissolution pits resulting from bacterial oxidation.

An attempt was made by Keller and Murr (1982) to determine the role of crystallographic directions in pyrite on the rate of bacterial oxidation. They observed complexed pitting on the crystal surfaces, and concluded that the crystallographic directions do play a role during the bacterial oxidation process. However, their observed rates of oxidation on various crystallographic directions were inconsistent.

During a study by Hansford (1986), hexagonal dissolution pores within a pyrite crystal were observed. He proposed that these pores were formed by bacterial leaching along screw dislocations within the pyrite crystal. Pooley (1987) observed that certain parts of particles are more readily attacked through pitting than others, and suggested that it might be due to crystallographic control or small chemical differences in the mineral. He also observed dissolution to occur around small mineral inclusions within the sulphides.

Preferential bacterial oxidation of certain sulphides in a multi-metal sulphide substrate is envisaged by numerous scientists as a direct result of the different oxidation potentials of the various minerals.

Panin *et al.* (1977) and Atkins (1978) established independently that arsenopyrite leaches more rapidly than pyrite, due to its lower oxidation potential and therefore its higher activity. Karavaiko and Pivovarova (1977) established that the pyrite with hole (p-type) conductivity is oxidized by *T. ferrooxidans* at a higher rate, and more continuously than pyrite with electron (n-type) conductivity, i.e. pyrites with cation deficiency is oxidized more readily than pyrite with anion deficiency. They further concluded that deviations from the ideal electron constitution in an electron structure of a sulphide mineral is important during bacterial oxidation. They envisaged such deviations to include the following: the presence of cation or anion deficiency in the composition of sulphides, the position of the Fermi level and the value of electrochemical and electrode potentials.

The electrochemical aspects during bacterial oxidation of multi-metal sulphides were studied by Natarajan (1988). He concluded that both bio- and electrochemical interactions are important in the bio-oxidation of sulphides. In a mixture of various sulphide minerals present in a leaching system, the mineral with the lowest oxidation potential will undergo preferential oxidation while the noblest mineral will stay passive.

Komnitsas and Pooley (1990) determined that arsenopyrite dissolution started immediately in the presence of bacteria and proceeded much faster than the dissolution of pyrite; thus arsenopyrite oxidation occurred at much lower Eh values than pyrite.

The mechanism of oxidation of sulphides was studied by Karavaiko and Pivovarova (1977). They observed that cells of *T. ferrooxidans* occurred in close contact with arsenopyrite crystals during oxidation, and that both the cells and the crystal around the cells were surrounded with a slime. This led to their conclusion that a bacterium-mineral micro-environment formed, which indicated that an enzymatic mechanism exists for the bacterial oxidation of sulphides. Studies by Murr and Berry (1976) and Bennet and Tributsch (1978) also give strong support for the direct contact mechanism of bacterial oxidation. This view is also supported by Natarajan (1988), who stated that the mere presence of bacteria in a solution is not enough to oxidize the sulphides; direct bacterial attachment to the mineral surfaces is a prerequisite for solubilization of sulphides.

The effect of ferric sulphate leaching on the sulphides was also studied. In 1982 Keller and Murr concluded that bacterial leaching of pyrite is more effective than ferric sulphate leaching. The difference in biological and chemical leaching of an auriferous pyrite/arsenopyrite flotation concentrate were investigated by Norman and Snyman (1988). They observed that during both leaching methods, arsenopyrite, rather than pyrite, was selectively attacked and destroyed. They concluded that acidic-ferric leaching was relatively unimportant during the bacterial oxidation process.

In summary, previous work on the mineralogical factors influencing bio-oxidation initially suggested the random distribution of bacterial activity on the sulphide surfaces, without any crystallographic influences. However, recent studies show that bacterial oxidation is directly dependent on the crystal structure. Although a number of mineralogical factors, such as dislocations, grain boundaries, inclusions, crystallographic orientations, etc., were suggested as determining the rate of bacterial leaching, it is not clear whether any one of them is of overriding importance. The effect of small deviations in the composition of sulphide minerals was, however, not directly investigated, and is one of the objectives of this study.

Knowledge of the mode of occurrence of refractory gold in sulphide minerals is essential in a study of the liberation of gold from sulphides by a pre-treatment method, as outlined by Cook and Chryssoulis (1990): "*The successful processing of sulphide-bearing refractory gold ore can clearly only be achieved by a better understanding of the mineralogy of the invisible gold and its distribution within and among coexisting common sulphide minerals*".

Submicroscopic gold may account for the major proportion of the gold and it appears to be preferentially concentrated in arsenopyrite. Studies by Schouwstra and De Villiers (1989) on the gold mineralisation at Sheba mine indicated that arsenopyrite is economically the most significant sulphide mineral due to its good correlation with high gold values.

The nature of *invisible gold* (either in solid-solution or as discrete inclusions of submicroscopic size) in sulphide minerals has been a subject of heated controversy and dispute and has been passionately debated in the literature for decades by numerous scientists, such as Stillwell and Edwards (1946); Schweigart (1965); McPheat *et al.* (1969); Henley (1975); Mironov *et al.* (1981); to name but a few. Boyle (1979) did an extensive review of evidence supporting the occurrence of gold in solid-solution or as discrete inclusions of submicroscopic size. He concluded that both these types can exist.

Recent research produced more detailed information, employing various new bulk analytical techniques and more sensitive microbeam analytical methods, such as Mössbauer spectroscopy, electron-probe, secondary-ion mass spectrometry (SIMS), micro-proton induced X-ray emission (μ-PIXE) spectroscopy and high-resolution transmission electron microscopy (HRTEM).

Boiron *et al.* (1989), Marcoux *et al.* (1989) and Cathelineau *et al.* (1989) investigated gold-bearing arsenopyrite from various deposits in France, using an electron microprobe. They observed compositional zoning within the arsenopyrite: with the periphery of the arsenopyrite crystals enriched in As and Au, correlating with a decrease in the S and Sb contents. Similar zoned arsenopyrites were studied by Johan *et al.* (1989). They concluded that the incorporation of gold in arsenopyrite is due to substitution of As or Fe, present in the Fe-sites, which indicated that gold occurs as chemically bound gold within the arsenopyrite crystal structure.

Although electron microprobe studies on gold distribution within sulphide minerals are widely used and are very popular, the minimum detection limit (mdl) for gold is relatively high at 200 ppm (Cabri, *et al.*, 1989), especially in pyrite, which usually contains low concentrations of gold. Graham *et al.* (1989) however, succeeded in reducing the mdl of electron microprobe analyses to 10 ppm. However, other techniques, with lower detection limits can yield better results.

The ion microprobe (also referred to as SIMS for Secondary Ion Mass Spectrometry) (mdl = 0.3 ppm) has been successfully used by Chryssoulis and Cabri (1990) and Cook and Chryssoulis (1990) in studies of gold-bearing sulphides. The in-depth profiling capability of the microprobe allowed them to identify gold inclusions (as small as 100 Å) and to distinguish it from gold in solid solution or dispersed in the crystal lattice. Investigations by Cabri *et al.* (1991), applying particle induced X-ray excitation (PIXE) analysis (mdl = 25 ppm) showed gold distribution within some pyrite crystals to be non-homogeneous.

None of the above investigations, however, provides direct evidence of structurally bound gold in the sulphide minerals.

^{197}Au Mössbauer spectroscopy, employed by Wagner *et al.* (1986) and Wagner *et al.* (1988) has shown that gold in arsenopyrite occurs as chemically bound cationic gold. Within pyritic ore the presence of chemically bound gold, as well as metallic gold inclusions, was revealed. High-resolution transmission electron microscopy (HRTEM) investigations of refractory arsenopyrite were performed by Cabri *et al.* (1989). No gold particles in the *colloidal* form, were found, which lead to their conclusion that the invisible gold within the arsenopyrite, is randomly distributed in solid-solution. However, Bakken *et al.* (1989) observed visible segregations of gold (colloidal particles less than 200 Å in diameter) in arsenopyrite from high-grade unoxidized Carlin ores during HRTEM investigations.

Wu and Delbove (1989) investigated the hydrothermal synthesis of gold-bearing arsenopyrite. They observed that the gold concentration, introduced as invisible gold into the arsenopyrite structure, varied in relation to the zoning in the crystals; the As-rich growth zones, essentially near the rims of the crystals, contain up to 1.7 weight per cent gold, while the cores are virtually gold-free.

Pyrite is frequently the most abundant sulphide in gold deposits (Cabri, *et al.,* 1991). Concentrations of submicroscopic gold in pyrite are, however, not as high as in arsenopyrite. Wells and Mullens (1973) studied pyrite crystals from the Cortez and Carlin gold mines, Nevada, and found a direct relationship between gold and arsenic in pyrite in the unoxidized ores.

The sorption of gold by pyrite was investigated by Mironov *et al.* (1981). They observed that pyrite is a semi-conductor which, when enriched in Ni and Co exhibits n-type conductivity, but when enriched in As exhibits p-type conductivity. They also concluded that the incorporation of arsenic into pyrite increases the capacity of the latter to take up gold.

Chryssoulis and Cabri (1990), utilizing the elemental distribution mapping facility on the SIMS, observed a positive correlation between arsenic and gold concentration in pyrite crystals. Cook and Chryssoulis (1990) observed that only if As is present in pyrite in amounts greater than 0.2 - 0.4 weight per cent, are significant amounts of gold incorporated into the structure.

Thus, evidence exists that *invisible gold* can occur both in solid-solution within the arsenopyrite and pyrite crystal structures and as submicroscopic inclusions. The existence of a sympathetic relationship between As- and Au-contents in both pyrite and arsenopyrite is also apparent.

4 AIM OF THIS STUDY

The mode of gold occurrence within sulphides has significant implications during bacterial oxidation and determines the manner in which a bacterial oxidation process may be employed (Pooley, 1987).

Lawrence and Bruynesteyn (1983) found that for some sulphide concentrates (mainly refractory pyritic) a sympathetic linear relationship exists between gold recovery and sulphide oxidation. By contrast, a non-linear relationship was found by Hansford (1986), during bacterial oxidation of a pyrite concentrate; 90 % of the gold was liberated after only 30 % pyrite oxidation. This is unexpected for ores containing mostly pyrite.

The gold recovery-pyrite oxidation curve obtained for a plant flotation concentrate from the Agnes goldmine in the Barberton Greenstone-belt (mainly pyritic ore) is shown in Figure 1 (Pinches, 1990). The concentrate was oxidized to different levels and the gold recoveries were estimated by cyanide leaching of the residues. The percentage gold recovered is largely sympathetic to the percentage of the pyrite oxidized. During the initial stages of sulphide oxidation (<30%) gold is liberated at a higher rate than in the later stages (above 30 %).

Figure 2 shows the typical gold recovery versus sulphide oxidation relationship obtained from a flotation concentrate from the Sheba goldmine (Pinches, 1990). The Sheba ore consists mainly of arsenopyrite and pyrite. Approximately 35 % of the gold in the sample was not refractory and could be recovered by direct cyanidation. The remaining 65 % of the gold occurred as refractory gold and was liberated by bacterial oxidation of the sulphides. The gold recovery and sulphide oxidation is non-linearly correlated, with the oxidation of only 35 per cent of the sulphides resulted in a 90 per cent gold recovery. Thus, two distinct stages of gold liberation exist, i.e. an initial rapid release of gold during the early stages of sulphide oxidation followed by a period of gold liberation with a much slower gold release.

Models to predict the gold recovery relationships were postulated by numerous scientists. Southwood and Southwood (1985) postulated a hybrid between the shrinking particle and their propagating-pore concept as a model for the bacterial oxidation process of sulphides. Their propagating-pore model was further also used in mathematical and kinetic models (respectively by Lazer, *et al.,* 1986 and Hansford, 1986) to describe the bacterial leaching process.

An attempt was made by Lazer *et al.* (1986) to describe the relationship between sulphide oxidation and gold release by means of a mathematical and mineralogical model. However, their mineralogical observations did not support their experimental data. They suggested that their assumption that *the amount of gold released is proportional to the amount of sulphide being oxidized* was wrong, and that bacterial leaching occurred preferentially at sites of greater gold concentration within the sulphide particles. They could however, not prove this and conclude that *"regrettably, it would be very difficult to obtain the mineralogical evidence needed to demonstrate conclusively the mode of occurrence of the sub-microscopic gold in the concentrates or to investigate any other possibilities for the fast release of gold from the sulphides"*.

One of the main purposes of this investigation is therefore an attempt to explain this enhanced rate of gold release from sulphide minerals during the bacterial oxidation process. In order to investigate this, mineralogical factors affecting the bacterial oxidation of gold-bearing sulphides from the Agnes, Sheba and New Consort goldmines were studied.

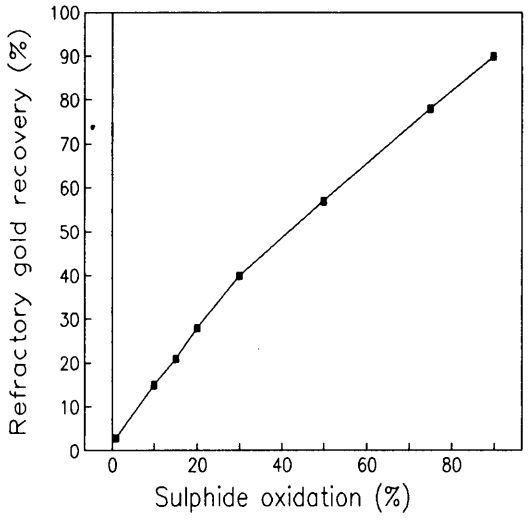

Figure 1: *Refractory gold recovered versus sulphide oxidation for a pyritic Agnes flotation concentrate.*

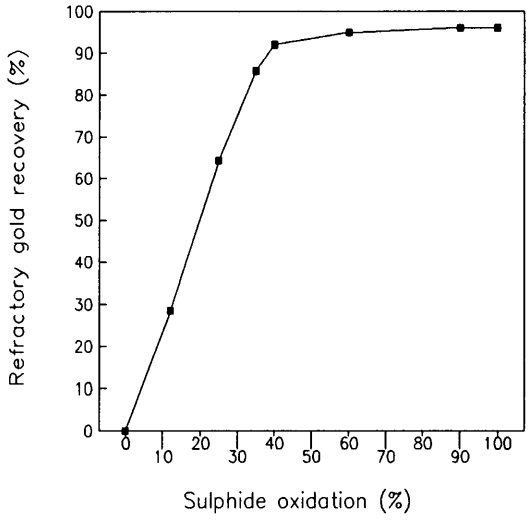

Figure 2: Refractory gold recovered versus sulphide oxidation for a Sheba flotation concentrate.

5 METHODS OF INVESTIGATION

5.1 Material

Ore samples from the Sheba, Agnes and New Consort goldmines near Barberton, Transvaal, South Africa, were used in this investigation. These goldmines are situated in the Barberton greenstone-belt, one of the major Archean nuclei of southern Africa (Anhausser, *et al.*, 1984). The three types of ore samples exhibit distinct differences in mineral assemblage and in modes of gold occurrence.

The Sheba ore is from the Main Reef Complex (MRC). This MRC is the widest and the richest ore zone in the Sheba mine (Wagener and Wiegand, 1986). Schweigart and Liebenberg (1966) found that approximately 70 % of the gold occurs as inclusions within sulphide minerals, mainly pyrite and arsenopyrite, and 30 % as free gold. This gold ore is classified as refractory, due to the presence of small gold inclusions in arsenopyrite and pyrite and submicroscopic gold, mainly in arsenopyrite (Schouwstra and De Villiers, 1989). Quartz is the main gangue mineral and smaller amounts of calcite, ankerite, sericite, muscovite and fuchsite are also present.

The ore from the Agnes Mine is mainly pyritic. Approximately 80 % of the gold occurs free and 20 % is intimately associated with sulphide minerals, mainly pyrite (Schweigart and Liebenberg, 1966). The gangue minerals are mainly quartz and sericite.

Mineralization at the New Consort Mine is largely associated with a fine grained siliceous zone known as the Consort Bar. Interlayered sulphide rich bands, containing arsenopyrite as the main ore mineral, are present in the Bar. Refractory gold, occurring mostly in association with arsenopyrite, was estimated at approximately 20 % of the total gold by Schweigart and Liebenberg (1966). The main gangue minerals include quartz, biotite, calcite and sericite.

Whole rock samples from these mines, forming part of a collection of samples located in the Mineralogy Division of Mintek, were used during the present study. These samples were originally collected by Dr. W.R. Liebenberg, Mr. A. Lombaard and Dr. R.P. Schouwstra.

5.2 Sample Preparation

The whole rock ore samples were leached with hydrofluoric acid, according to the Neuerburg method (1975). This treatment involves the dissolution of the siliceous matrix, but it does not attack or alter gold, pyrite, arsenopyrite and the majority of other sulphides. The leached residues contained mainly pyrite and/or arsenopyrite crystals. From each of these residues crystals were selected and mounted in epoxy resin and polished surfaces were prepared. Where the quantity of sulphide residue was large enough gold assay values were also determined. The sample numbers of the polished sections investigated in this study, together with their original numbers and gold assay values where available, are listed in Table I.

5.3 Analytical Methods

Suitable crystals, containing few inclusions or cracks, were studied by means of incident light microscopy, whereafter more detailed analytical techniques were used.

5.3.1 *Scanning electron microscopy*

Detailed surface observations were carried out using a Scanning Electron Microscope (SEM). Initial observations were done at 20 kV with a probe current of 2.45 nA to enhance the differences in average atomic concentration of the different phases within the sulphide crystals. Using the SEM the apparent brightness of the mineral phases is directly related to the atomic number (Z) of the elements present. This is known as the *Z effect*. Heavier elements with a higher atomic number produce more secondary electrons and therefore appear brighter than elements with a lower atomic number.

Table I: Sample numbers and gold assay values (where available) of the sulphide residues

Sample No.	Original No.	Gold assay value (g/t)
SHEBA		
RC1006 RC1007 RC1024	RPS980	1759
RC1008 RC1013 RC1018 RC1019 RC1025 RC1041	RPS353	1225
RC1009 RC1014 RC1016 RC1017 RC1026 RC1042	RPS275	
RC1037 - apy RC1038 - py	RPS341	58.2
RC1039 - apy RC1040 - py	RPS323	39.1
RC1033 RC1034 RC1076 - RC1085	SHB1	1053
RC1035 RC1036 RC1086 - RC1095	SHB2	1032
AGNES		
RC1004 RC1005 RC1053 - RC1056	Agnes ROM	77.3
RC1061 - RC1068	A73	
RC1069 RC1070	A74	
RC1071 - RC1073	A35	
RC1074 RC1075	A69	
NEW CONSORT		
RC1022 RC1023A RC1023B RC1057 - RC1060	52E11	107
RC1043 RC1044	52E2	
RC1051 RC1052	Consort A	
RC1045 RC1046	Consort B	
RC1047 RC1048 RC1049 RC1050	Consort C	

For example in pyrite, gold (Z = 79) generates more secondary electrons than iron (Z = 26) and sulphur (Z = 16) in pyrite, and would appear very much brighter. Arsenopyrite is again brighter than pyrite due to the presence of arsenic (Z = 33). In arsenopyrite or pyrite, therefore, any zone or area that contain a higher amount of arsenic than the surroundings, will appear slightly brighter. By using a high probe current, this Z-effect is enhanced and therefore any minor compositional inconsistency (approximately higher than 0.5 %) within the crystals is discernible as a difference in brightness of the image.

During the initial SEM study, the nature of any inclusions present in the sulphide crystals were identified. Simultaneously, the dimensions and mode of occurrence of any gold inclusions encountered, were recorded. Furthermore, the microtexture, morphology and compositional zoning within the crystals, were noted.

The crystals were examined both before and after bacterial leaching and the effects of the leaching were recorded by means of both secondary electron and electron backscatter images.

5.3.2 *Electron microprobe analyses*

Electron microprobe analyses were conducted at an accelerating voltage of 15 kV, a beam current of 20 nA on a Faraday Cage, using a counting time of 40 seconds for gold and 20 seconds for all the other elements. The following elements were analysed for: As, Ag, Bi, Pb, S, Sb, Sn, Au, Zn, Cu, Ni, Co and Fe. The minimum detection limit (mdl) for gold was established at 450 ppm, at a confidence level of 95 %. Only analyses that total between 98.0 and 101.0 wt % were used, in accordance with the requirements of Kretschmar and Scott (1976).

5.4 Bacterial Leaching

The laboratory grown mixed culture consisted predominantly of the bacterium *Thiobacillus ferrooxidans*, but minor amounts of the bacterium *Leptospirillum ferrooxidans* were also present. Figure 3 shows the mixed culture used. *Thiobacilli* is rod-shaped and *Leptisperilli* has a sinuous form. This spirillium-type organism oxidizes iron only (Balashova, *et al.*, 1974).

A medium, known as a 9 K medium (Silverman and Lundgren, 1959) was used as lixiviant during the bacterial leaching tests. Its constituents and their respective proportions, are listed in Table II. Bacterial leaching testwork was conducted continuously in 1.5 ℓ P.V.C. pachuca air-lift vessel. Figure 4 is a schematic representation of the typical apparatus used during this investigation.

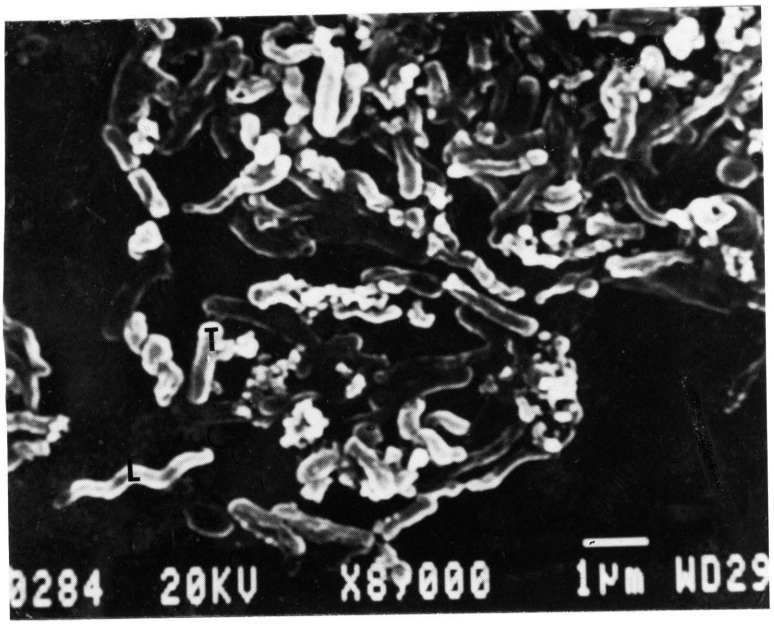

Figure 3: *A secondary electron image of a mixed bacterial culture with bacteria Thiobacillus ferrooxidans (T) and Leptospirillum ferrooxidans (L).*

Table II: *List of substances constituting the lixiviants used; 9 K for bacterial oxidation tests, 0 K for sterile tests.*

MEDIUM	SUBSTANCE	MASS (g/l)
9 K	$(NH_4)_2SO_4$	3.0
	KCl	0.1
	K_2HPO_4	0.5
	$MgSO_4.7H_2O$	0.5
	$CaNO_3.4H_2O$	0.1
	$FeSO_4.7H_2O$	44.0
0 K	$Fe_2(SO_4)_3.xH_2O$	69.1

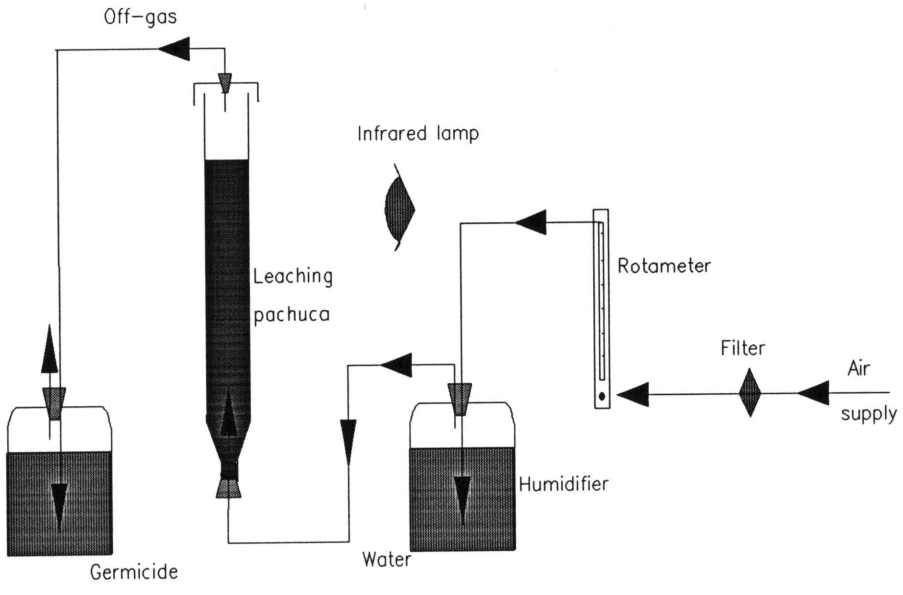

Figure 4: Illustration of the apparatus used during testwork.

During the bacterial tests the 9K lixiviant medium in the pachuca was inoculated with the mixed bacteria culture. An arsenopyrite-pyrite concentrate was added to the solution. The conditions used during this investigation were those previously established as optimum for these types of ores. The appropriate density of pulp was established at 10 per cent solids. Throughout the tests the pH value was adjusted and kept at 1.4 by the addition of either lime, sodium hydroxide or sulphuric acid. The oxidation-reduction potential remained approximately at 600 mV. The temperature was maintained between 35 and 37 °C by the proximity of an infra-red lamp, and the use of a preheated air-supply. The laboratory supply of compressed air was filtered at 0.2μm and regulated through a rotameter at a rate of 2 ℓ/min. into the humidifier. Humidified air was used to minimise water evaporation from the agitated pulp, and thus fluctuations in iron concentration. The ferric iron concentration within the bacterial solution was determined by titration and established at 15.2 g/ℓ.

After every three days, a third of the pulp was removed and replaced by fresh concentrate and lixiviant. Thereby the bacteria retained an elevated active state and the redox potential remained high throughout the tests.

Polished sections were suspended and submerged in the bacterial leach pulp in the puchucas for various periods of time. The effect of sulphide oxidation was monitored by observations of the leached sections using an optical microscope and a SEM. The nature of dissolution features was recorded by SEM backscatter or secondary electron images. After the SEM inspections, the sections were re-introduced to the bio-solution for a further period of leaching.

5.5 Ferric-Sulphate Leaching

In addition to the bacterial leaching test pachucas a separate pachuca containing a 0K solution was set-up to conduct non-bacterial acid leaching tests. The 0K medium consists of the same constituents as the 9K medium, except that no bacteria and no ferrous sulphate were added. The ferrous sulphate was replaced by ferric sulphate (Table II). 69.1 g of ferric sulphate was added to the solution to establish a ferric iron concentration of 15 g/ℓ, i.e. identical to that in the bacterial leach solution. No pulp was added to the solution. The rest of the conditions that prevailed during bacterial leaching, were not adjusted during the acid leaching.

Three additional acid leach tests, with concentrations of ferric iron at 30, 45 and 60 g/ℓ respectively, were performed. The prevailing conditions during each test are listed in Table III.

Polished sections were subjected to a sterile ferric sulphate leach for various periods of time. After removal of the sections from the solution, the sections were examined using a SEM. Backscatter images of the appearance of the exposed surfaces were recorded. Afterwards the sections were re-introduced to the acid solution for a further period of time.

Table III: Conditions of various ferric-sulphate leach tests.

Test	Conc (g/ℓ)	pH	Redox (mV)	Temp (°C)
1	15	1.41	608	35.5
2	30	0.81	613	36.0
3	45	0.78	619	36.5
4	60	0.48	620	36.0

6 RESULTS

6.1 RESULTS OF MICROSCOPE, SEM AND MICROPROBE INVESTIGATIONS

6.1.1 New Consort Arsenopyrite

Arsenopyrite, together with minor amounts of loellingite, are the predominant ore minerals present in the New Consort samples.

The arsenopyrite is As-rich, with an As/S atomic ratio higher than 1, reaching a maximum of 1.19. A summary of the microprobe analyses appears in Table IV, while Appendix 1 lists the complete analyses of these arsenopyrites. In Figure 5 the variation in arsenopyrite composition is plotted in the ternary system Fe-As-S. The As-rich nature of the New Consort arsenopyrite is evident. The composition of the arsenopyrite can in general be expressed as $FeAs_{1.1}S_{0.9}$, but small variations do occur. The variation in both S- and As-content between the different compositional zones, is only about 2 weight per cent. Arsenopyrite usually occurs as subhedral to anhedral crystals.

The New Consort arsenopyrite exhibits only faint compositional zoning. When this zoning is distinguishable within a crystal, it usually occurs as As-rich centres surrounded by slightly less As-rich rims. An arsenopyrite crystal, showing subtle zoning of this type, is illustrated in Figure 6. Kretschmar and Scott (1976) established that such an As-rich assemblage would form at a temperature of approximately 650 °C. From their results, the crude zoning in the arsenopyrites, from As-rich cores (As = 36 at %) to relatively As-depleted rims (As = 34 at %), can be explained by a progressive decrease in temperature, or decrease in log aS_2.

In the New Consort arsenopyrite a weak negative relationship exists between the As- and S-content (Figure 7). An enrichment in nickel occurs within the arsenopyrite, with Ni-concentrations reaching a maximum value of approximately 0.85 atomic per cent (Table IV). A plot of Ni- versus As-content (Figure 8), indicates that two distinct trends exist. The trend with the higher Ni-values represents arsenopyrite without any loellingite inclusions. However, when loellingite inclusions are present, the Ni-content of the arsenopyrite drops. In both these cases, however, a positive relationship exist between Ni and As. Cobalt is also present in relatively high amounts, as high as 2 000 ppm. A linear positive relationship exists between cobalt and nickel.

Numerous nickeliferous loellingite grains, with an approximate composition of $FeNi_{0.3}As_{2.5}S_{0.1}$ (Table IV), occur as inclusions within or in contact with the arsenopyrite crystals. These loellingite inclusions vary in dimensions: from a few micrometers to hundreds of micrometers in diameter. Figure 9 exhibits a loellingite inclusion within an arsenopyrite crystal.

Table IV: *Summary of the microprobe analyses of As-rich arsenopyrite and loellingite inclusions.*

	ARSENOPYRITE						LOELLINGITE				
	Atomic %				ppm		Atomic %				ppm
	Fe	As	S	Ni	Au	As/S	Fe	As	S	Ni	Au
min	31.91	34.11	29.89	0.06	< mdl	1.08	24.54	58.72	0.62	7.17	< mdl
max	34.41	36.13	32.1	0.85	1660	1.19	26.56	65.58	3.06	8.73	402
avg	32.98	35.46	30.95	0.39	381	1.14	25.61	63.56	2.22	7.78	123
std	0.63	0.53	0.60	0.26	408	0.03	0.62	1.95	0.93	0.59	150

min - minimum value
max - maximum value
avg - average value
std - standard deviation
mdl - minimum detection limit, 450 ppm

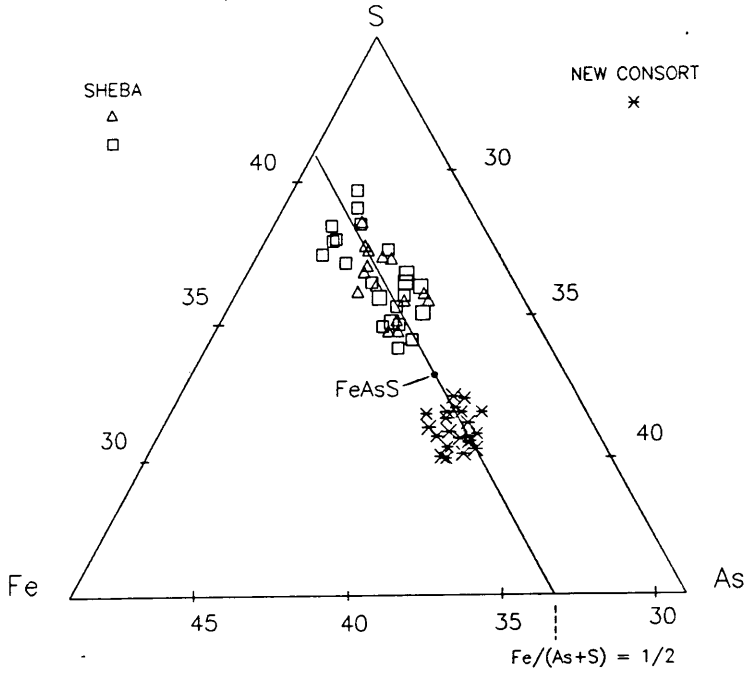

Figure 5: *The variation in composition of New Consort and Sheba arsenopyrite in the Fe-As-S ternary system*

Figure 6: *An arsenopyrite crystal, with an As-rich centre, containing numerous inclusions (black), partially surrounded by a S-rich rim - RC 1022 (electron backscatter image)*

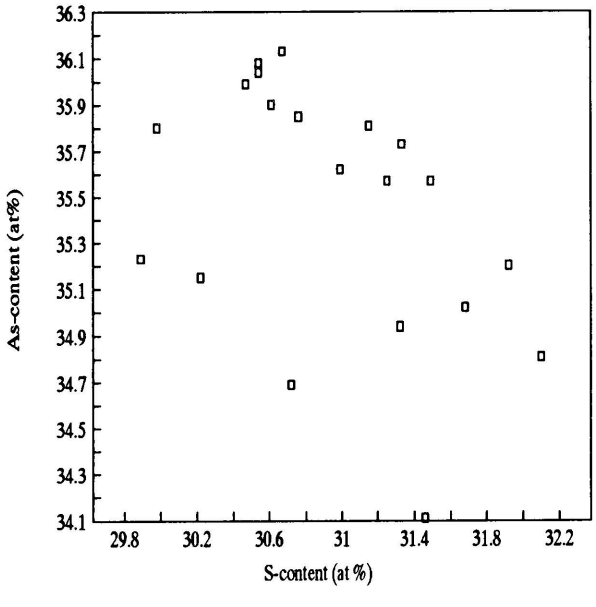

Figure 7: As- versus S-concentration in the New Consort arsenopyrite

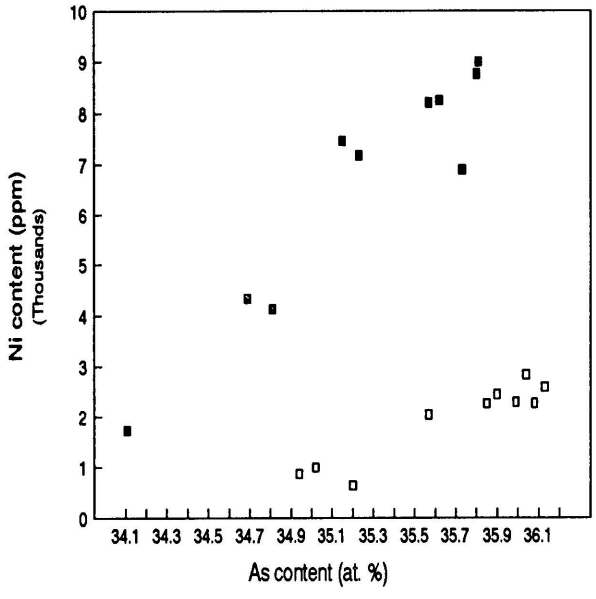

Figure 8: *Ni-content against As-content, showing a positive correlation between them. (Filled symbols - arsenopyrite without any loellingite inclusions; empty symbols - with loellingite inclusions)*

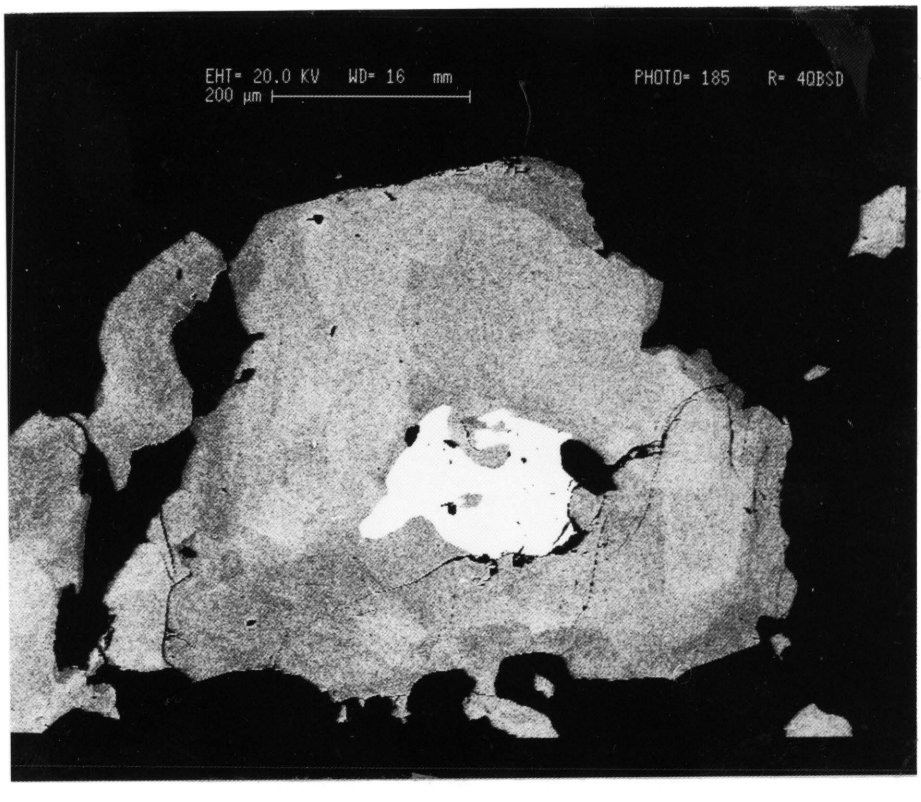

Figure 9: *Electron backscatter image of a loellingite inclusions (white) within arsenopyrite - (RC 1043)*

Most of the gold in New Consort arsenopyrite, occurs as particulate gold. Table V indicates the dimensions and the association of the gold particles observed within the arsenopyrite. On average, these gold inclusions have areas smaller than 10μm^2. However, some of them are relatively large, with the largest having an area of approximately 750μm^2. Gold particles in the arsenopyrite can occur as inclusions within loellingite, within arsenopyrite and on the contact of loellingite and arsenopyrite (Figure 10). Gold inclusions in loellingite are frequently associated with Ni-enriched areas, as is evident from Figure 11. Numerous quartz veins, which cut across the arsenopyrite crystals, are also hosts for gold particles. Figure 12 shows gold particles along a quartz vein.

The submicroscopic gold content of the New Consort arsenopyrites is low; with a maximum of slightly more than 1 600 ppm and an average value below the minimum detection limit (mdl). The gold content varies slightly from zone to zone, without any distinct pattern. No direct relationship exists between the Au-content and the As-content in the New Consort arsenopyrite (Figure 13), but the highest amount of submicroscopic gold occurs in the zones with high As/S ratios.

The following minerals, of varying dimensions, occur as inclusions in arsenopyrite: loellingite, pyrrhotite, gold, tetradymite, Bi-telluride, Pb-telluride, monazite, xenotime, tetrahedrite, ilmenite, Ni-arsenide, galena, muscovite and quartz.

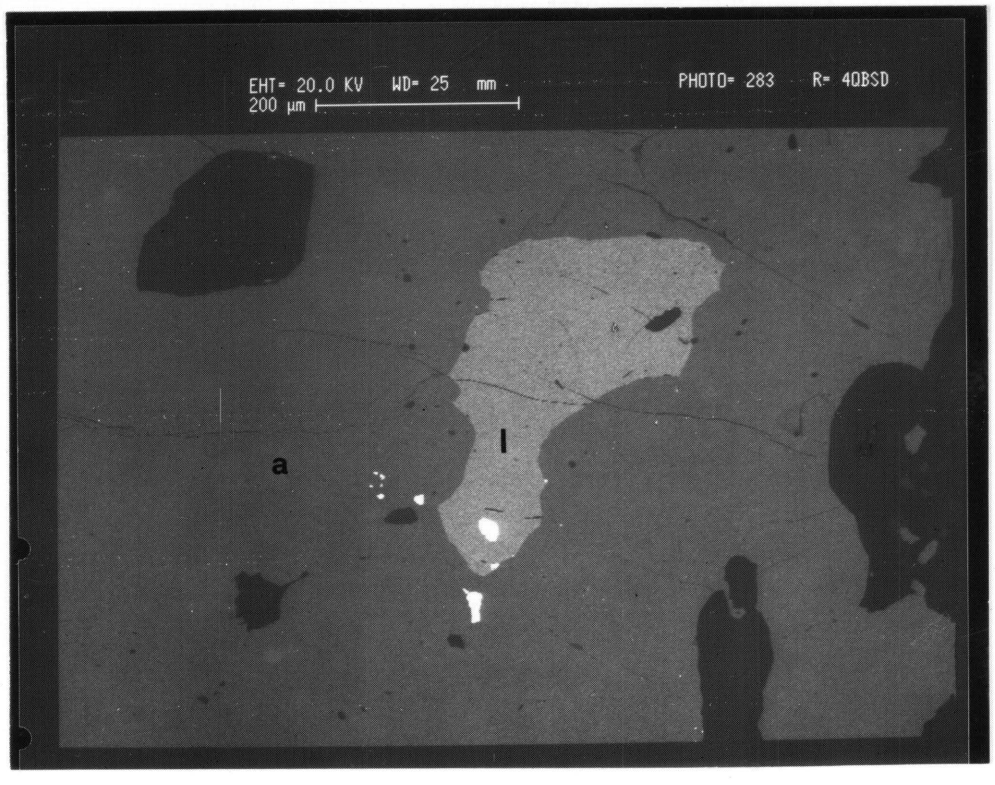

Figure 10: Gold inclusions within loellingite (l), arsenopyrite (a) and on the contact of loellingite and arsenopyrite - RC 1044. (electron backscatter image)

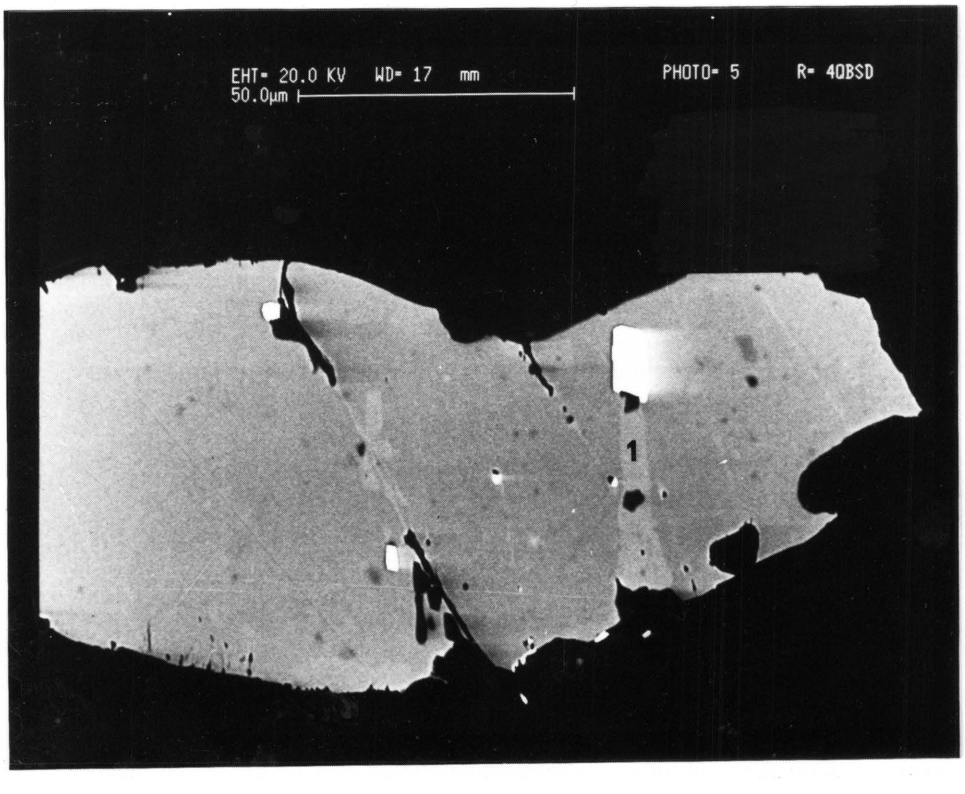

Figure 11: Gold inclusions (white), associated with Ni-enriched loellingite (light grey - 1) and quartz (black) all enclosed in loellingite - RC 1022 (electron backscatter image)

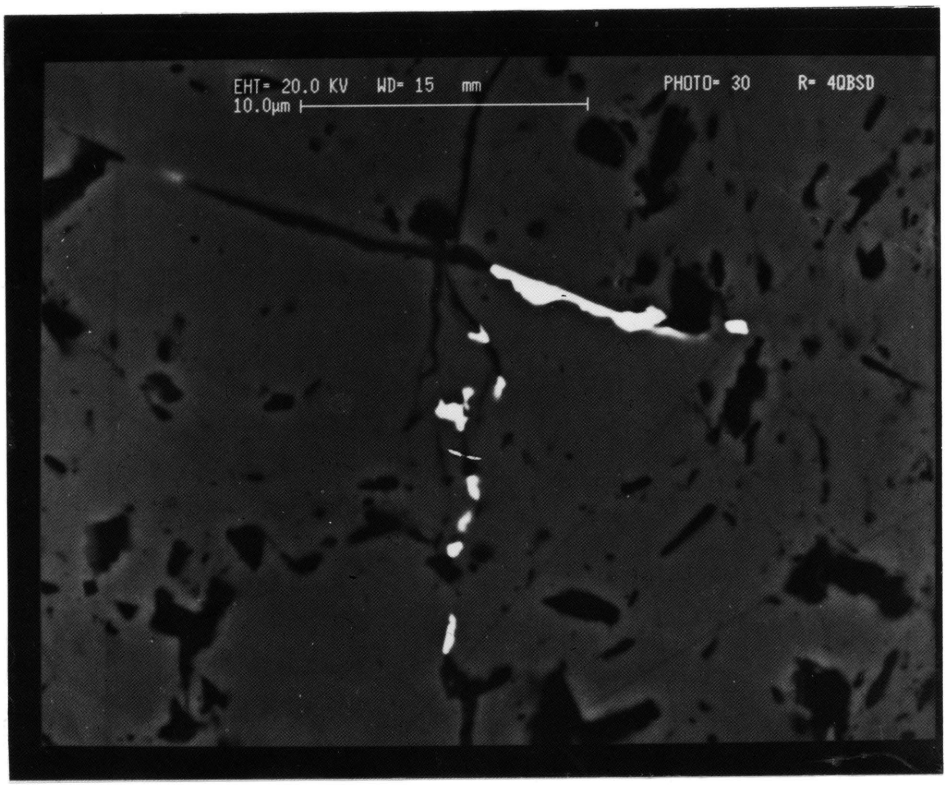

Figure 12: Gold inclusions (white) along quartz veins (black), within an arsenopyrite particle - RC 1043 (electron backscatter image)

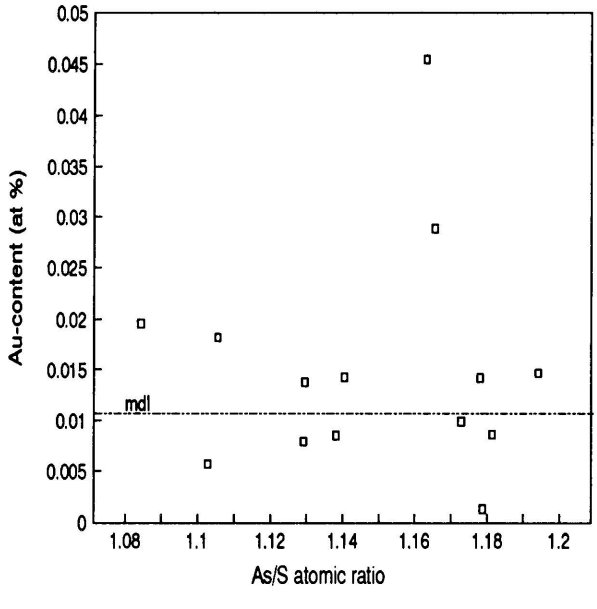

Figure 13: As/S atomic ratio against Au concentrations

6.1.2 Sheba Arsenopyrite and Pyrite

Arsenopyrite and pyrite are the major sulphides present in the Sheba ore, with minor and trace amounts of galena, chalcopyrite, pyrite, Pb-Sb-sulphide, tetrahedrite, sphalerite, stibnite, tennantite, rutile, quartz and monazite. The minor minerals are in general economically insignificant and usually occur as inclusions in arsenopyrite and pyrite crystals.

6.1.2.1 *Sheba arsenopyrite crystals*

The Sheba arsenopyrite occurs as euhedral, needle-like crystals, owing to preferential crystal growth along the c-axis. These thin needles of arsenopyrite occur either as individual single crystals or as clusters.

The Sheba arsenopyrite is S-rich, with an As/S atomic ratio below 1 and an approximate composition of $FeAs_{0.9}S_{1.1}$. From Figure 5 the S-rich nature of the arsenopyrite and the variation in As- and S-contents, in comparison with New Consort arsenopyrite, is evident. This variation in the As- and S-content can be as high as 6 at %.

The majority, if not all, of the Sheba arsenopyrite crystals are chemically zoned, in some cases delicately, as shown by SEM photomicrographs Figures 14, 15 and 16. Electron microprobe analyses illustrating the variation in major element composition of the different zones are given in Appendix 2. A summary of the data, presented in two sets of analyses corresponding to As-rich zones (As/S ratio > 0.85) and As-poor zones (As/S at ratio < 0.85), is given in Table VI. Compositional zoning is therefore characterized by lateral enrichments in As-content and simultaneously in impoverishments in S-content, and vice versa.

The crystal illustrated in Figure 14 is apparently formed by a cluster of crystals of the same crystallographic orientation. Crystals of this type are considered to form by continued crystallization around an initially complex skeletal crystal (Phillips, 1963).

Figure 15 shows a S-rich arsenopyrite with complex compositional zoning in a plane approximately perpendicular to the *c-axis*. Delicate rhythmic reversals in chemical composition, with alternating enrichments in As- and S-content, are visible. From one zone to the other the variation in atomic As-content may be as high as 6 atomic per cent. Figure 16 shows the compositional zoning in a plane approximately parallel to the *c-axis* of an arsenopyrite crystal.

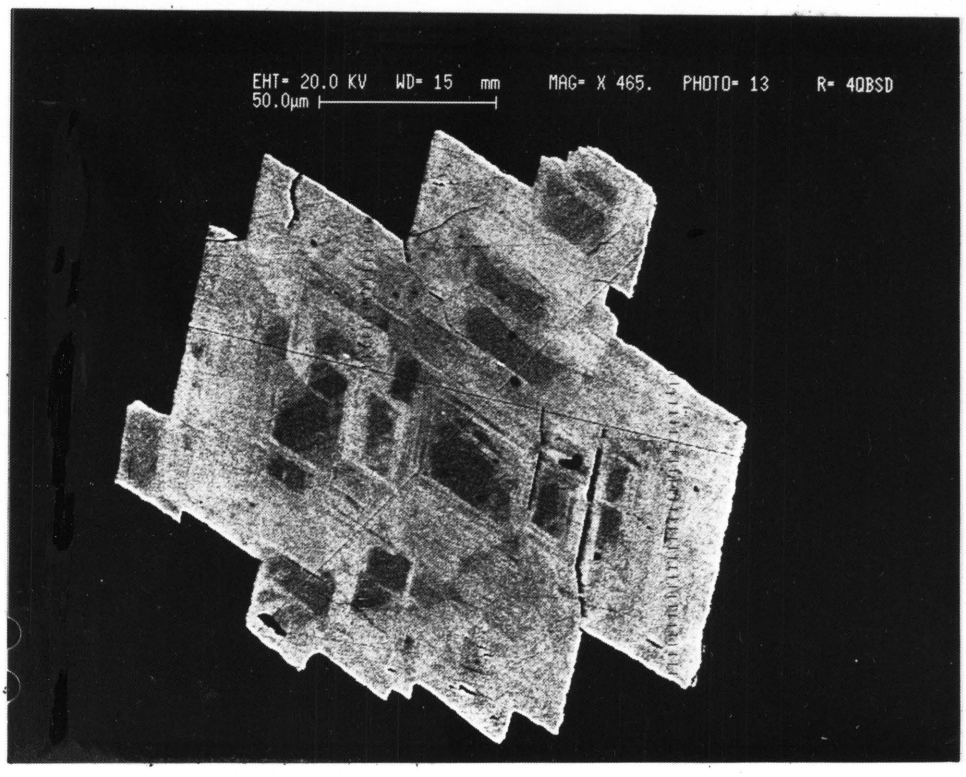

Figure 14: An arsenopyrite crystal formed by parallel crystal growth. The darker areas are S-rich, while the lighter regions contain more arsenic - RC 1009 (electron backscatter image)

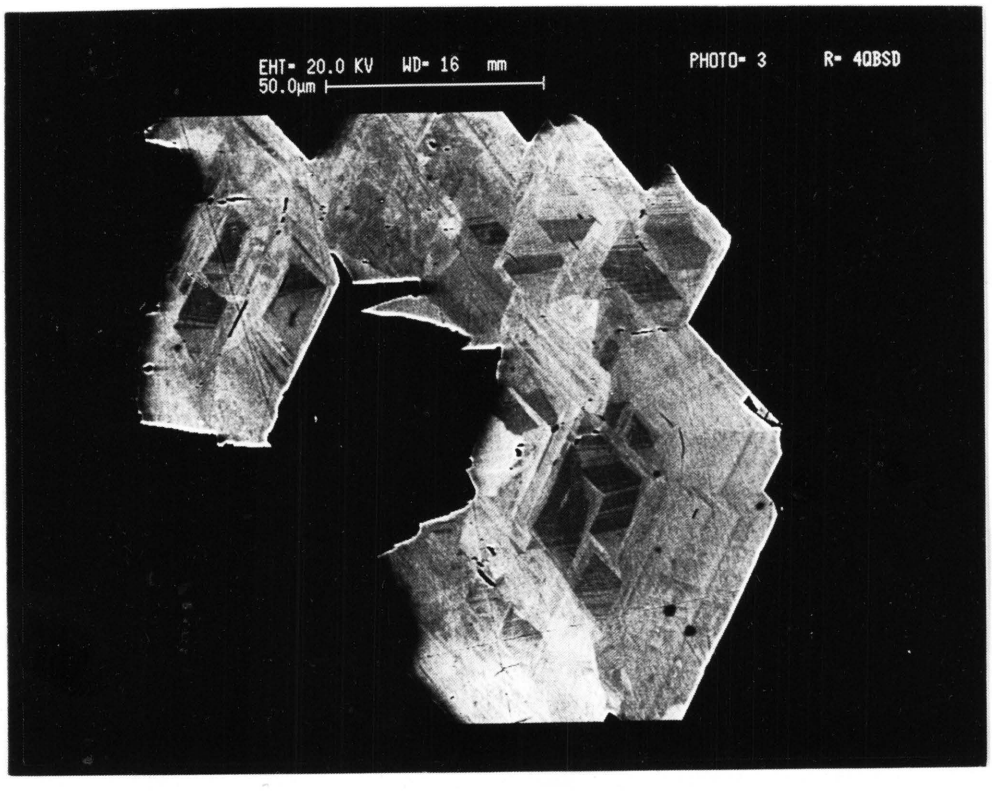

Figure 15: An arsenopyrite crystal showing complex compositional zoning - RC 1008 (electron backscatter image)

Figure 16: Zoned arsenopyrite crystal, orientated approximately parallel to the c-axis - RC 1026 (electron backscatter image)

Table VI: Summary of the microprobe analyses of zoned Sheba arsenopyrite. (Analyses of 55 As-rich and 40 As-poor zones)

	As-rich Zones						As-poor Zones					
	Atomic %				ppm		Atomic %				ppm	
	Fe	As	S	As/S	Sb	Au	Fe	As	S	As/S	Sb	Au
min	31.98	30.24	33.63	0.84	n.d.	574	31.90	27.72	35.77	0.71	336	< mdl
max	34.60	33.73	36.49	0.96	2014	6876	34.56	30.29	39.50	0.84	4351	1233
avg	32.94	31.43	35.37	0.89	413	1741	33.09	29.11	37.51	0.78	2457	416
std	0.64	0.53	0.73	0.03	427	977	0.63	0.81	0.90	0.04	1005	559

min - minimum value
max - maximum value
avg - average value
std - standard deviation
mdl - minimum detection limit, 450 ppm
n.d. - not detected

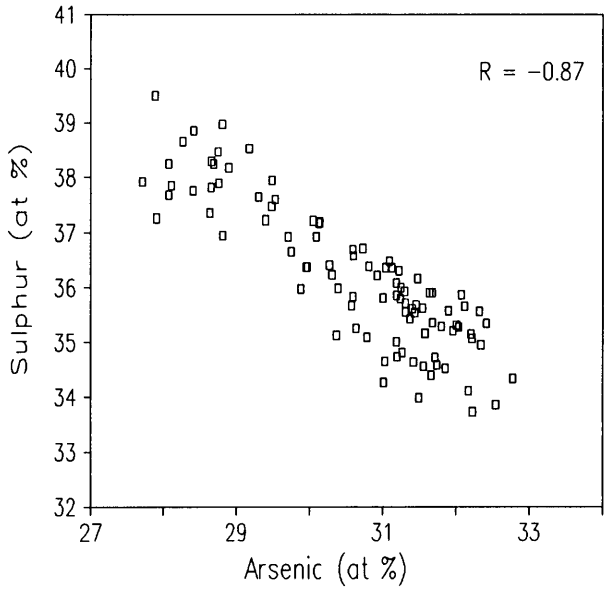

Figure 17: As- against S-content in the Sheba arsenopyrite, indicating a negative relationship, and a variation of up to 6 % in both As and S.

From the electron microprobe data, relationships between the different chemical constituents in the arsenopyrites were determined. A linear negative relationship exists between As- and S-content with a correlation coefficient of -0.87 (Figure 17).

The Sheba arsenopyrite contains on average 1 700 ppm submicroscopic gold in the As-rich zones (Table VI). The gold-content not only varies from one zone to another, but fluctuations also occur within the zones themselves. The highest gold concentration of 6 876 ppm, occurred within an As-rich zone in an arsenopyrite inclusion in pyrite. The Sheba arsenopyrite also contains antimony in relatively high amounts, concentrated primarily in the As-poor zones (Table VI). Thus, the As-Au-rich zones are depleted in Sb, while the opposite is true for the Au-As-poor zones. A plot of the Au- against the Sb-concentration reflects this antipathetic relationship (Figure 18).

The As-, S- and Fe-contents are plotted against the Au- and Sb-concentrations, respectively, in Figures 19 to 23. From these graphs the following is evident:

Au-content is positively, but non-linearly, related to As-content (Figure 19). It seems that a threshold As-content exists at approximately 30 atomic per cent: above it gold occurs in high concentrations, but below it gold concentrations are low, and on average less than

the mdl. A similar, but inverse trend exists in Figure 20, where gold is negatively related to the S-content. Here, high gold values occur below a S-content of approximately 37 atomic per cent. The data partly suggests that gold occurs in solid solution in the arsenopyrite, but the apparent exponential relationship may be due to the fact that at high gold concentrations gold may be present as discrete grains.

Near-linear relationships exist between the Sb-content and both As- and S-content. In the case of As the correlation is negative, and in the case of S it is positive (Figures 21 and 22).

No distinct correlations were found between the atomic Fe-content and Au- or Sb-contents (Figure 23).

In Figure 24 the As/S atomic ratios are plotted against the percentage gold in the arsenopyrite. From this graph it is evident that the As-rich S-poor zones (As/S ratio > 0.84) usually contain high amounts of submicroscopic gold.

The above results therefore illustrate that the gold is heterogeneously distributed in the Sheba arsenopyrite and is specifically enriched in zones having a relatively moderate Fe-content, a high As content (> 30 at.%) and a low S- (<37 at. %) and Sb-content. The distribution of gold is therefore a function of the distribution of the As-rich zones within the crystals.

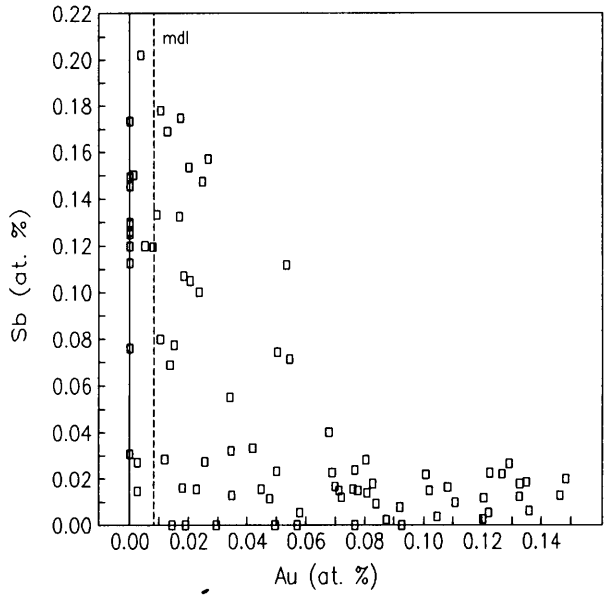

Figure 18: Concentrations of Sb against gold, showing an inverse relationship.

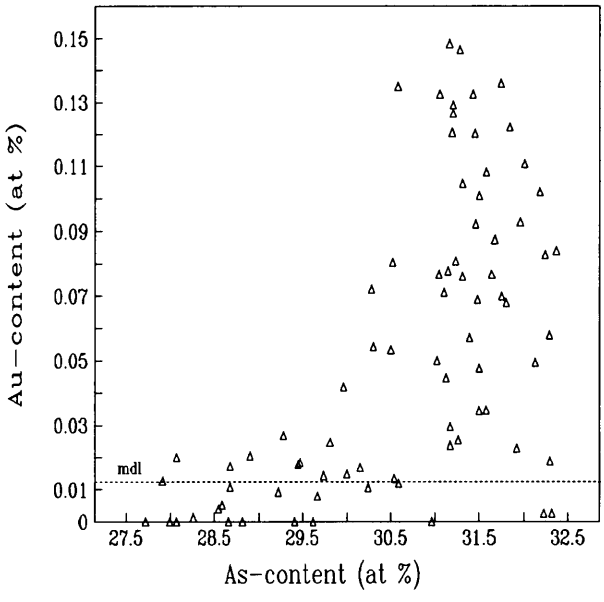

Figure 19: Gold concentration against atomic As-content

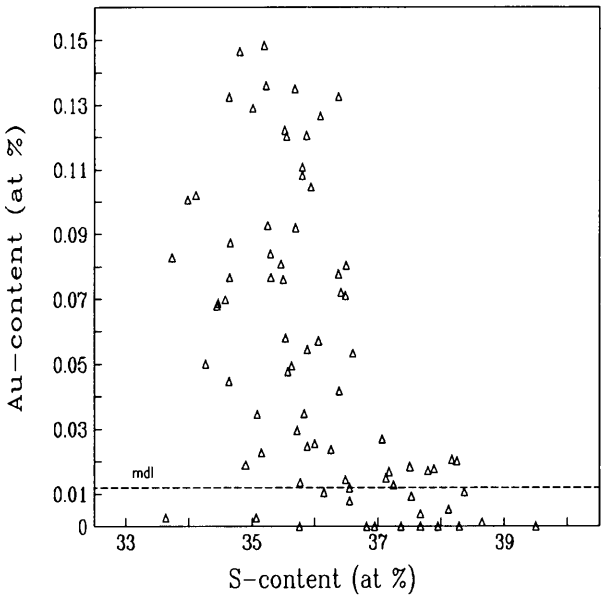

Figure 20: Gold concentration against atomic S-content

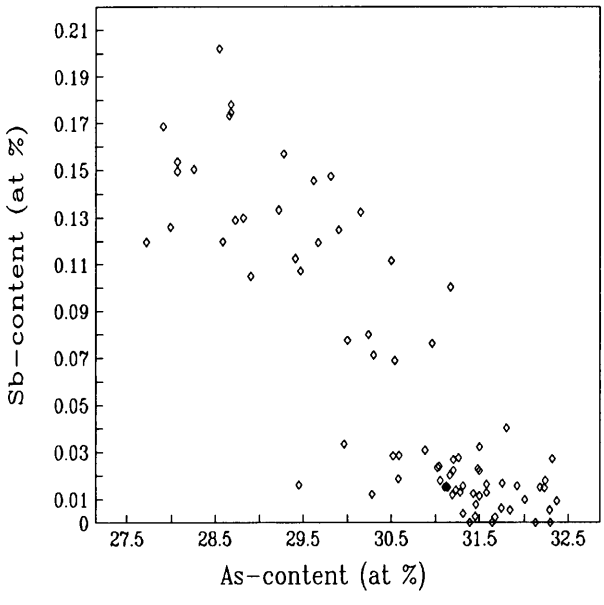

Figure 21: Antimony concentration against atomic As-content

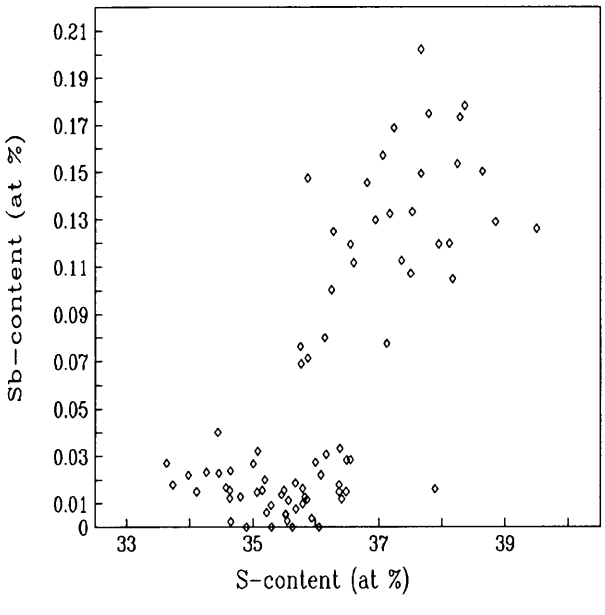

Figure 22: Antimony concentration against atomic S-content

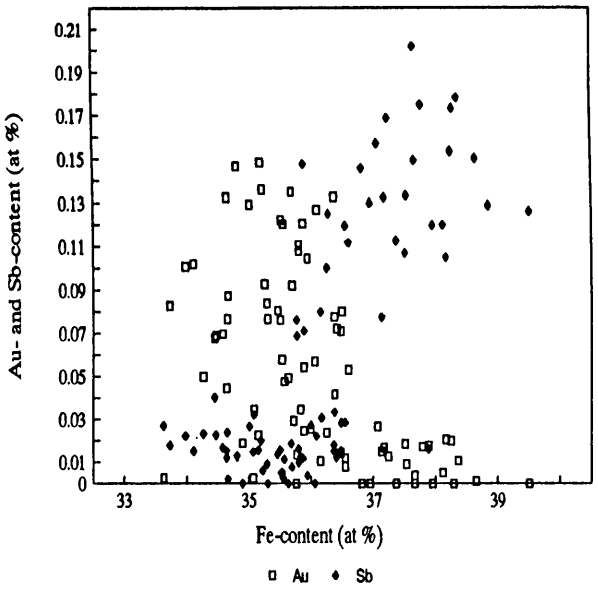

Figure 23: Gold and antimony concentration against atomic Fe-content.

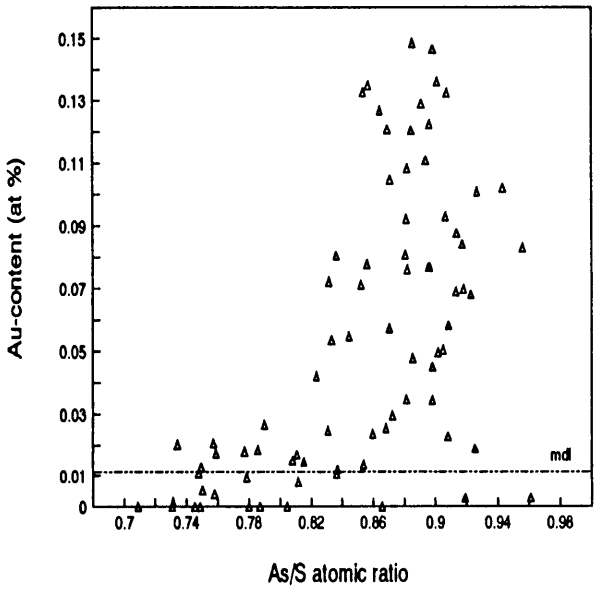

Figure 24: As/S atomic ratios against the concentration of gold

From the microprobe analyses, the crystal-chemical formulae of the Sheba arsenopyrite were calculated on the basis of 3 atoms per formula unit (as suggested by Johan, *et al.,* 1989, who studied the mechanism of Au substitution in arsenopyrites). As long ago as 1936 Buerger indicated that mixed As and S populations exist at the As- and S-sites, while the Fe-sites can also be occupied by As. He stated that Fe(III) exists in the non-polar state in the arsenopyrite crystal structure, and can be substituted by As(III). Mössbauer studies by Wagner *et al.* (1986) and Marion *et al.* (1986) indicated that gold is present in arsenopyrite in a combined state, i.e. either as Au(III) or Au (I). This implies that gold and antimony, substituting elements in the arsenopyrite lattice, are in the Au(III) and Sb(III) states (Johan, *et al*. 1989).
The distribution of As among structural sites was thus calculated using the same rules as Johan and his co-workers. The following rule was used in this study:

- *when* $(As/S)_{at} < 1$*, the excess of S is attributed exclusively to As-sites and the excess of As thus formed is transferred to Fe-sites.*

During this recalculation antimony and gold were also attributed to the Fe-sites. The resulting crystal-chemical formulae calculated in this way, are given in Appendix 3.

Various plots of this data were made to determine relationships between the elements present in different sites. Figure 25 displays a plot of atomic percentages of Au and Sb against S[As], i.e. S present in the As-site. It indicates that zones with high gold content have low amounts of S in the As-sites. This is simply a reflection of the high gold content of As-rich zones. In the Au-rich zones most of the As is present in the As-sites, and little As is present in the Fe-sites (Figure 26). The Au content is negatively, non-linearly correlated with the As[Fe], with gold values reaching a maximum if As[Fe] is below 0.04. An increase in As[Fe], thus correlates with a decrease in the gold content.

The behaviour of Sb is the inverse of that of the gold, i.e. antimony shows a nearly direct relationship with S[As] (Figure 25), while a linear positive correlation exists between antimony and As[Fe]. It is evident from Figure 27 that the amount of Fe[Fe] has a negative correlation with the Sb-content.

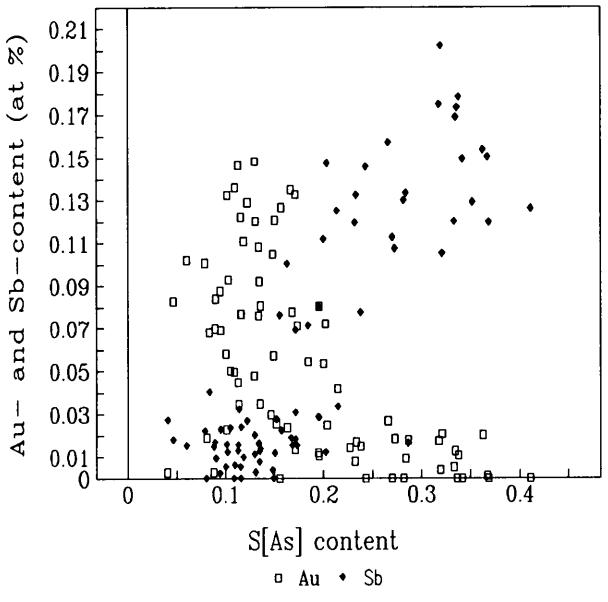

Figure 25: Au- and Sb-concentrations against the amount of S[As]

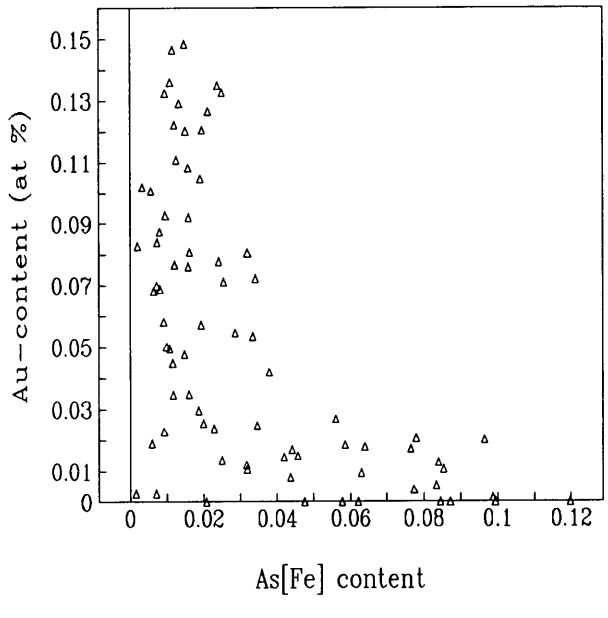

Figure 26: Au-concentrations against the As[Fe] content

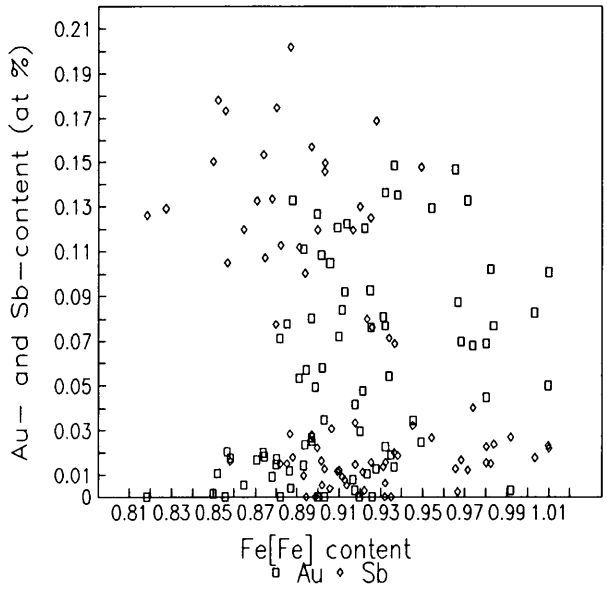

Figure 27: Au- and Sb-concentrations against the amount of Fe[Fe]

From these graphs the mode of substitution of Au and Sb in the arsenopyrite crystals can be determined. The negative relationship between Au-concentration and the amount of As[Fe] (Figure 26) and the negative correlation of Sb-concentration with Fe[Fe] suggest that Au(III) and Sb(III) can substitute for Fe in the Fe-sites, where As and Fe also occur in oxidation states of (III).

In addition to the submicroscopic gold present in the arsenopyrite, visible gold particles also occur as inclusions within the arsenopyrite. The surface area of these inclusions is in general smaller than $10\mu m^2$, with an average of approximately $7\mu m^2$. The mode of occurrence and dimensions of gold particles observed, are listed in Table VII. The majority of gold inclusions occur directly at the contact between two chemically different zones, (Figures 28 and 29). The occurrence of particulate gold along these zone contacts indicates that possible remobilization of the gold has occurred. This would have taken place during a later stage of metamorphism, when some of the gold in a solid solution state, may have exsolved in order

to minimise the free energy of the sulphide lattice. This gold would migrate and coalesce by means of solid state diffusion to low energy sites, such as fractures, grain boundaries and lattice dislocations (Clark, 1960).

From the results cited above it is evident that gold in the Sheba arsenopyrite occurs in two modes: firstly as invisible gold (probably chemically bound in the crystal lattice), within As-rich zones, with low S- and Sb-contents, and secondly as particulate gold inclusions mainly at the zone contacts.

The compositional zoning and mode of occurrence of submicroscopic gold in the Sheba arsenopyrite are similar to those observed in arsenopyrite from hydrothermal deposits in Spain and France by French scientists (Cathelineau, *et al.,* 1989; Johan, *et al.*, 1989; Marcoux, *et al.*, 1989 and Boiron, *et al.,* 1989). They observed that As and Au are linearly, positively related. However, they found that Fe and Au are negatively correlated, suggesting that the Au-rich zones were Fe-deficient. A negative relationship between Au and Fe was also found by Wu and Delbove (1989) who studied the hydrothermal synthesis of gold bearing arsenopyrite. They detected a maximum gold content of 1,7 wt % in the As-rich zones of their synthesized zoned arsenopyrites. However, in both these studies, submicroscopic gold only, and no particulate gold, was present in the arsenopyrite crystals, in contrast to the Sheba arsenopyrite. No such trend was thus observed in the Sheba arsenopyrite, because of the presence of gold particles. This can further be due to the relatively low submicroscopic gold content (max = 7 000 ppm) of the Sheba arsenopyrite, compared to the submicroscopic gold content of 17 000 ppm present in the synthesized arsenopyrite crystals.

An attempt to explain the compositional zoning within arsenopyrite and the incorporation of submicroscopic gold in the arsenopyrite structure follows below:

The mechanism of incorporation of submicroscopic gold in the arsenopyrite has been the subject of much research. In the arsenopyrite crystal structure the iron atoms are octahedrally coordinated, while the dianions (As and S) are also in sixfold coordination. According to Cook and Chryssoulis (1990), arsenopyrite can be expressed as $[Fe]^{3+}$ $[AsS]^{3-}$. In order to retain the trivalent negative charge, the dianions are inversely correlated. This linear substitution relation between arsenic and sulphur is thus also evident from the results obtained during this study. Furthermore, arsenopyrite is a semi-conductor with a low magnetic moment. This implies that adjacent pairs of Fe^{3+} ions are bonded, resulting in alternating long and short Fe-Fe bond distances. Buerger (1936) indicated that mixed As and S populations exist on the As- and S-sites, while the Fe-sites can also be occupied by As. According to him the small radius of Fe in arsenopyrite can be correlated with iron in the ferric state (Fe^{3+} radius 1.12 Å). He proposed that an excess of As is incorporated in the arsenopyrite crystal, with As^{3+} (radius 1.20 Å) substituting for Fe^{3+}.

Table VII: *Dimensions and associations of the gold particles observed in Sheba arsenopyrite*

Dimension (μm)	*Association*
4.2 X 1 *1 X 1.4* *5.3 X 2* *1 X 1.7* *1 X 0.5* *2.4 X 2* *1.2 X 1* *0.8 X 0.3* *1.2 X 0.5* *1 X 0.3* *6.4 X 0.5* *0.7 X 0.7* *0.3 X 0.2* *1.2 X 1* *0.7 X 0.2* *0.4 X 0.4* *0.4 X 0.3* *2.5 X 0.5* *2.4 X 1.5* *1.4 X 1* *2 X 0.6*	*as inclusions at the contact between As-rich and S-rich zones*
1.5 X 1 *2.2 X 0.7* *1 X 0.5* *1 X 1* *2.3 X 0.5* *7.4 X 4* *2 X 1*	*along cracks in arsenopyrite*
2.7 X 1 *1 X 0.5*	*within tetrahedrite*
0.8 X 0.8	*chalcopyrite*

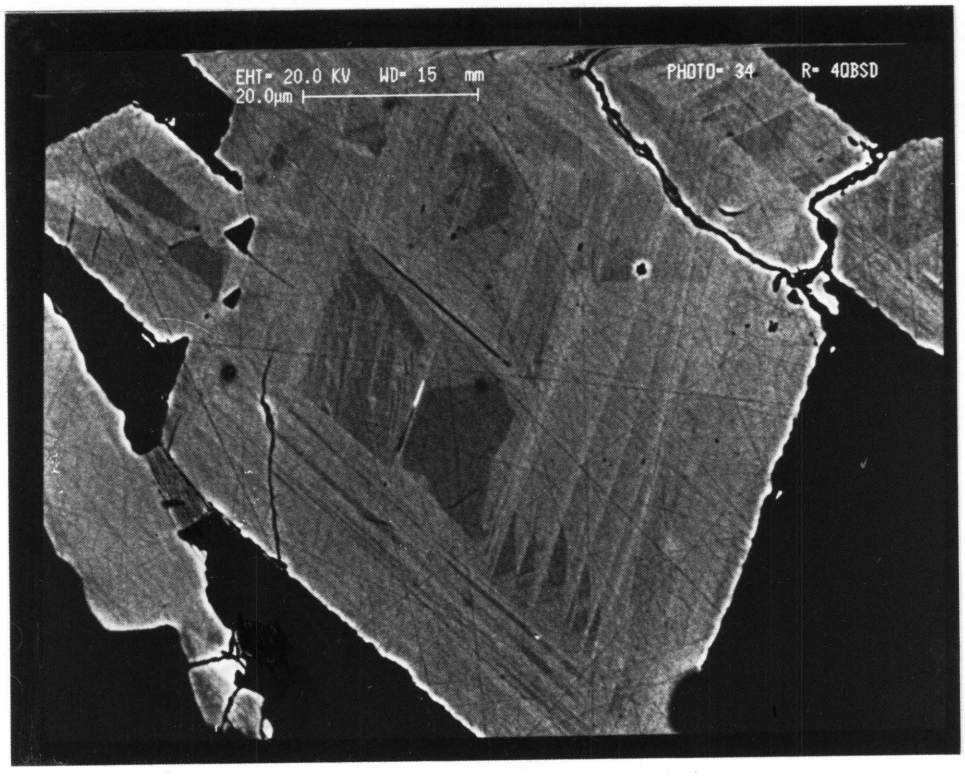

Figure 28: Gold particles (white) at the contact between S-rich and As-rich zones - RC 1019 (electron backscatter image)

Figure 29: Numerous small gold particles at the contact between S-rich and As-rich zones - RC 1033 (electron backscatter image)

Arsenopyrite can thus rather be expressed as $[FeAs]^{3+}$ $[AsS]^{3-}$. Thus, it is easy for other trivalent metal cations (such as Sb^{3+}, Au^{3+}, etc) to substitute for Fe^{3+} or As^{3+}. In fact Mössbauer studies by Wagner *et al.* (1986) and Marion *et al.* (1986) have indicated that gold is present in arsenopyrite in a combined state, i.e. either as Au^{3+} or Au^{1+}. The similar sizes of the As and Au atoms explain the relative ease of substitution of gold for arsenic in arsenopyrite.

An attempt was made to apply this mechanism (of incorporation of gold by substitution for Fe^{3+} or As^{3+}) to the Sheba arsenopyrite. The calculated crystallochemical formulae of different zones in the S-rich arsenopyrites, outlined previously, indicate that an excess of S is present in the Sheba arsenopyrite. Therefore, the S-sites are totally filled, and the excess of S is present in the As-sites.

In the recalculated formulae for the different zones, it is evident that at high S-content (which correlates with a high Sb-content), the total S[As] (i.e. S in the As-site) is high, and thus As tends to occupy Fe-sites. The amount of As[Fe] is therefore high, and this reduces the amount of Fe[Fe]. High amounts of Sb is also incorporated in the Fe-sites when Fe[Fe] is low. This is evident from the negative near-linear relationship that exists between Fe[Fe] and the Sb-content. The overall effect is that high Sb-values are associated with zones in the arsenopyrite which contain a high amount of S-atoms in the As-sites, i.e. S-rich zones.

However, in relatively As-rich zones, the amount of S present in the As-sites is low, and most of the As occurs in the As-sites. The amount of As in the Fe-sites is therefore also low, which correlates with high amounts of Au[Fe]. The overall effect is that high Au-values are correlated with zones in the arsenopyrite which contain low amounts of As-atoms in the Fe-sites. This mechanism of gold incorporation within the arsenopyrite structure, explains the presence of the submicroscopic gold in the Sheba arsenopyrite.

However, to explain the variation in the zonal composition within the Sheba arsenopyrite, the work of Kretschmar and Scott (1976) has direct relevance. They have studied the phase relations for the Fe-As-S system and determined that arsenopyrites from a S-rich environment have a temperature of formation below 491 °C. This geothermometer gives temperatures ranging from less than 300 ° to 500 °C when applied to the compositional range of Sheba arsenopyrite crystals, from 27.7 at % As (As-poor zones) to 33.7 at% As (As-rich zones). Such large temperature fluctuations are unlikely and the temperatures obtained are probably unrealistic. These incorrect results may be due to the presence of Au or Sb in the arsenopyrite crystal, or a lack of chemical equilibrium between arsenopyrite and other minerals. However,

the results of Kretschmar and Scott show that an increase in aS_2 will lead to a decrease in at % As-content. Compositional zoning can therefore be considered as a non-equilibrium feature, reflecting the kinetics of the arsenopyrite growth and local fluctuations in the $a(S_2)/a(As_2)$ ratio.

It was also postulated by Cathelineau, *et al.* (1989) that gold is transported in a hydrothermal solution as a gold thioarsenide complex, $AuAsS_2$. In order to form S-rich As-poor zones the activity of S in the hydrothermal solution will necessarily be high relative to the low activity of As . The zones thus formed, will contain high amounts of S in the As-sites, resulting in high As[Fe]. Under these circumstances the Au-As complex will be stable in the solution and the Au-content of these zones will be low, while the Sb-content will be high.

However, the formation of the relatively As-rich zones reflects a decrease in S-fugacity of the solution, and a corresponding decrease of the S[As]. The amount of As[As] sites will therefore be high, resulting in a decrease of As[Fe]. Under these circumstances the As-Au complex can be incorporated in the arsenopyrite crystal structure with Au^{3+} occupying the Fe-sites and the As occupying the As-sites. Therefore, zones that formed while the S activity of the solution was low, will contain high amounts of submicroscopic gold.

Periodic fluctuations between the activity of the As-Au complexes and S-Sb complexes would therefore result in the rhythmic compositional zoning of the arsenopyrite, the heterogeneous distribution of Au in arsenopyrite crystals and the sympathetic correlation of Au with As-rich zones. Ultimately, it would appear that the Au-content of the various zones of the Sheba arsenopyrite was controlled by fluctuations in the S-fugacity of the hydrothermal solution.

The above interpretations closely correspond to the experimental results obtained by the French scientists, i.e. Cathelineau *et al.* (1989); Johan *et al.* (1989); Marcoux *et al.* (1989) and Boiron *et al.* (1989) who studied zoned S-rich arsenopyrites from hydrothermal deposits in Spain and France.

6.1.2.2 *Sheba pyrite crystals*

Pyrite from Sheba goldmine occurs as euhedral cubic or pyritohedral crystals and as anhedral grains. Euheral crystals only occur in the samples where pyrite is the most abundant sulphide mineral. More than one generation of pyrite formation is generally observed in the case of the euhedral crystals.

The first generation usually comprises a core, with numerous inclusions of gold, galena, arsenopyrite, tetrahedrite and a Fe-Pb-Sb-sulphide (Figure 30). In the absence of arsenopyrite inclusions, the core is generally compositionally zoned. Alternating enrichments and depletions in arsenic resulted in the formation of fine oscillatory zones, as narrow as 1 μm. Figures 31 and 32 display such compositional zoning in the first generation core. A variation in the As-content from one zone to another can be as high as 2 atomic per cent. Clark (1960) stated that the maximum As that can be incorporated in the pyrite structure under equilibrium conditions is about 0.1 wt %. Fleet *et al.* (1989) however, studied natural pyrite with up to 8 wt % arsenic. It is not clear however, whether all this As was in the pyrite structure. The compositional zoning can be explained by periodic fluctuations in the activity of As (or a_S/a_{As}) in the hydrothermal solution during pyrite crystallization.

The second generation exhibits crystal growth around the first generation core. Silicates and arsenopyrite occur as inclusions within this pyrite generation (Figures 30 to 32). The third generation is separated from the second by a thin zone containing numerous quartz and sometimes sulphide inclusions (Figures 30 and 31).

More than one generation of pyrite is present, suggesting a multiphase ore genesis. The chemistry of the ore fluids probably had a complex evolution during the crystallization of pyrite. Such an evolution is recorded by the changes in the trace and major element content of the different generations.

Anhedral zoned pyrite was only observed in samples where arsenopyrite is the most abundant sulphide. These pyrite particles exhibit crude compositional zoning from As-depleted cores to As-enriched edges. Frequently, quartz, rutile and ilmenite inclusions occur within the As-poor core (Figure 33). The chemical zonation is usually not concentric, since the As-rich regions are mostly irregularly distributed (Figure 34).

A)

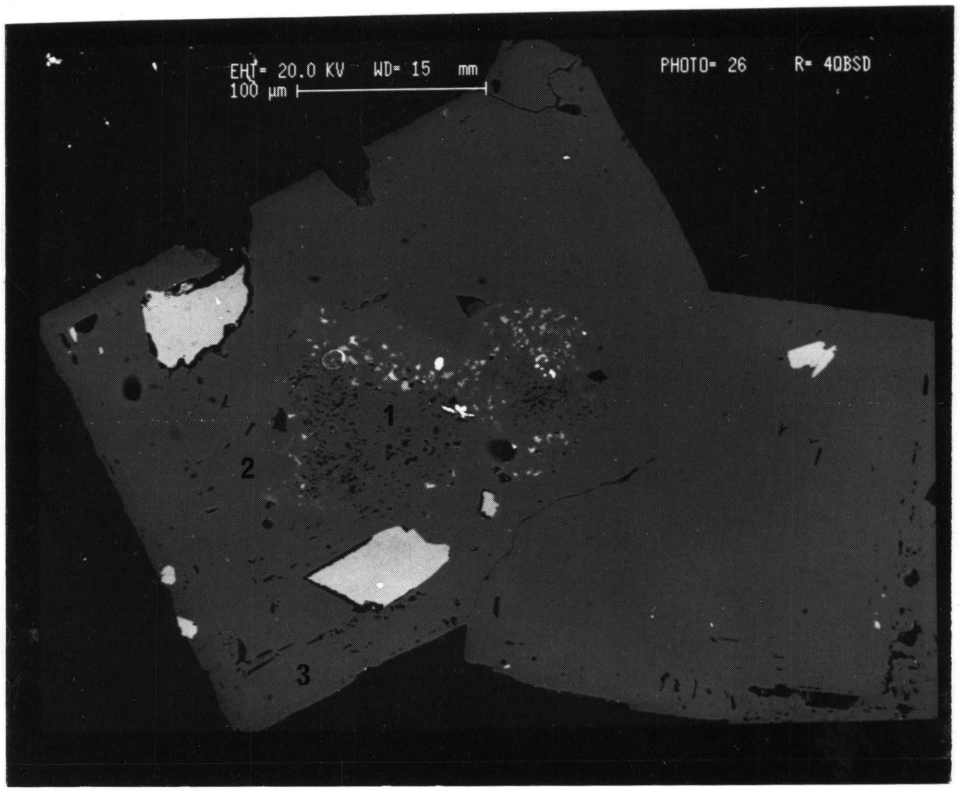

B)

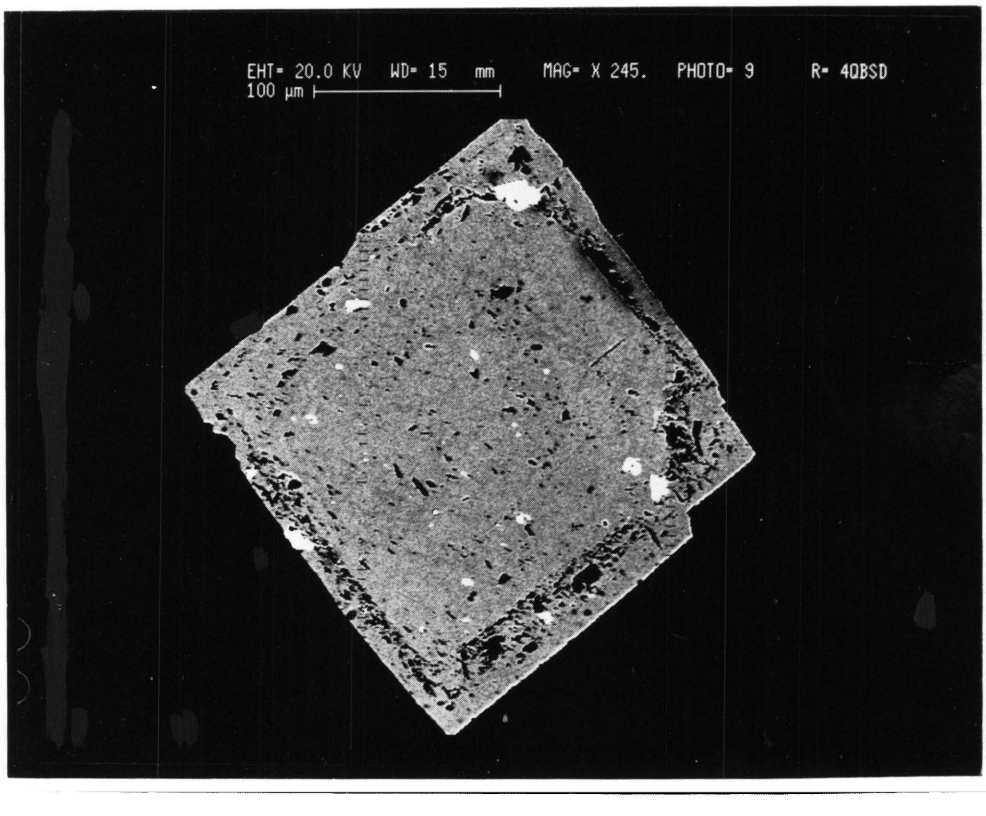

Figure 30: Unzoned Sheba pyrite crystals, exhibiting more than one generation of crystal growth: A) three different generations (1-3) of pyrite formation are present B) two generations are present - the final generation is separated from the earlier generation by a zone of silicate and sulphide inclusions - RC 1016 (electron backscatter image)

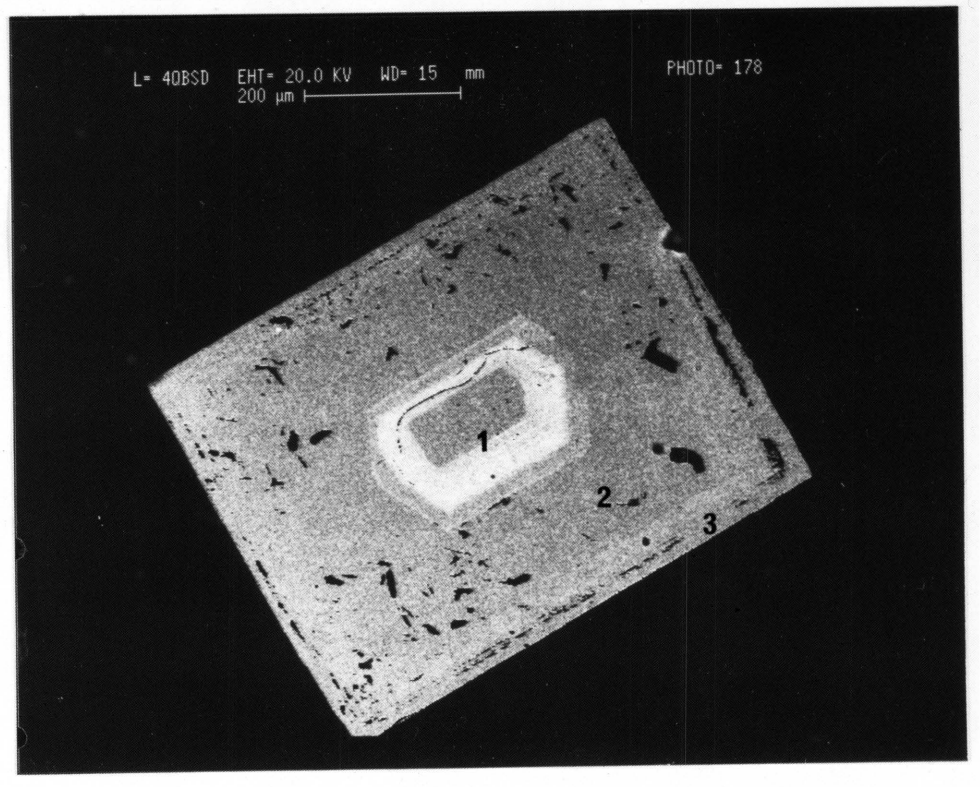

Figure 31: A crystal showing three generations of pyrite: 1) zoned As-rich core, (2) an As-poor intermediate generation, separated from the outer generation (3) by a zone of quartz inclusions - RC 1038 (electron backscatter image)

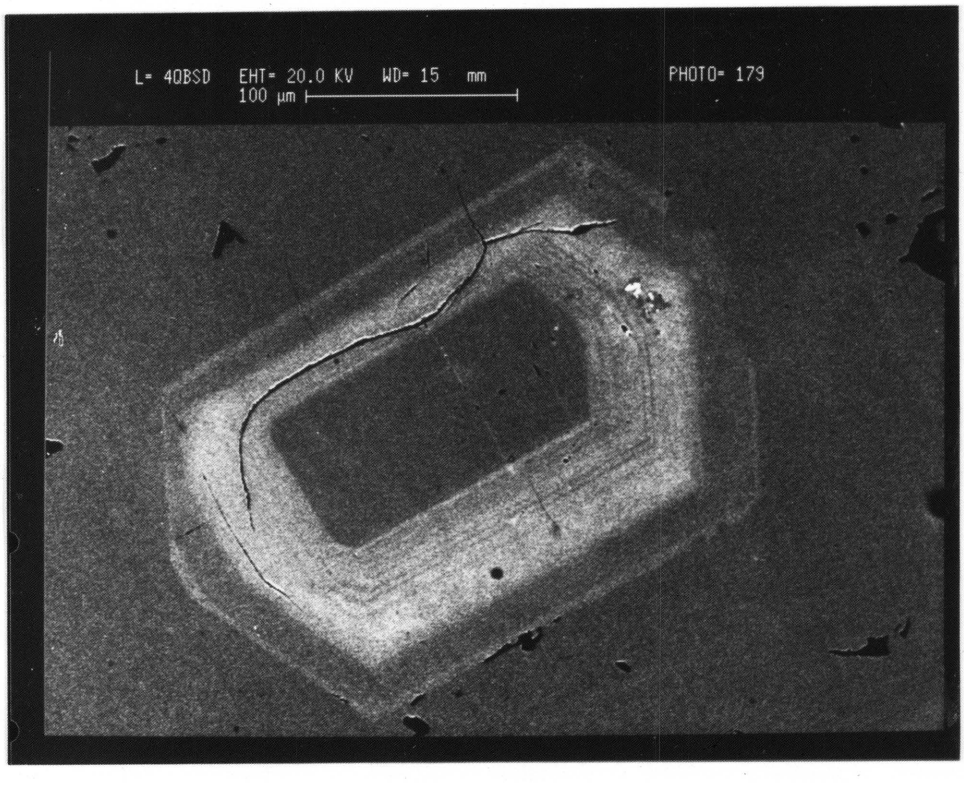

Figure 32: Euhedral core of a pyrite grain, exhibiting fine compositional zoning, due to alternate enrichment and depletion in As-content - RC 1038 (electron backscatter image)

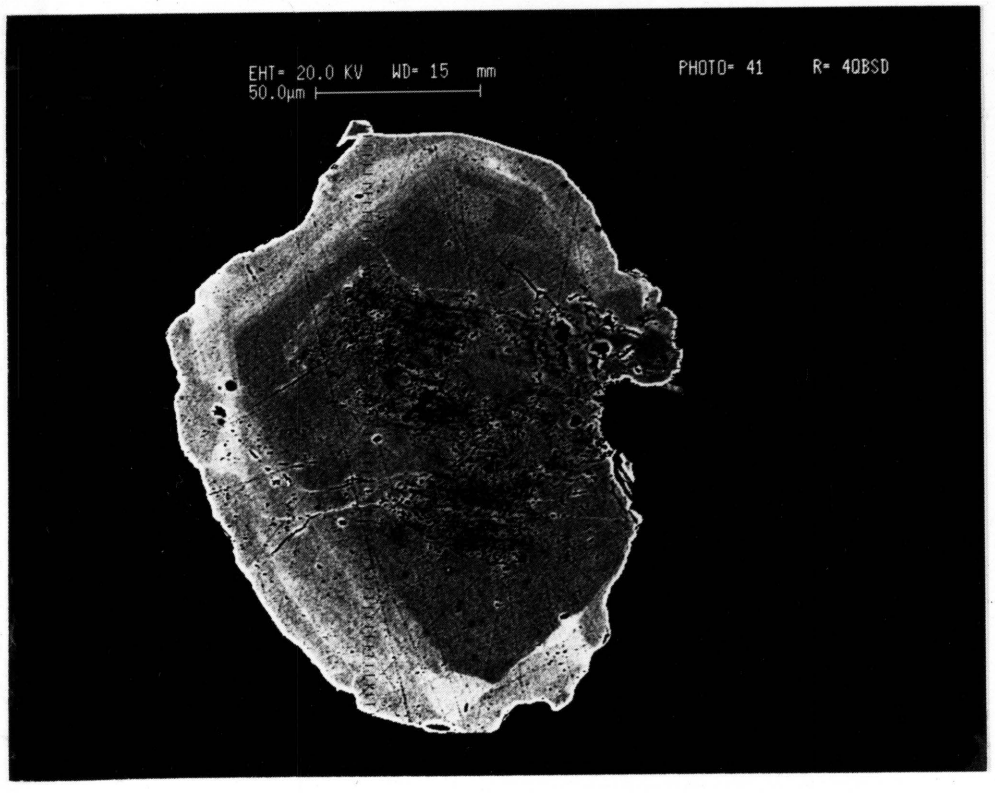

Figure 33: Pyrite showing As-rich areas along the outer edges, with an As-poor centre - RC 1024 (electron backscatter image)

Figure 34: Pyrite with unevenly distributed As-poor areas (dark grey), and As-rich regions along the outer edges - RC 1016 (electron backscatter image)

Microprobe analyses of the different types of pyrite crystals are listed in Appendices 4 and 5. A summary of the results appears in Table VIII. These analyses were used to determine relationships between the different constituents in pyrite.

A plot of Fe- against S-content present in the pyrite crystals (Figure 35) exhibits a weak negative trend. In the lower regions of S-content a broad spread in Fe-content occurs. Due to the stoichiometrical relation between Fe and S within pyrite, this scatter in data points is unexpected.

A significant linear trend exists between the sulphur and arsenic concentrations (Figure 36). This inverse relationship between As- and S-content explains the low correlation coefficient obtained between Fe- and S-content (Figure 35). If Fe is plotted against S plus As, a linear inverse relationship is obtained, with a very high correlation (Figure 37). This clearly indicates that As substitutes for S in the Sheba pyrite. The chemical formulae of Sheba pyrite can thus be modified to $Fe(S+As)_2$, where As is less than 2 atomic per cent.

The relationship between the Fe- and As-content is however not well-defined. A plot of the atomic percentage of iron against that of arsenic, illustrates high arsenic concentrations at moderate iron-contents (Figure 38).

Table VIII: Summary of the composition of Sheba pyrite crystals (at%)

	As	*Ag*	*S*	*Au*	*Ni*	*Fe*
min	*n.d.*	*n.d.*	*64.09*	*< mdl*	*n.d.*	*32.43*
max	*2.23*	*0.038*	*67.16*	*0.021*	*0.690*	*34.15*
avg	*0.58*	*0.007*	*65.94*	*0.007*	*0.093*	*33.22*
std	*0.61*	*0.009*	*0.72*	*0.006*	*0.167*	*0.32*

min - minimum value
max - maximum value
avg - average value
std - standard deviation
n.d. - not detected
mdl - minimum detection limit

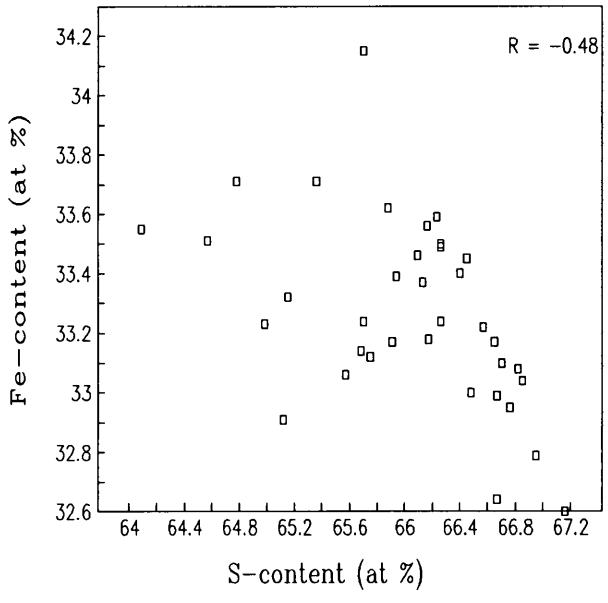

Figure 35: The correlation between the Fe- and S-content in Sheba pyrite crystals

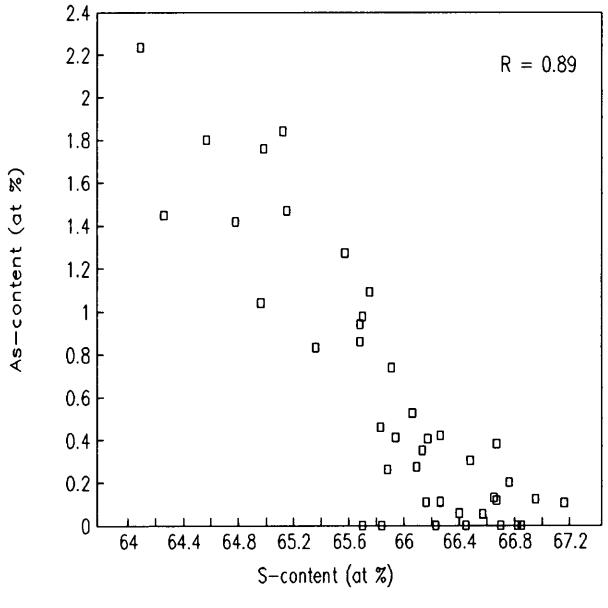

Figure 36: Arsenic versus sulphur in the Sheba pyrite crystals

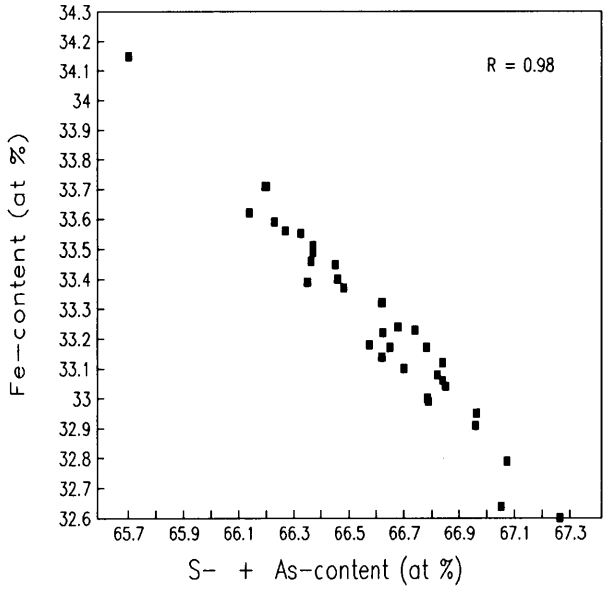

Figure 37: Fe-content versus S- plus As-content, displaying an inversely linear correlation

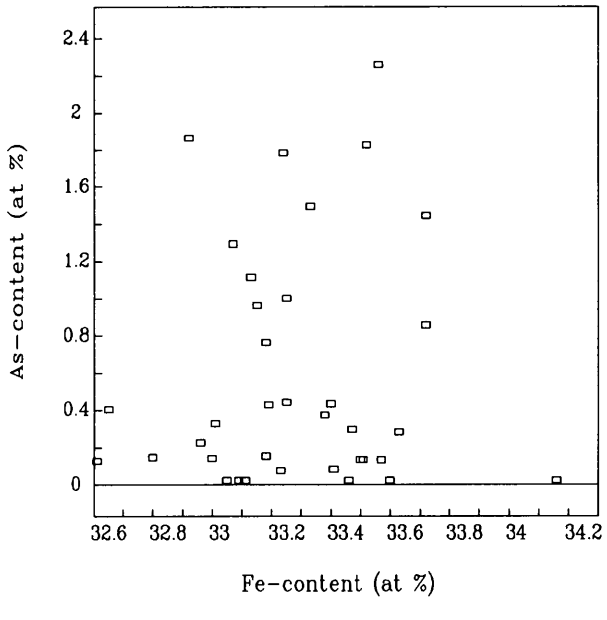

Figure 38: Fe- versus As-content in Sheba pyrite crystals

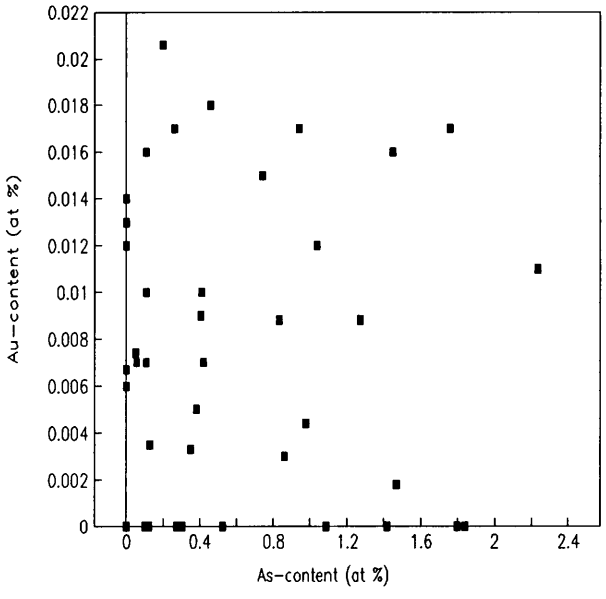

Figure 39: As-content versus concentrations of submicroscopic gold in the pyrite.

The submicroscopic gold content reaches a maximum of 1 500 ppm in the Sheba pyrite crystals. However, no clear relationship exists between the amount of submicroscopic gold and As-content (Figure 39).

In addition to the submicroscopic gold, the Sheba pyrite crystals also contain particulate gold; either as irregular inclusions in pyrite, or at the contact between different pyrite generations, or where a later generation cuts across zoned pyrite. The dimensions of several of the observed gold particles are listed in Table IX.

Table IX. Dimensions of some gold inclusions observed in the Sheba pyrite crystals

Dimension (μm)
1.4 X 0.7
2 X 1.2
2 X 0.5
1.3 X 1
0.5 X 0.6
2.4 X 1
1.4 X 0.5
0.8 X 0.4

An attempt to explain the incorporation of arsenic and gold in pyrite crystals follows:

In the pyrite structure each iron atom is octahedrally coordinated by six sulphur atoms and each sulphur atom has a pyramidal coordination with three iron ions and one sulphur atom to which it is bonded covalently (Wuensch, 1974). The centre of the dumb-bell shaped disulphide ions (S_2^{2-}) pairs is analogous to the Cl in the NaCl-type crystal structure. As discussed by Cook and Chryssoulis (1990) a simple pyrite structure can be written as $[Fe]^{2+}$ $[S_2]^{2-}$. They further postulated that As is introduced into the structure as anion pairs of $[AsS]^{3-}$. Thus As^{2-}--S^{1-} replaces the normal S^{1-}--S^{1-} anionic dumb-bell shaped pairs in the pyrite structure. It is envisaged that a substitution occurred whereby anionic As^{3-} substitutes for S^{2-} in the anion pairs, and can be expressed as $[Fe]^{2+}[(S,As)_2]^{3-}$. This explains the linear inverse correlation that exists between the As and S atomic concentrations within these pyrite crystals.

However, there will be a charge imbalance in the pyrite crystals, due to a trivalent anion As^{3-} substituting for a divalent anion S^{2-}. This can be satisfied by replacing the divalent iron with trivalent cations, such as As^{3+}, Fe^{3+}, Sb^{3+}, etc. The pyrite formula can thus be written as $(Fe^{2+},Fe^{3+})(S,As)_2$. Au^{3+} can therefore enter the pyrite crystal by substituting for Fe^{3+} or As^{3+}. This should result in a direct correlation between arsenic and gold in these pyrite crystals. However, this correlation was not observed during the present study, possibly as a result of the occurrence of particulate gold in the pyrite crystals. Furthermore, due to the very high detection limit and the very low gold concentration in pyrite, any relationship between gold concentration and that of other elements is not apparent.

6.1.3 Agnes Pyrite

Pyrite crystals from the Agnes gold mine constitute a complex assemblage with variations in chemical composition and textures.

Two main textural types exist:
a) Irregular intergrown masses of small euhedral crystals, with numerous inclusions of quartz, ilmenite, chalcopyrite, monazite, pyrrhotite, arsenopyrite or calcite (Figure 40), and
b) Large zoned pyrite crystals with few inclusions (Figure 41).

Within these types of pyrite, various regions are distinguished by differences in texture and chemical composition. This indicates multiphase ore genesis, so that more than one generation of pyrite can be distinguished. The first pyrite generation typically exhibits compositional zoning (Figure 42 and 43). The zoning is due to rhythmic enrichment and impoverishment in arsenic. After the first crystallization period, a resorption period followed during which part of the zoned generation was destroyed. The later second generation, with a homogeneous As-poor composition, crystallized after this resorption period. In Figures 43, 44 and 45 the corroded remnants of the first generation pyrite can be seen overgrown and cut by the second generation pyrite.

Microprobe analyses of the pyrite crystals are listed in Appendices 6 and 7. The compositional difference between the two generations, and between the As-poor and As-rich zones within the first generation, is given in Table X. A significant difference exists in the As-content of the two generations. Both the As-rich and As-poor zones of the first generation pyrite contain high amounts of As, while an insignificant amount of As is present in the second generation. The first generation of pyrite is characterized by zones low in As-content (average 0.19 at %), alternating with As-rich zone (average 1.1 at %). The highest amounts of trace elements are also present within these As-rich zones; the most important being gold (as high as 1 500 ppm), silver (2 200 ppm) nickel (8 200 ppm) and cobalt (4 000 ppm). The second pyrite generation contains low amounts of arsenic (average 0.02 at % As), and the highest Fe -and S-contents (Table X).

The relation between sulphur and iron within *both pyrite generations*, is shown in Figure 46. A negative linear correlation exists, with a certain amount of scattering (correlation coefficient = -0.82). An upper limit is defined by non-stoichiometrical pyrite from the As-poor first generation and the second generation.

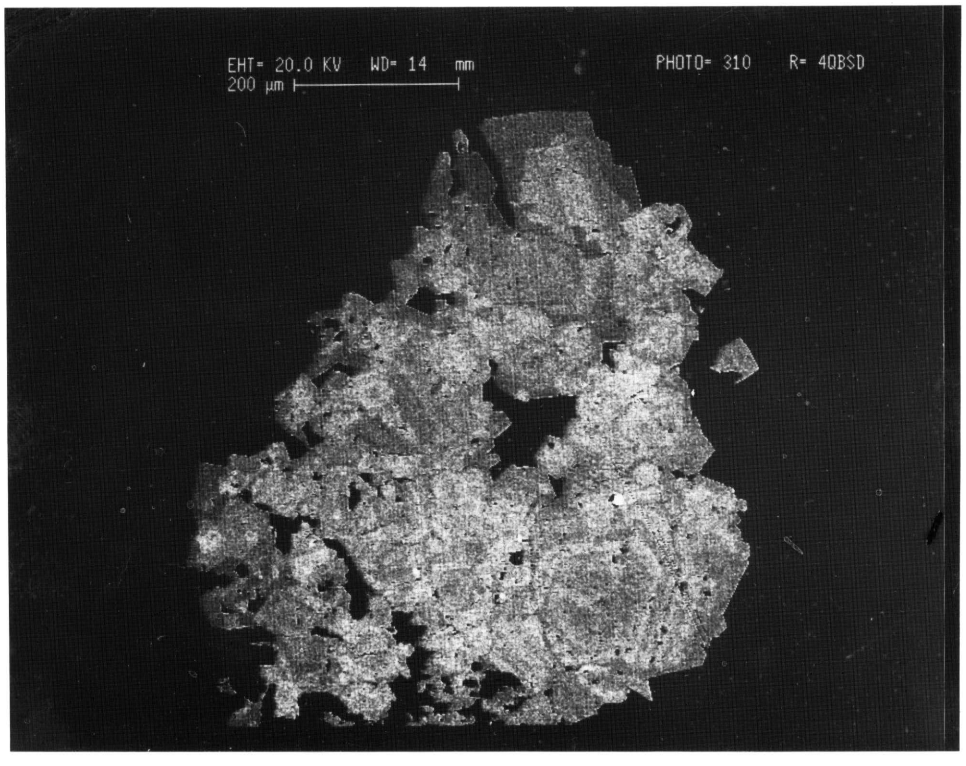

Figure 40: Intergrown mass of small pyrite crystal - RC 1056 (electron backscatter image)

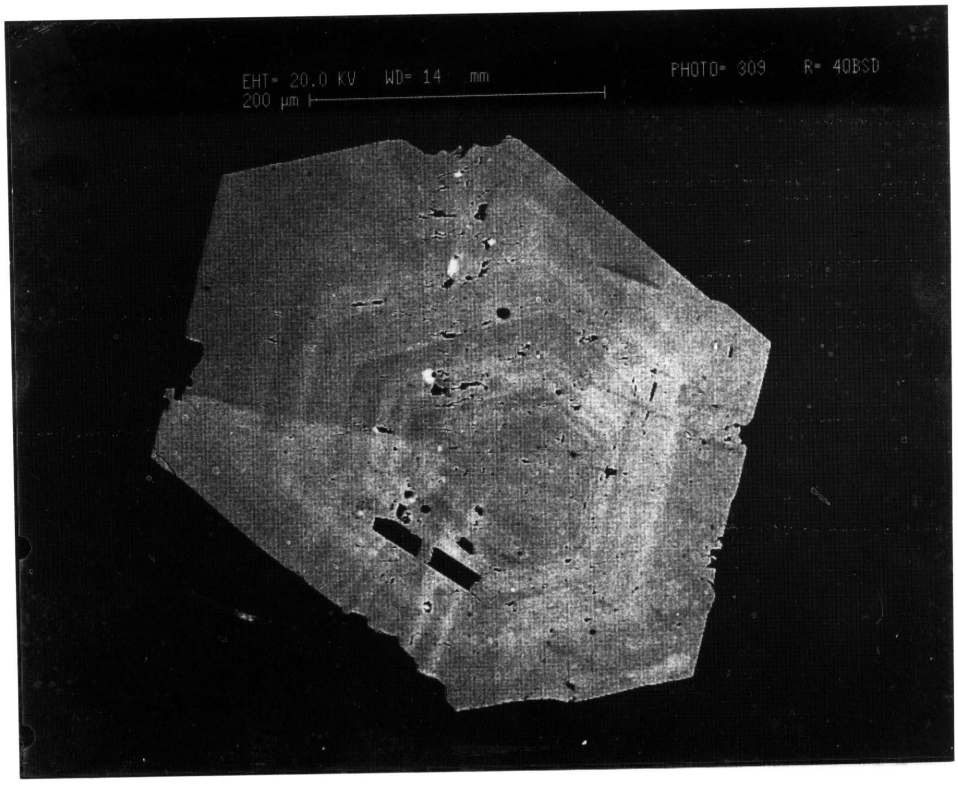

Figure 41: A pyrite crystal, exhibiting concentric compositional zoning due to fluctuations in the As-content - RC 1056 (electron backscatter image)

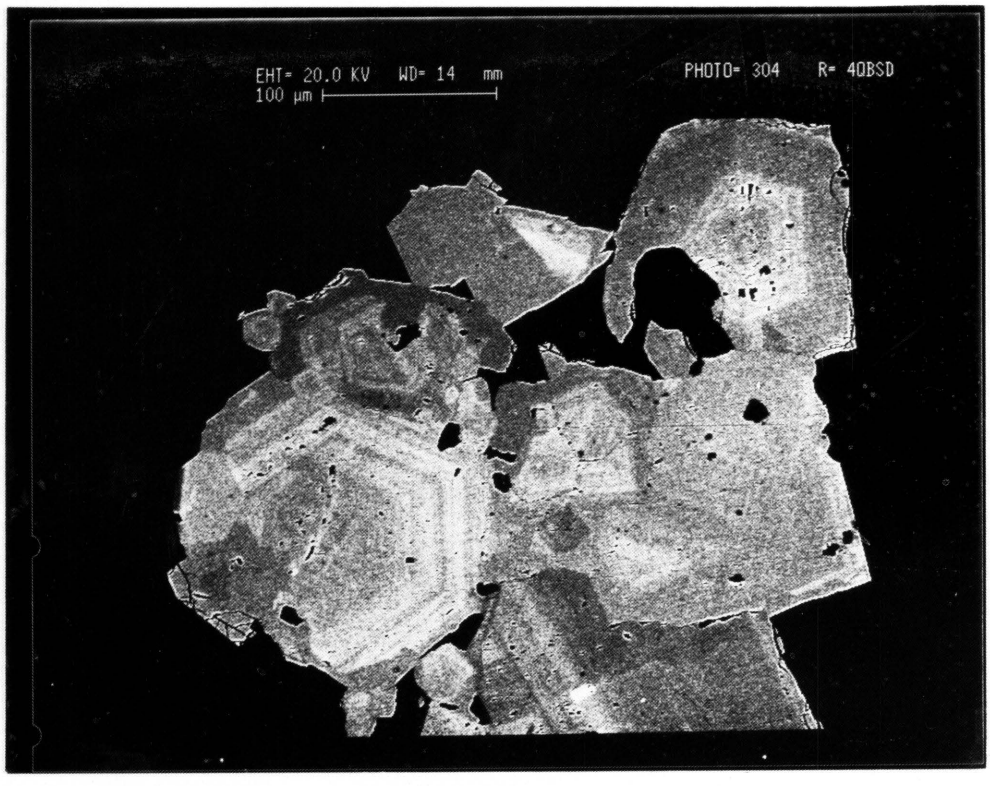

Figure 42: An intergrowth of pyrite crystals, exhibiting zoning due to fluctuations in As-content. The dark grey regions constitute a second generation (As-poor) partially surrounding the earlier generation - RC 1055 (electron backscatter image)

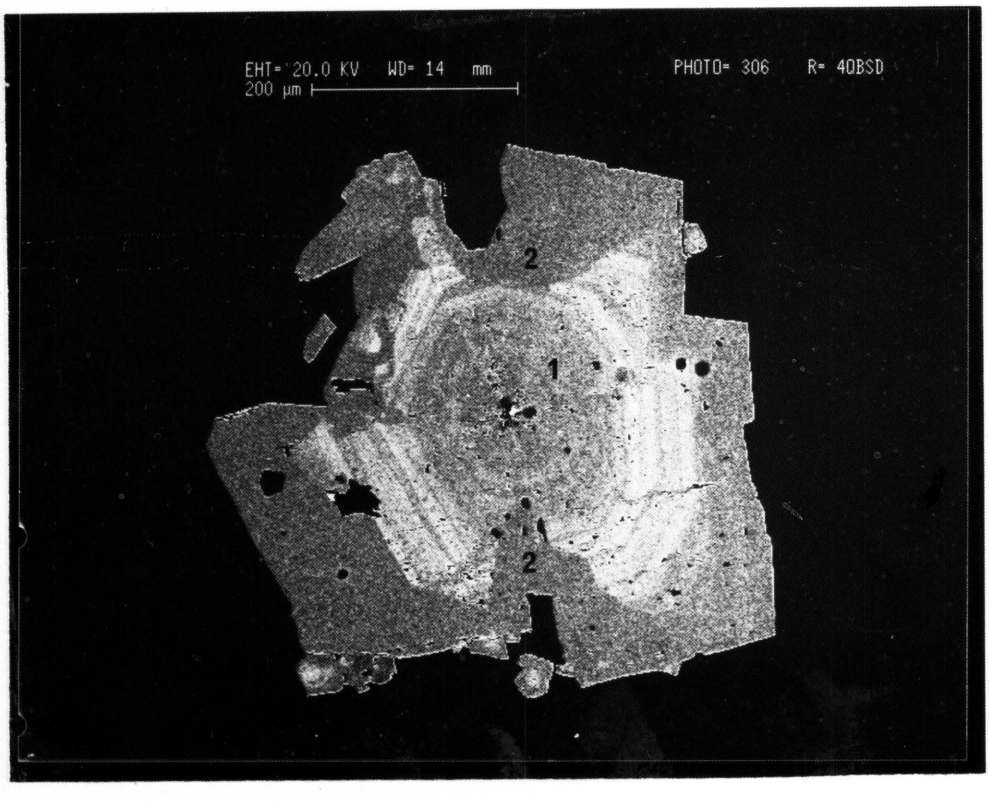

Figure 43: A crystal showing two generations of pyrite: the first generation (1) constitutes concentric growth zones with rhythmic variations in As-content; the second generation (2), As-poor (darker grey), crystallized after a period of resorption RC 1055 (electron backscatter image)

Figure 44: A crystal exhibiting more than one generation of pyrite: the first generation (1) is chemically zoned, the second generation (2) is chemically more or less homogeneous, and the third generation (3) is depleted in As and cuts across the earlier generations.

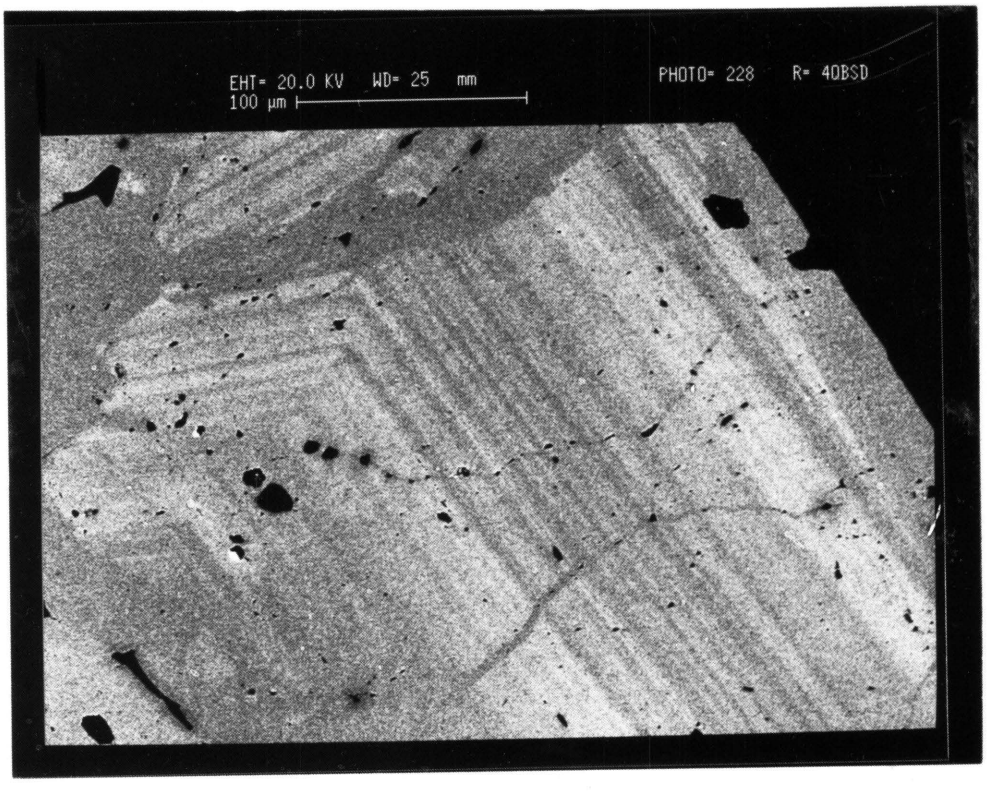

Figure 45: The same crystal illustrated in Fig. 44, at higher magnification. The very fine rhythmic changes in composition within the first generation are apparent. The third generation can be seen cutting across the first generation zoning - RC 1056 (electron backscatter image)

Table X: *A summary of the microprobe analyses of both the As-poor and As-rich zones within the first generation and also the second generation Agnes pyrite composition*

	As (at%)	S (at%)	Fe (at%)	Au (ppm)	Ni (ppm)	Co (ppm)
First generation pyrite: As-poor zones						
min	n.d.	63.47	32.46	< mdl	n.d.	n.d.
max	0.52	67.28	36.04	804	2548	1898
avg	0.19	65.79	33.91	215*	138*	478*
std	0.16	0.94	0.89	260*	451*	353*
First generation pyrite: As-rich zones						
min	0.09	63.5	31.82	< mdl	n.d.	n.d.
max	1.91	66.86	35.15	1507	8151	3962
avg	1.09	65.27	33.42	322*	462*	646*
std	0.45	0.76	0.82	392*	1665*	697*
Second generation pyrite						
min	0.00	63.37	31.99	< mdl	n.d.	220
max	0.2	67.93	36.55	1269	1723	1022
avg	0.02	65.84	34.03	249*	246*	524*
std	0.04	1.30	1.31	367*	414*	250*

min - minimum value
max - maximum value
avg - average value
std - standard deviation
n.d. - not detected
mdl - minimum detection limit
* - note - this amount may be below the mdl

If the S- and Fe-contents of *only the first generation As-poor zones* are plotted against one another, an extremely high correlation coefficient of -0.98 is obtained (see Figure 47). Similarly, the correlation between S- and Fe-content of the *second generation* pyrite is very high (R = -0.99) (Figure 48). However, the correlation between Fe- and S-content of the *first generation As-rich zones* is lower (R = -0.89) (Figure 49).

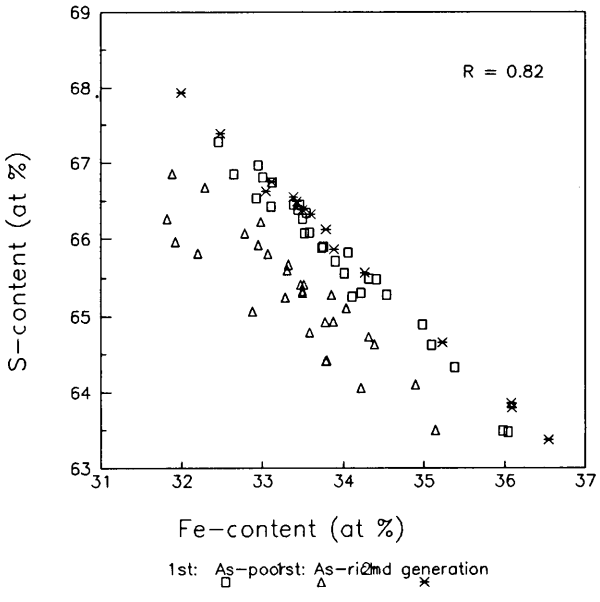

Figure 46: *S-content against Fe-content in the first generation (As-poor and As-rich zones separately) and the second generation pyrite.*

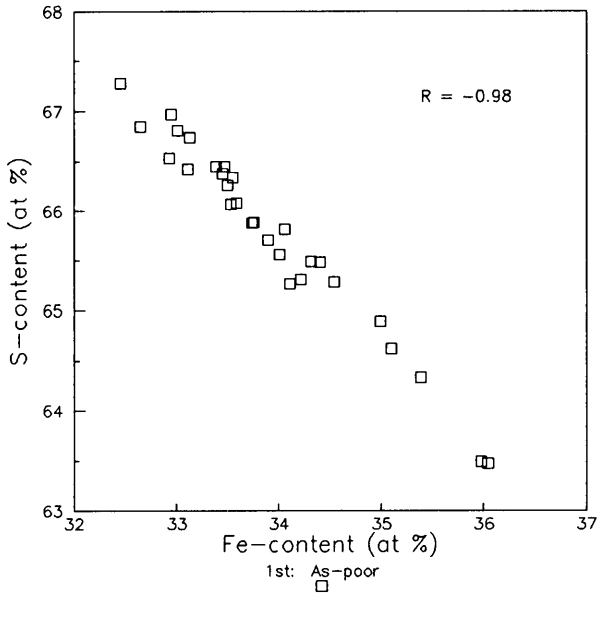

Figure 47: S-content against Fe-content in the first generation As-poor zones

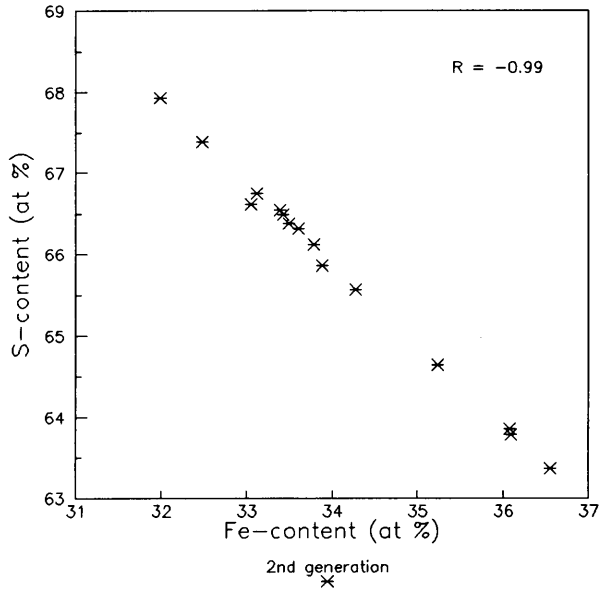

Figure 48: S-content against Fe-content in the second generation pyrite

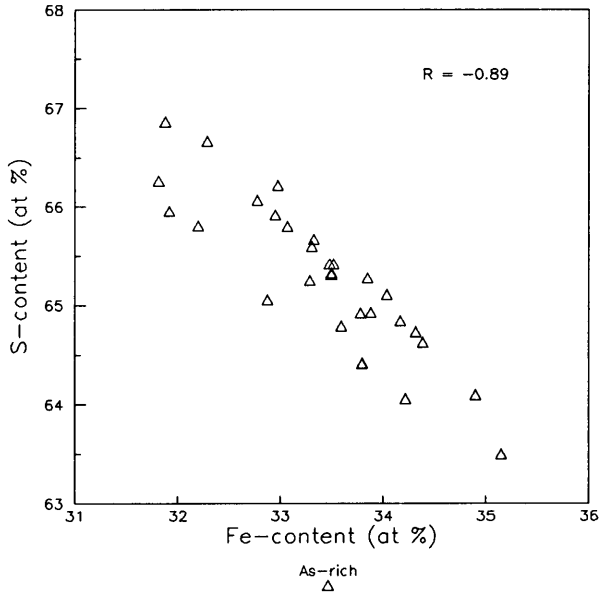

Figure 49: S-content against Fe-content in the first generation As-rich zones

From the previous series of graphs, it is evident that the correlation between sulphur and iron is the lowest in the As-rich zones, while a high correlation exists in both the As-poor zones and the second generation pyrite. The scatter in the data-points in Figure 46, is therefore due to scatter in the points from the As-rich zones. Significant amounts of arsenic and trace elements occur within these zones, and will therefore alter the ideal relationship between sulphur and iron.

The relation between As- and S-concentrations within the pyrite, is, however, not so well-defined, but a crude negative correlation exists in the first generation pyrite. A similar weak negative trend exists between As- and Fe-contents. This indicates that a coupled substitution of As for both S and Fe occurred. This is in contrast with the Sheba pyrite, where a linear negative relationship exists between As and S.

The submicroscopic gold content of the Agnes pyrite reaches values as high as 1 500 ppm within the As-rich zones. No direct relation exists between the As- and Au-content in the pyrite (Figure 50). The second generation pyrite, containing no or very little arsenic, has on average gold concentrations below the detection limit, but it can reach values as high as 1 300 ppm. The As-rich zones of the first generation pyrite display high gold values at moderate As-content.

In addition to the submicroscopic gold present in the Agnes pyrite, particulate gold also occur as inclusions in the crystals. Table XI lists the dimension of some gold inclusions observed. These gold particles usually occur at the contact between the different generations and the zone contacts.

In summary, more than one generation of pyrite is present in the ore from the Agnes goldmine. The first generation is compositionally zoned, expressed by varying amounts of arsenic. The As-rich zones within this first generation pyrite contain the highest amount of submicroscopic gold. The second generation pyrite is depleted in arsenic. Gold particles occur at the contacts between different generations and zones.

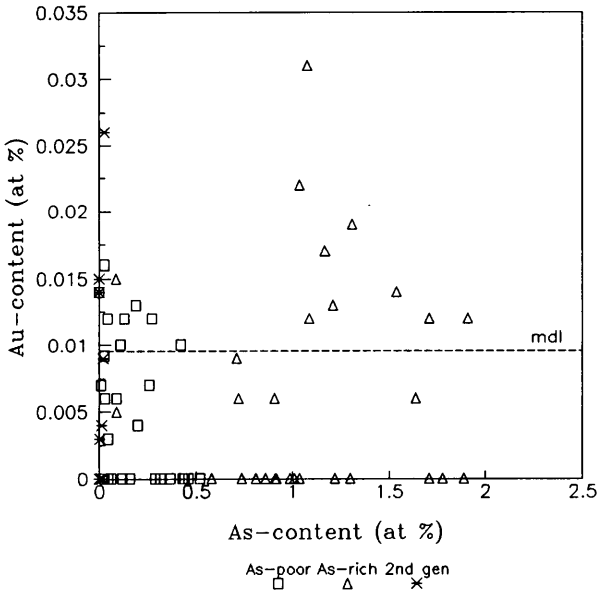

Figure 50: Bimodal distribution of submicroscopic gold, in relation to the As-content of pyrite

Table XI. Dimensions of the several gold particles observed in the Agnes pyrite crystals

Dimension (μm)
70 X 15
5 X 3
4 X 4
2 X 1
1 X 1
3 X 1
8 X 2
6 X 2
2 X 2
1 X 1
3 X 1

6.2 RESULTS OF BACTERIAL OXIDATION

6.2.1 New Consort Arsenopyrite and Loellingite

The response of loellingite and arsenopyrite to bacterial leaching differed markedly.

The loellingite inclusions within the arsenopyrite crystals reacted rapidly and developed dissolution pits during the initial stages of bio-leaching. Figure 51 illustrates the typical appearance of loellingite inclusions after bacterial leaching for five hours. Within some crystals the dissolution pits that developed on the surface of loellingite particles were orientated in well-defined directions, parallel to one another (Figure 52). With an increase in leaching time, extensive dissolution of the loellingite inclusions took place. Pits and leaching depressions were abundant on the loellingite crystal surfaces, as is evident from Figure 53.

Arsenopyrite leaches extremely slowly, in comparison to loellingite. Only after 24 hours of leaching did the arsenopyrite crystals display any effects of bacterial activity. These effects consisted of dissolution channels which developed mainly along pre-existing cracks and other lineations within the arsenopyrite crystals. With an increase in residence time (30 hours), further leaching occurred along these channels, but additional smaller dissolution channels (with an average length approximately 10μm, and width 2μm) and sparsely distributed pits also developed on the leached surfaces (Figure 54).

Dissolution pits also developed on the exposed surfaces of some arsenopyrite crystals after 36 hours of bio-leaching. These dissolution pits produced a surface with a finely dotted appearance (Figure 55).

With extended leaching times, the widths of the larger dissolution channels, which cut across the crystals in random directions, increased to approximately 5μm. The dissolution pits became more abundant and more closely spaced in certain zones. Figure 56 exhibits the presence of large dissolution channels, while zoning is discernible due to a variation in the concentrations of pits. From Figure 57 it is evident that pitting occurred more abundantly in certain zones, than in others. Dissolution pits also developed along the zone contacts.

A)

B)

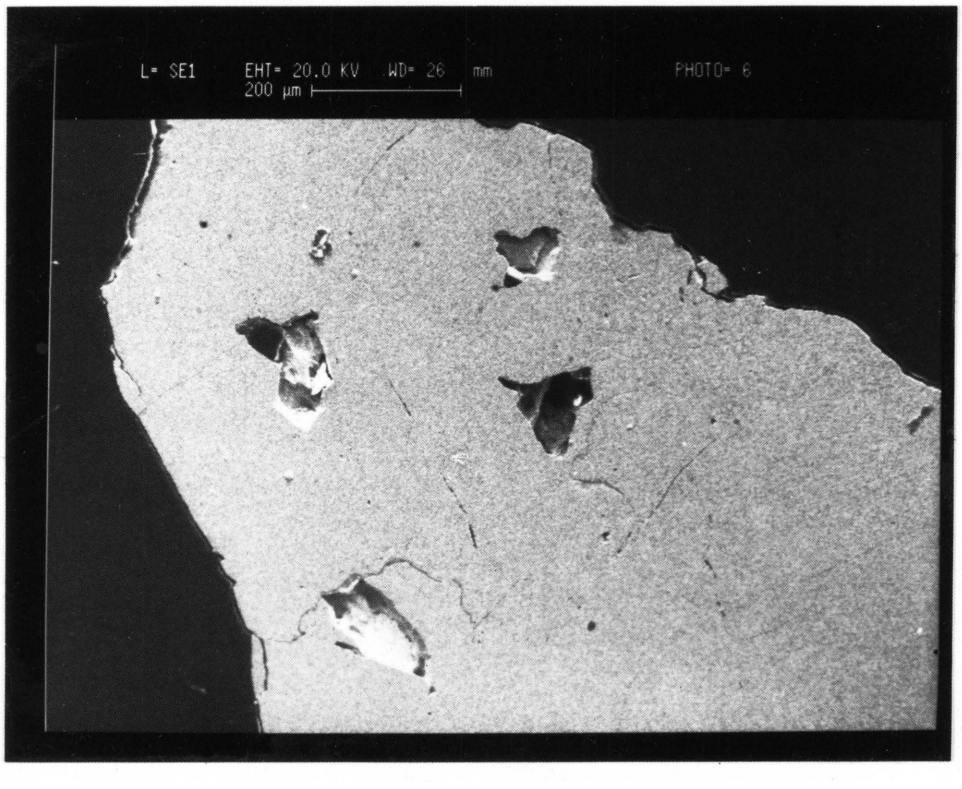

Figure 51: An arsenopyrite particle with loellingite inclusions (white) and numerous cracks:
A) prior to bacterial leaching (electron backscatter image)
B) after 5 hours of bacterial leaching - extensive leaching of loellingite inclusions is evident - RC 1022 (secondary electron mode)

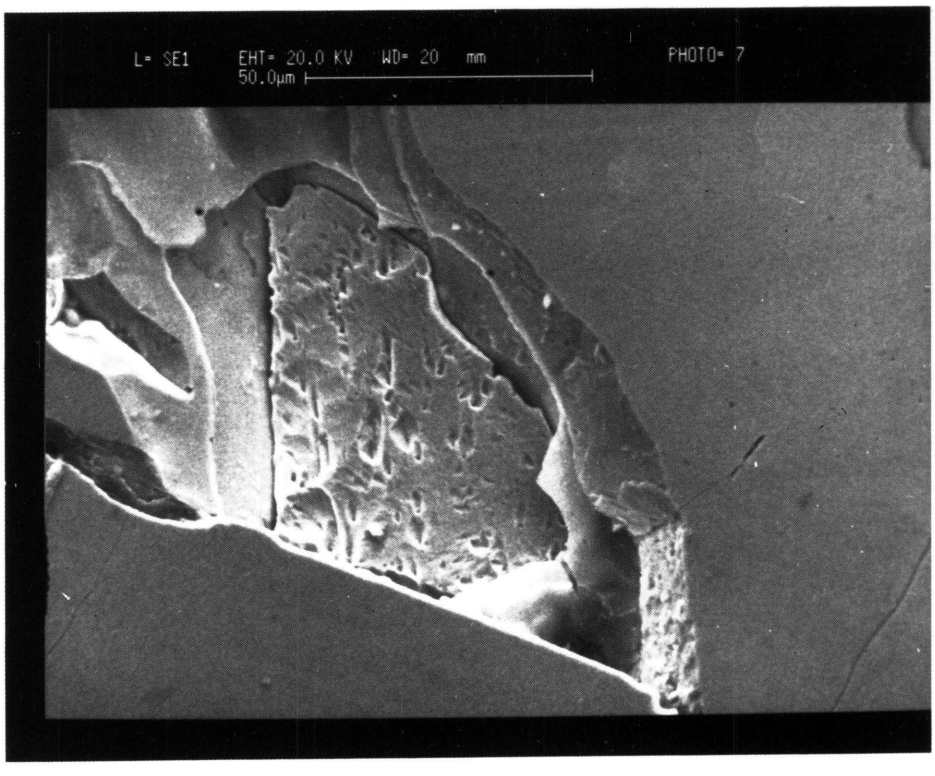

Figure 52: A leached loellingite inclusion exhibits dissolution pits on its surface, while the enclosing arsenopyrite shows no evidence of leaching - RC 1023A (secondary electron mode)

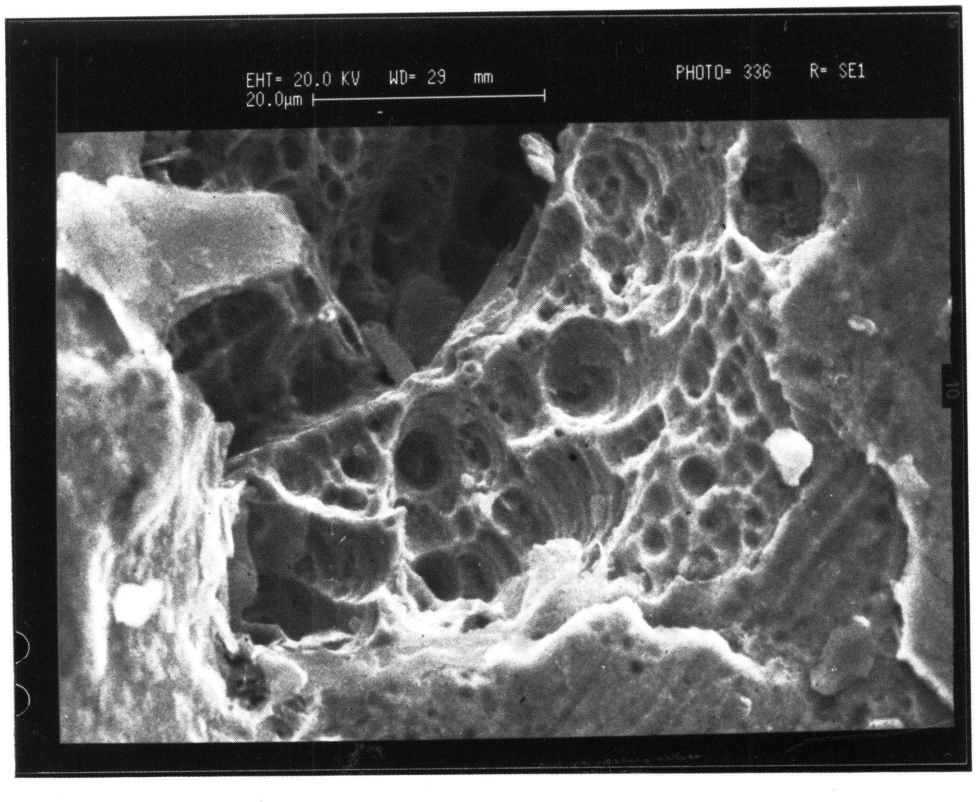

Figure 53: A partially leached loellingite inclusion showing extensive pit formation - RC 1023B (secondary electron mode)

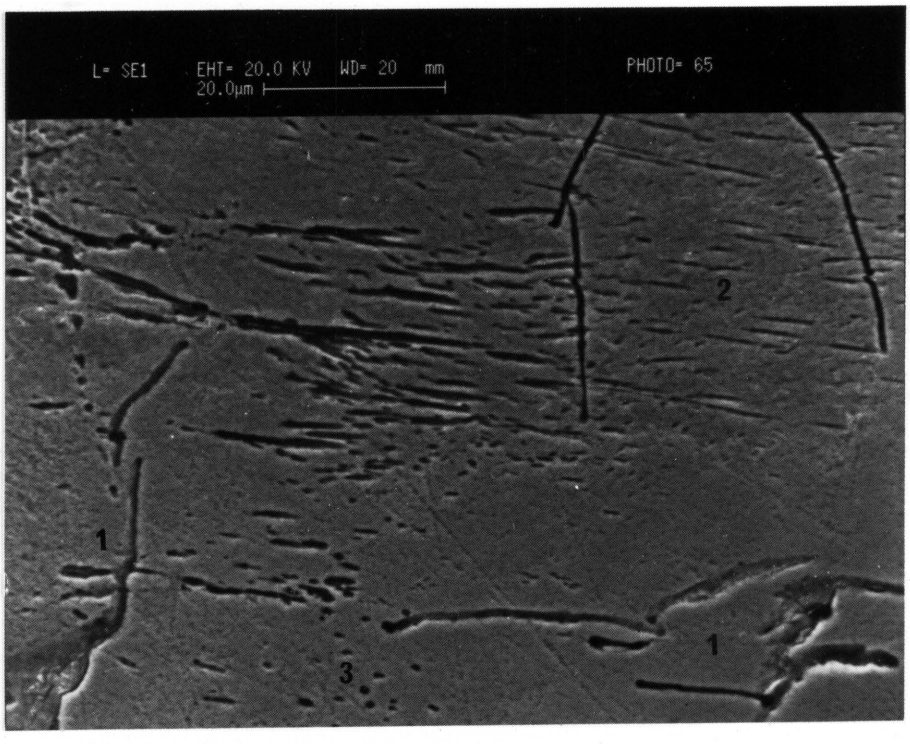

Figure 54: An arsenopyrite crystal after 30 hours of bacterial leaching - the following features are visible: (1) - large dissolution channels along pre-existing cracks, (2) - smaller channels approximately parallel to one another and (3) dissolution pits - RC 1023 A (secondary electron mode)

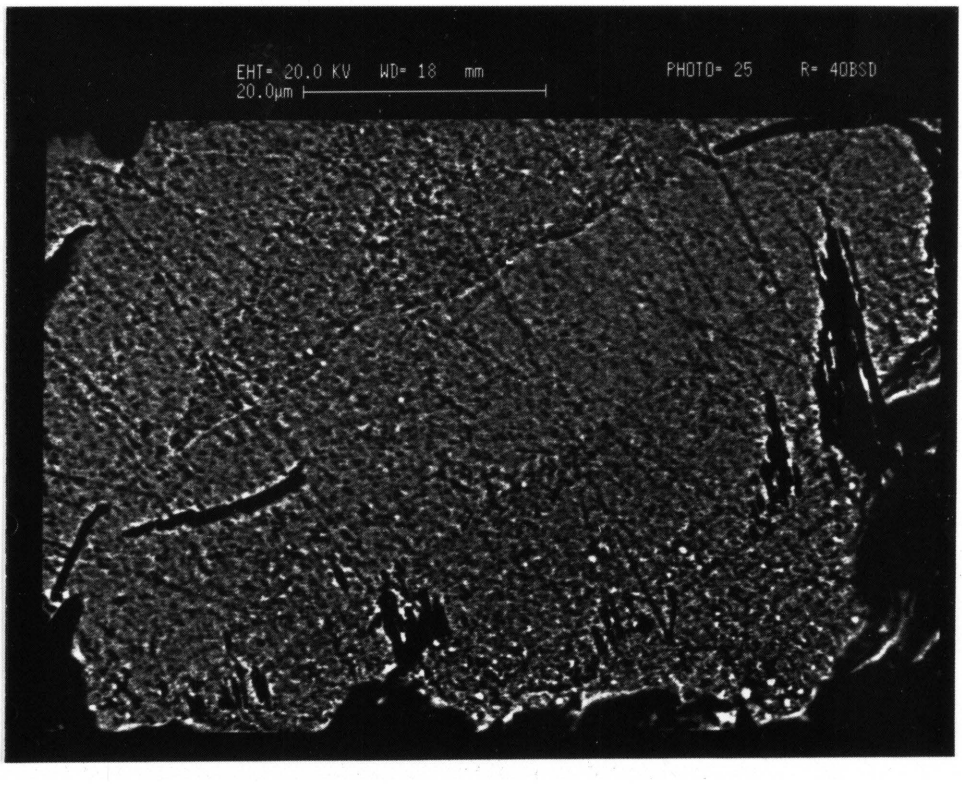

Figure 55: Dissolution pits (smaller than 1µm) developed on an arsenopyrite crystal surface after 36 hours of bio-leaching -RC 1022 (electron backscatter image)

After the arsenopyrite had been leached for approximately 72 hours, a diversity of leaching features developed, as is evident form Figure 58. Dissolution channels of varying dimensions cut randomly across the crystals. Narrow, short channels (less than 1μm in width) had developed mostly within the outer zone of the arsenopyrite crystal. These channels are in general perpendicular to the crystal edge or zone contacts. From the variation in leaching effects, different crystallographic orientations in the crystals can be distinguished. Zoning is also revealed by a variation in the intensity of pitting within the different zones.

During further periods of oxidation, dissolution cavities within the loellingite were sometimes clogged with solids and leach precipitates, which prevented the leach liquor from reaching the loellingite surface. Further oxidation of the loellingite inclusions only occurred when access for the leach liquor was provided by either the development of dissolution channels in the arsenopyrite adjacent to them, or by the lowering of the enclosing arsenopyrite surface by further extensive leaching.

Due to the extensive development of dissolution channels within the arsenopyrite crystals and the very rapid rate of leaching of loellingite inclusions, disintegration of the crystals occurred and the arsenopyrite crystals were therefore lost from the section (Figure 59).

Most of the particulate gold in the New Consort ore is associated with the loellingite inclusions. Therefore, due to the reactive nature of loellingite, most of the gold inclusions within the loellingite were liberated during the early stages of bacterial oxidation. Gold inclusions, associated with arsenopyrite, were released much more slowly during continuous leaching of the arsenopyrite crystals. Figure 60 shows a gold particle exposed during leaching and which can now be recovered by cyanidation.

The recovery of the submicroscopic refractory gold from arsenopyrite is more or less proportional to the degree of oxidation of arsenopyrite. However, this gold represents a minor amount of the refractory gold present in New Consort arsenopyrite.

In summary, during bacterial oxidation of the New Consort arsenopyrite crystals, the loellingite inclusions were leached very rapidly, liberating a high amount of gold particles. The oxidation of the arsenopyrite itself occurred predominantly along pre-existing fractures, cracks and lineations. Large dissolution channels resulted, which cut irregularly and randomly across the arsenopyrite particles. Bacterial oxidation through pitting and the development of small channels occurred at a later stage. Crystallographic orientations seemed to play a role in the development of these leaching features and patterns, and therefore also in the mode of bacterial activity. The faint zoning within the arsenopyrite played a role in the rate of bacterial leaching of the arsenopyrite, but no distinct preferences could be identified.

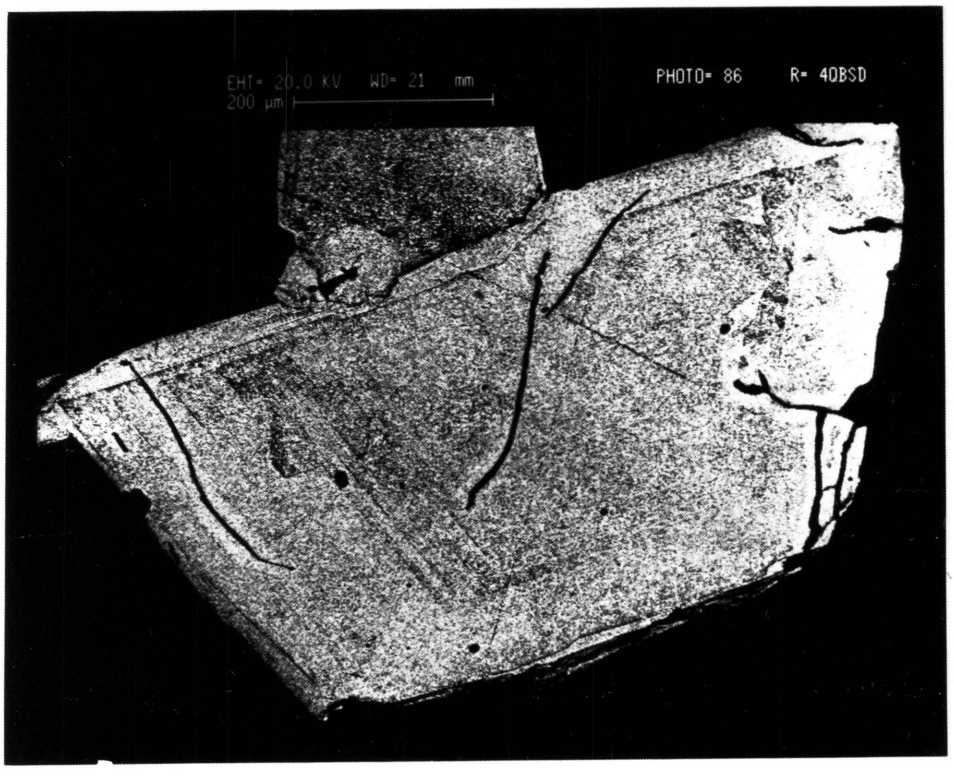

Figure 56: Bacterially leached arsenopyrite after 40 hours. Dissolution channels formed by intensive leaching along former cracks are visible; while zoning within the arsenopyrite crystal is revealed by variations in the intensity of pitting - RC 1022 (electron backscatter image)

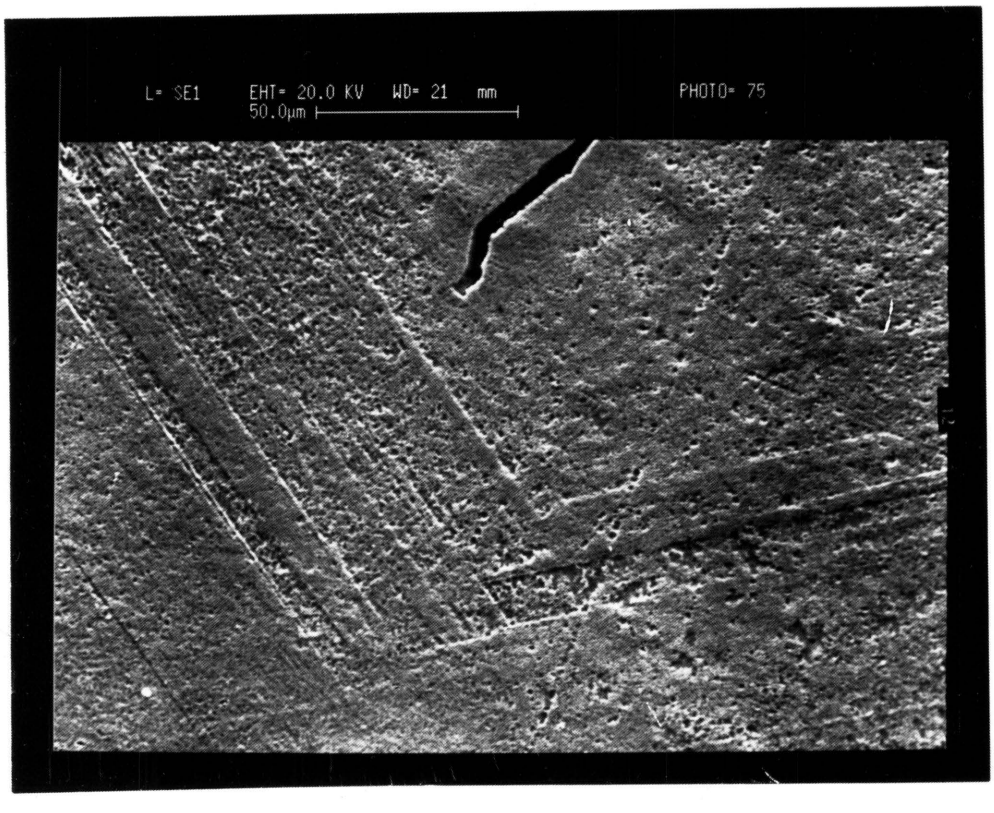

Figure 57: The arsenopyrite shown in Figure 56, at higher magnification - a dissolution channel can be seen, and also pit formation along zone contacts and within zones (secondary electron mode)

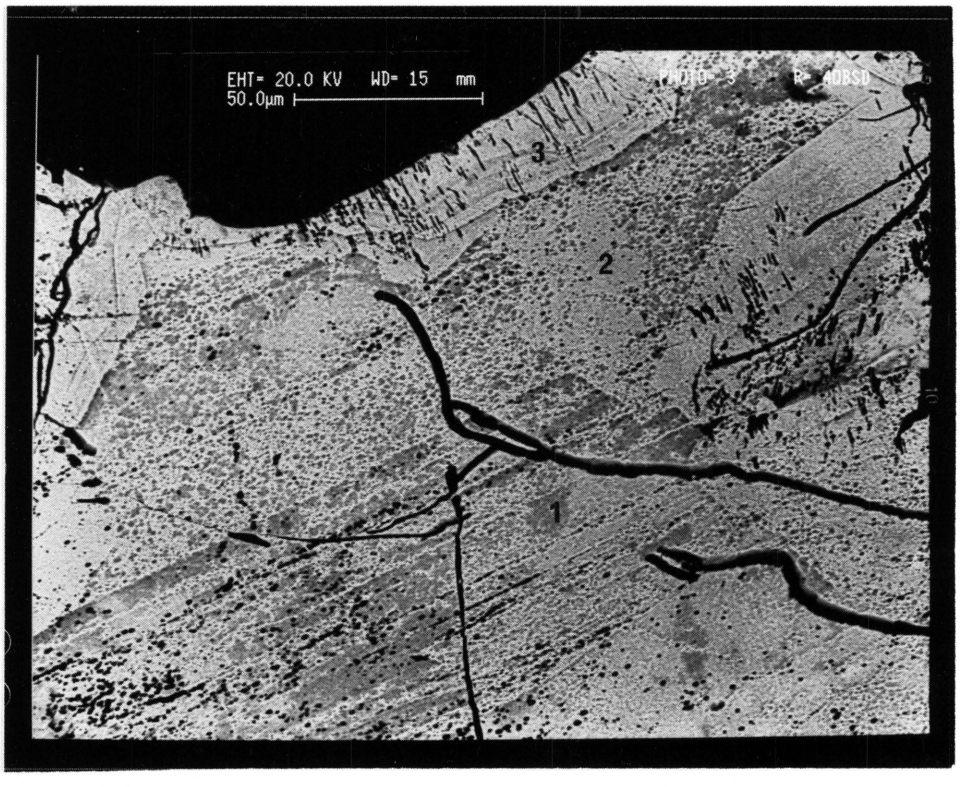

Figure 58: An arsenopyrite crystal after 72 hours of leaching. From the difference in dissolution features, three different crystallographic orientations (1-3) can be distinguished. In addition, the crystal is cut by dissolution channels representing the sites of former cracks. - RC 1023 B (electron backscatter image)

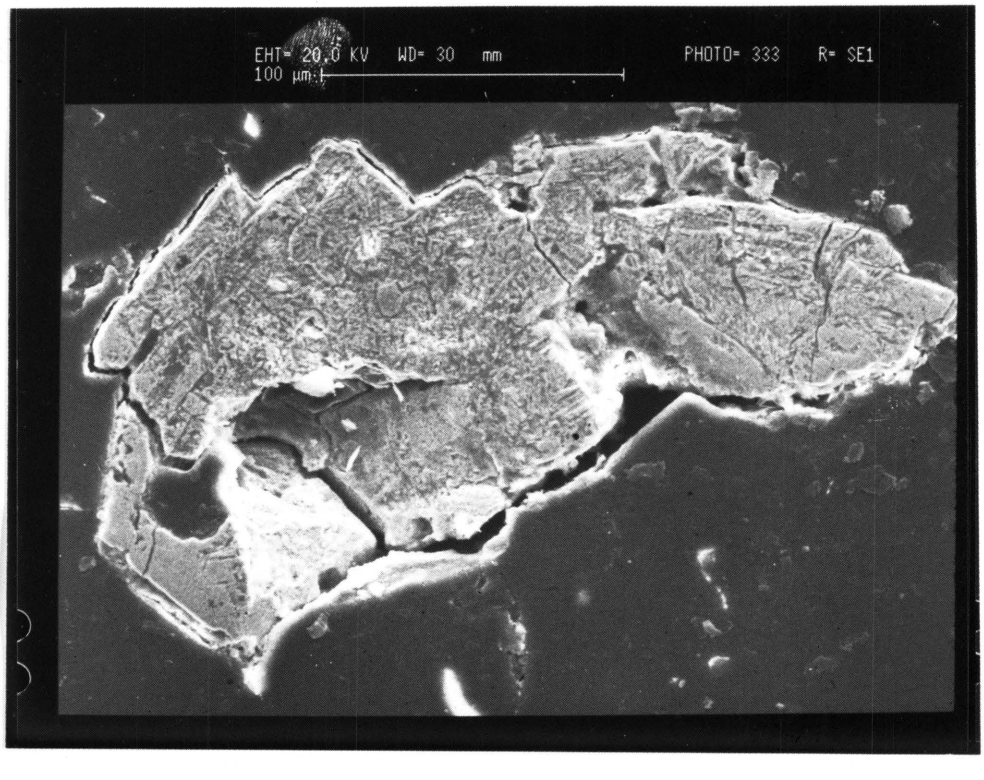

Figure 59: An arsenopyrite after 120 hours of leaching. The crystal shows signs of disintegration due to extensive leaching along cracks and the boundary of the grain - RC 1022 (secondary electron mode)

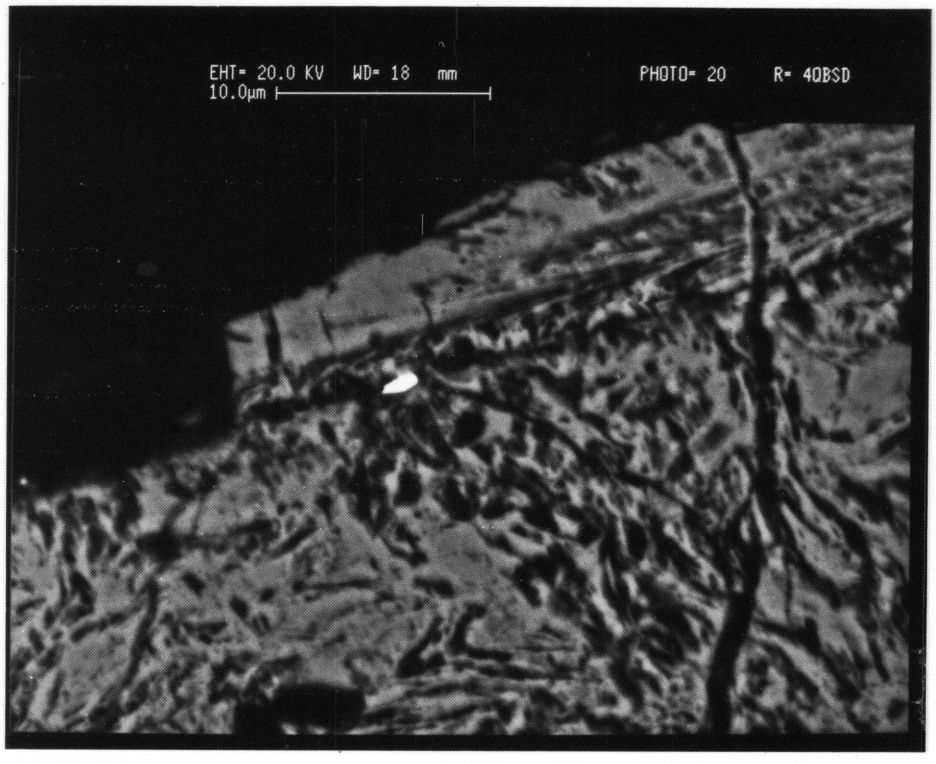

Figure 60: A partially liberated gold particle (white), at the contact between an As-rich zone and a S-rich rim - RC 1044 (electron backscatter image)

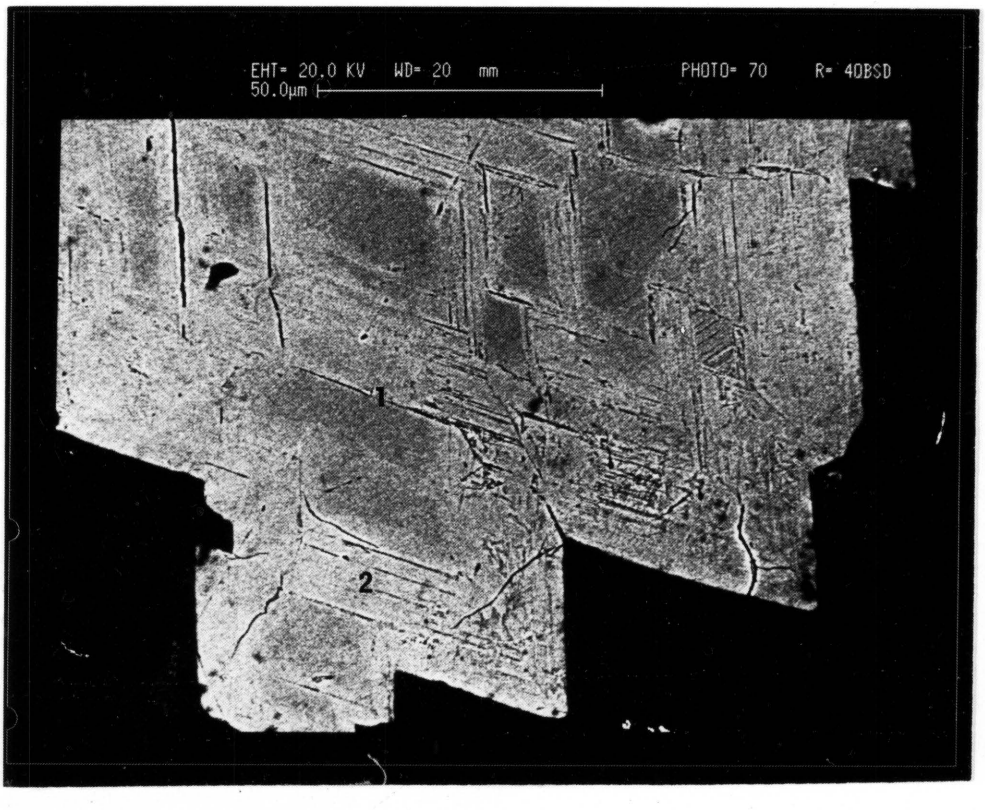

Figure 61: A zoned arsenopyrite crystal after 1 hour of bioleaching - dissolution channels can be seen at the contact between As- and S-rich zones (1) and also within the As-rich zones, parallel to the zone contacts (2) - RC 1018 (electron backscatter image)

6.2.2 Sheba Arsenopyrite

The Sheba arsenopyrite crystals were leached more readily than the New Consort arsenopyrite.

The bacterial attack on the arsenopyrite crystals was rapid, producing spectacular dissolution features. Even after only one hour of bio-leaching dissolution features developed on the exposed surfaces. This initial bacterial activity resulted in the formation of dissolution channels along the contacts of neighbouring As- and S-rich zones. Figure 61 illustrates the leached surface and the nature of the leaching channels. These dissolution channels have unequal lengths, but retain more or less a constant width, i.e. less than 1μm. Observation of the channels during successive leaching stages indicated that these channels developed from tiny dissolution pits (< 1μm), which initially formed along the zone contacts and later merged to form channels.

Gold particles, that generally occur at the zone contacts, were released during this very early stage of oxidation. An arsenopyrite crystal, with gold particles at the zone contacts, is shown in Figure 62 (A). The same crystal after 1 hour of leaching, is shown in Figure 62 (B). It is apparent that leaching occurred along the zone contacts, thereby liberating the gold particles, to such an extent that they were released from the surface of the crystal.

After increasing the leaching time to 6 hours, a complex leaching pattern was observed on the surface of the arsenopyrite crystals. Dissolution channels and pits formed along the zone contacts only within the As-rich zones, while the S-rich zones showed few signs of leaching. Figure 63 (A) shows an arsenopyrite crystal, before oxidation, while Figure 63 (B) shows the same crystal after it had been bacterially oxidized for 6 hours. Extensive channeling and pitting are visible in the As-rich zones, while the As-poor zones contain few dissolution features. At higher magnification (Figure 64) the effect of compositional zoning on the oxidation of the arsenopyrite is evident.

A)

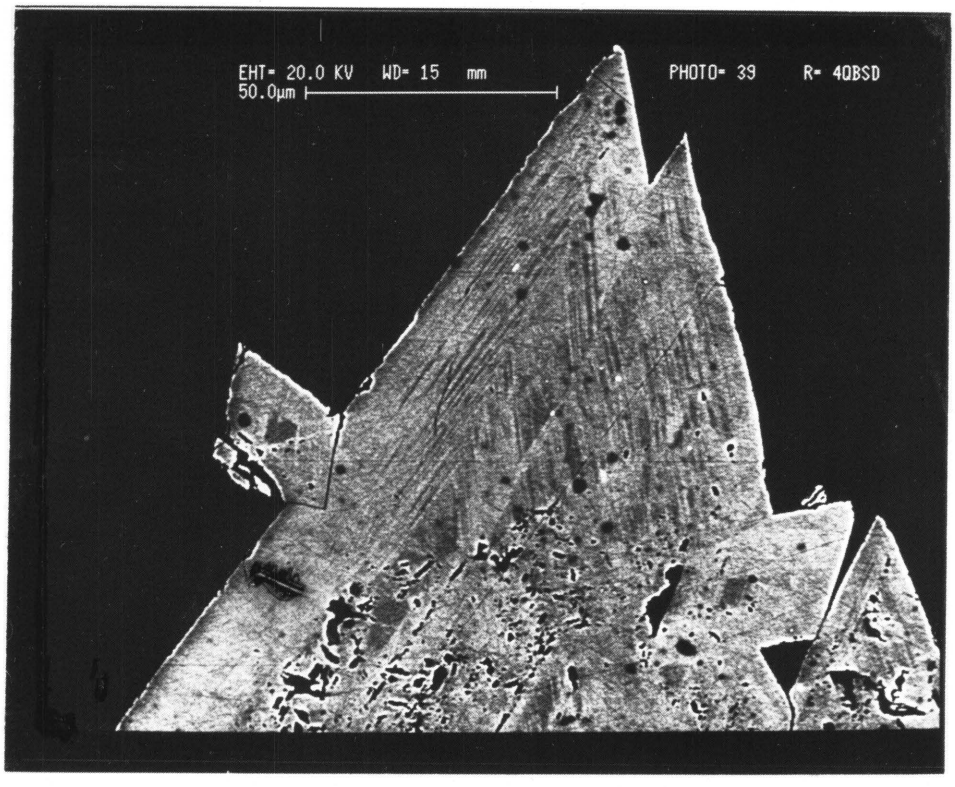

B)

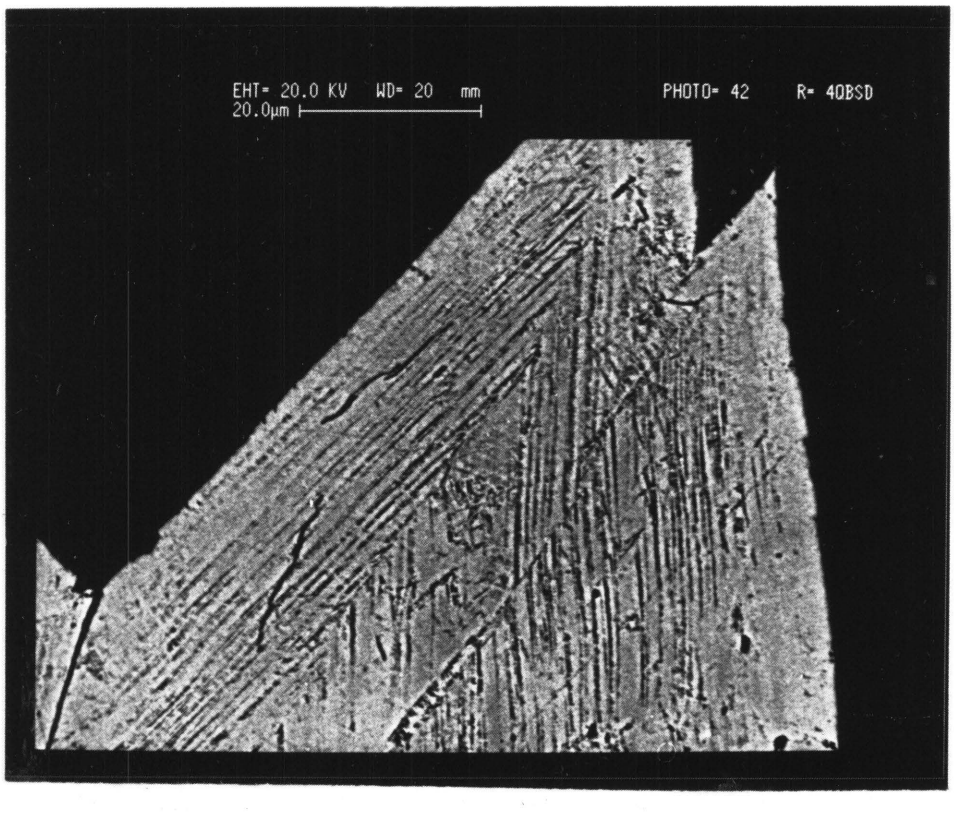

Figure 62: An arsenopyrite crystal: (A) before leaching, showing rhythmic compositional zoning, with some gold inclusions (white) along the zone contacts and B) after bioleaching for 1 hour: leaching has occurred along the zone contacts, liberating the gold particles (no longer visible) - RC 1008 (electron backscatter image)

A)

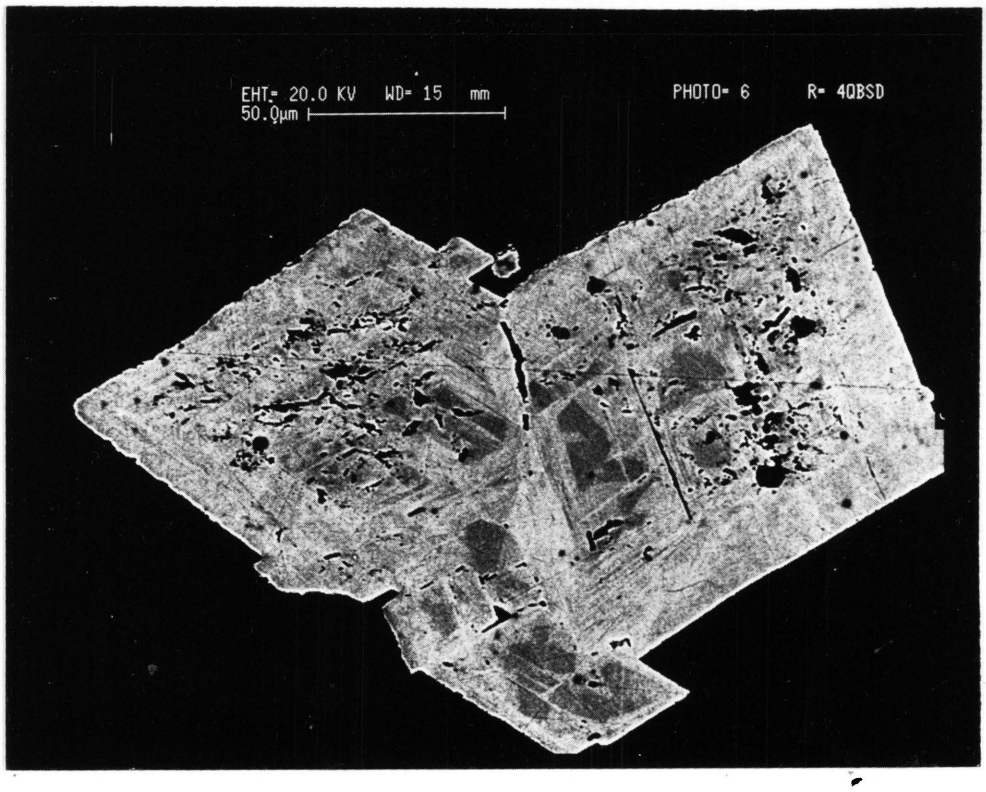

B)

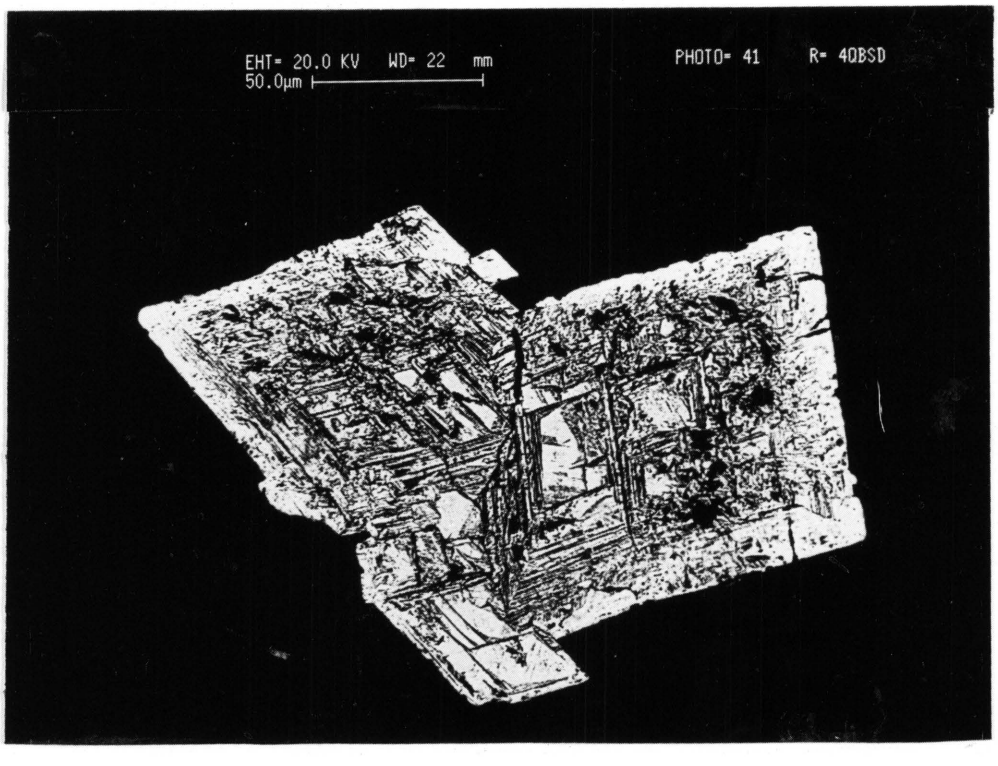

Figure 63. A zoned arsenopyrite crystal with S-rich areas (dark grey) and As-rich areas (light grey): (A) - before leaching and (B) - after being bacterially leached for 6 hours - the As-rich areas have been leached, while the S-rich regions were not attacked at all - RC 1008 (electron backscatter image)

A)

B)

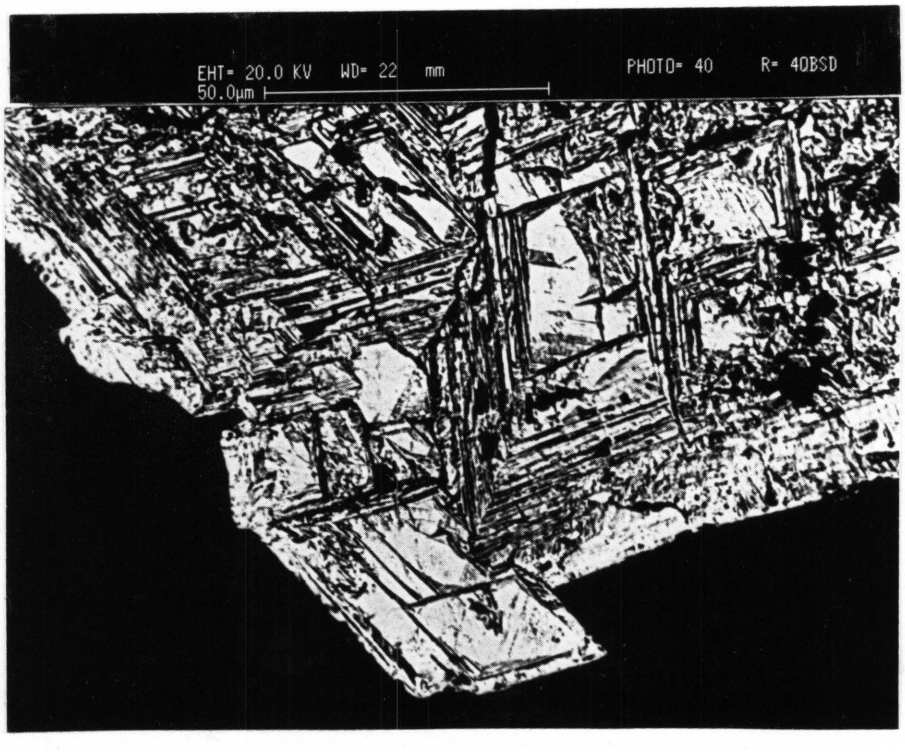

Figure 64: The arsenopyrite crystal shown in Fig. 63, at higher magnification: (A) - before leaching and (B) - after being bacterially leached for 6 hours. Preferentially leaching of As-rich zones is evident - RC 1008 (electron backscatter image)

However, no well-defined individual pits were observed on the surface of the As-rich zones. This is probably due to the rapid rate of dissolution of the entire As-rich zone, resulting in the merging of any small pits that may have developed.

Extensive preferential oxidation of the As-rich zones continued after 24 hours of bacterial leaching, while initial oxidation of the S-rich zones started. Thus, oxidation of the S-rich zones in the arsenopyrite only commences after the crystals had been subjected to the bacteria for one day. After the crystals were bacterially leached for 36 hours, they started to break apart. This was due to enhanced leaching along channels, which caused disintegration of the crystals (Figure 65), with the result that crystals were lost from the polished sections.

The bacterial activity described above has a direct effect on gold liberation from the arsenopyrite. During the very early stages of bacterial oxidation, leaching occurred mainly along zone contacts, where much of the particulate gold is situated. These gold particles were therefore liberated during this initial period of oxidation. Further bio-oxidation led to the leaching of the As-rich zones, releasing the submicroscopic gold, which is present in large amounts in these zones. Therefore, high amounts of refractory gold were released during the initial stages of bacterial oxidation. Further periods of bacterial oxidation resulted in the dissolution of the S-rich zones. However, these zones only contain minor amounts of refractory gold. Thus during the later stages of arsenopyrite oxidation, low amounts of refractory gold were released.

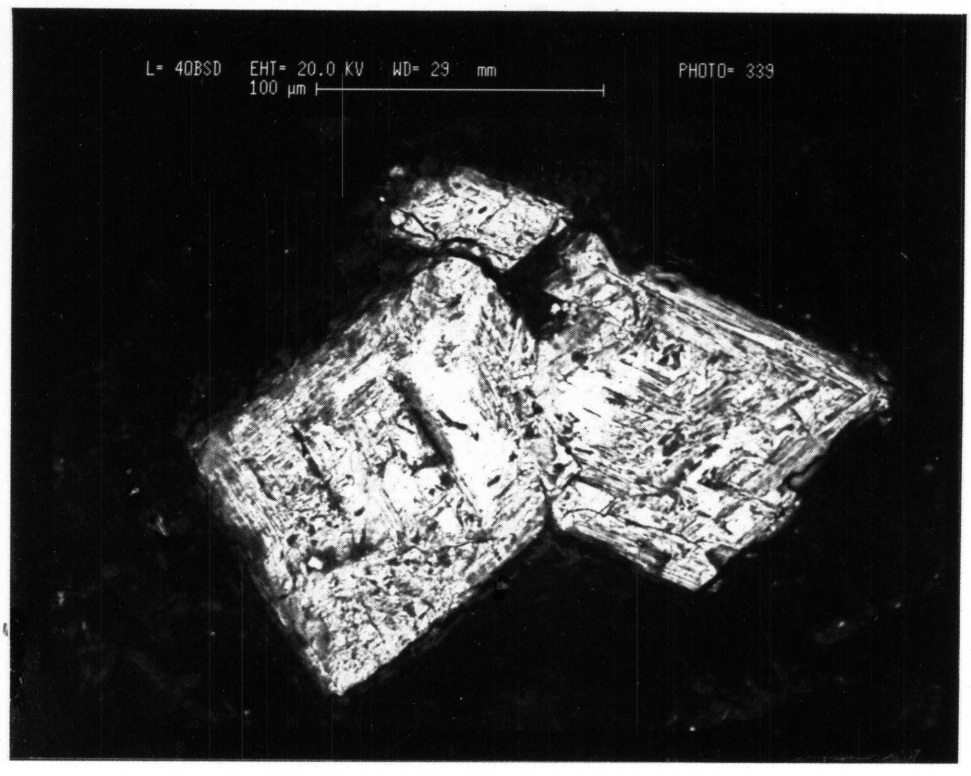

Figure 65: An arsenopyrite crystal after 36 hours of bacterial leaching; the crystal exhibits signs of disintegration due to extensive leaching along the As-rich zones. - RC 1008 (electron backscatter image)

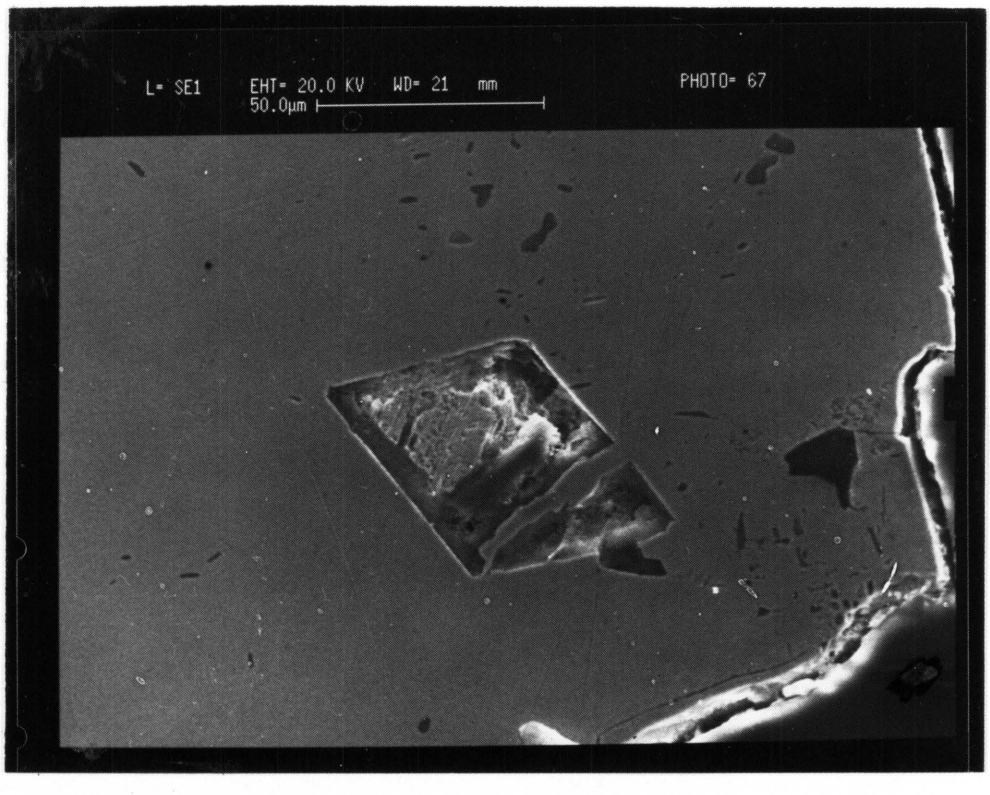

Figure 66: Preferential leaching of an arsenopyrite inclusion within an unleached pyrite crystal, after two hours of bacterial leaching. - RC 1016 (secondary electron image)

6.2.3 Sheba Pyrite

The Sheba pyrite crystals were much more slowly leached than the arsenopyrite crystals. However, arsenopyrite inclusions within unzoned pyrite crystals were leached rapidly during the incipient stages of bacterial leaching in a manner similar to that described in the previous section. Figure 66 shows the leached remnant of an arsenopyrite inclusion after 2 hours of leaching, while the enclosing pyrite exhibits no leaching effects. With an increase in leaching time the pyrite crystals were bacterially oxidized.

The effects of the initial bacterial activity on the zoned and unzoned pyrite crystal surfaces first became visible after 6 hours. Dissolution channels formed along pre-existing cracks, which cut randomly across the crystal faces (Figure 67), at the boundaries between pyrite of different generations or composition (Figures 67 and 68), and around inclusions.

These dissolution channels consist of individual pits, which upon merging formed continuous dissolution channels. Figure 69 shows pit formation during the transition from pearl-string-like chains to continuous channel-like dissolution structures. By using the SEM at higher magnification the dissolution pattern and shape of the dissolution pits can be distinguished. It is evident from Figure 70 that the pits have a square outline, with a consistent orientation.

The channels therefore consist of square-shaped, parallel-orientated pits, coalescing along a pre-existing zone of weakness (such as compositional or generational boundaries, dislocations, etc.) within the crystals.

Sometimes, unusual dissolution features are observed on the surface of the pyrite particles. Figure 71 displays such leaching features.

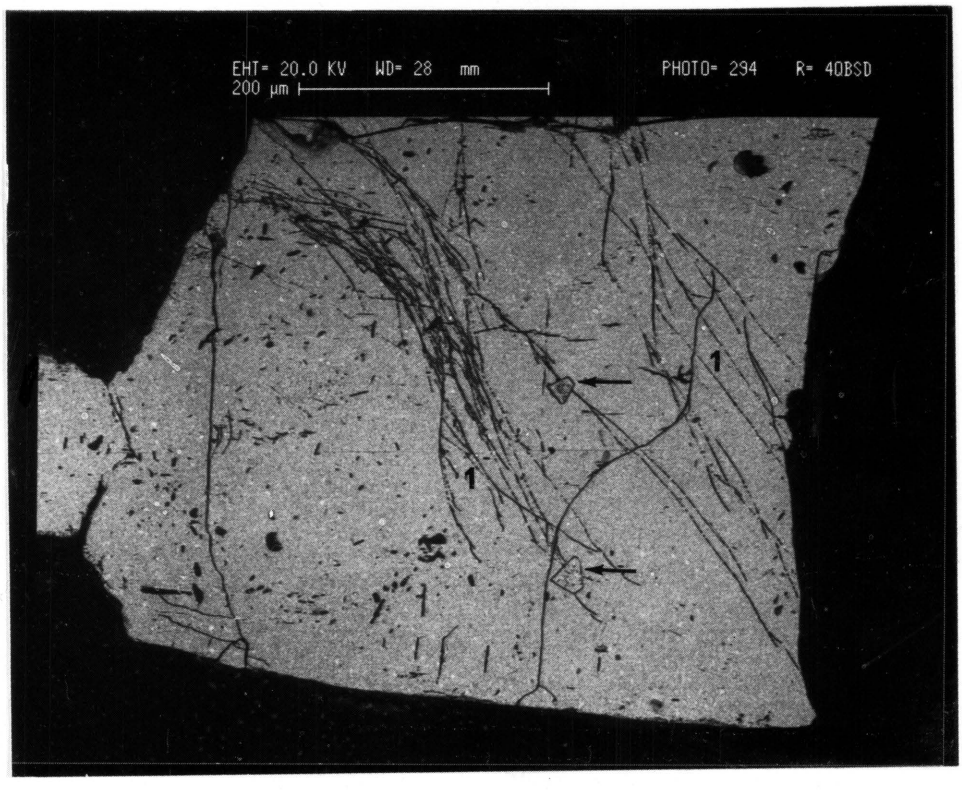

Figure 67: A pyrite crystal after 6 hours of bioleaching - leaching effects include dissolution channels that have developed along former cracks (1) and along the contacts between regions of varying compositions (arrows) - RC 1024 (electron backscatter image)

Figure 68: A bacterially leached pyrite particle after 6 hours - dissolution channels have developed along the grain boundaries (1) and along the contacts between compositionally diverse regions (2) - RC 1001 (electron backscatter image)

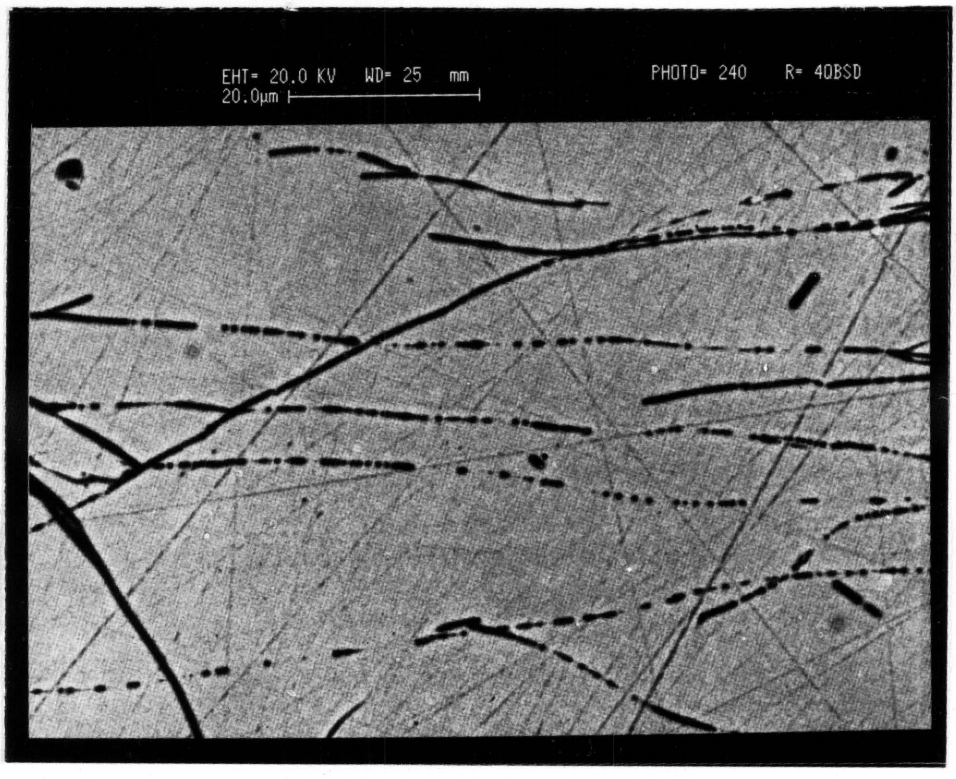

Figure 69: A leached arsenopyrite crystal, illustrating the development of dissolution channels by coalescence of closely-spaced pits along former cracks - RC 1024 (electron backscatter image)

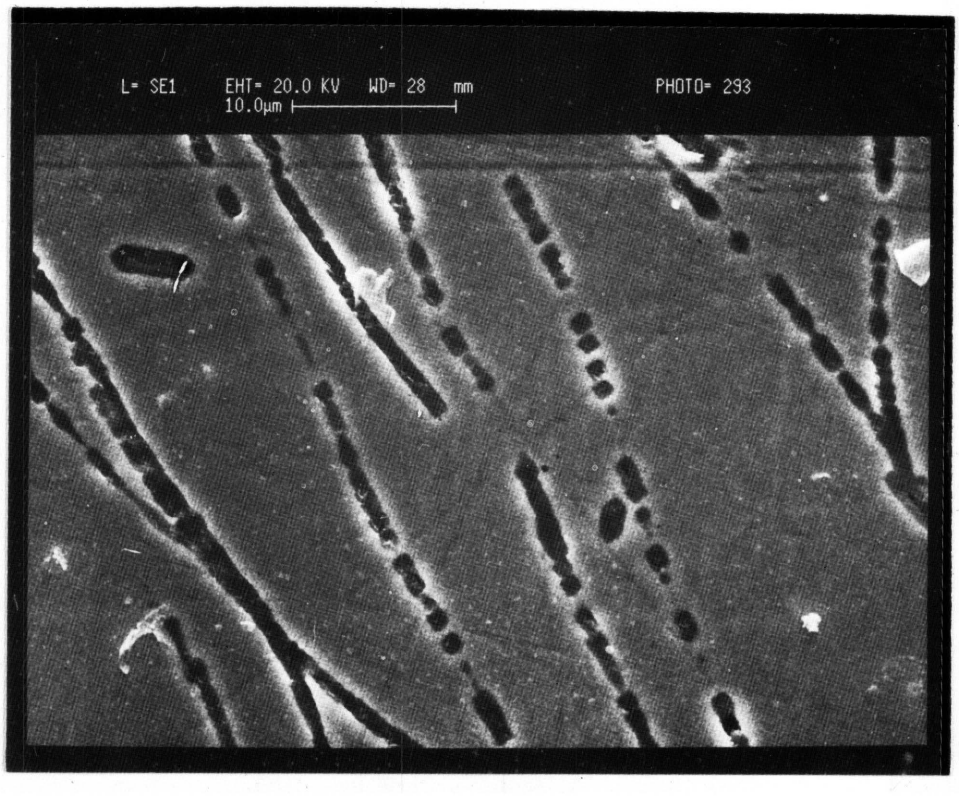

Figure 70: Dissolution channels similar to those shown in Fig. 69, at higher magnification. Pits with square outlines are evident. - RC 1024 (secondary electron image)

In zoned pyrite crystals an increase in leaching time resulted in a preferential attack on the As-bearing areas, with the development of short dissolution channels and pits. These channels mostly formed perpendicular to the contact with other domains of differing composition (Figure 72). The shape of the pits, distributed on the surface of the As-rich zones, have a square outline, similar to those forming channels (Figure 73).

With increased leaching times, the As-bearing zones were oxidized far more extensively than the other zones. Leaching also continued along the channels that cut across the pyrite crystal surfaces. These channels therefore increased in width and depth, until disintegration of the crystals occurred along them (Figure 74). Pieces of such fractured crystals were usually lost from the polished sections.

The liberation of gold particles from both the zoned and unzoned pyrite crystals during bacterial leaching took place mainly during the early stages of pyrite oxidation. The dissolution channels that formed during the early stages of oxidation, were located along the contact between different generations of pyrite or along contacts of domains of different chemical composition. In the zoned pyrite crystals, the As-bearing zones, where much of the submicroscopic gold occurs, were attacked in addition.

Thus, most of the gold in the pyrite crystals was liberated during the initial stages of oxidation.

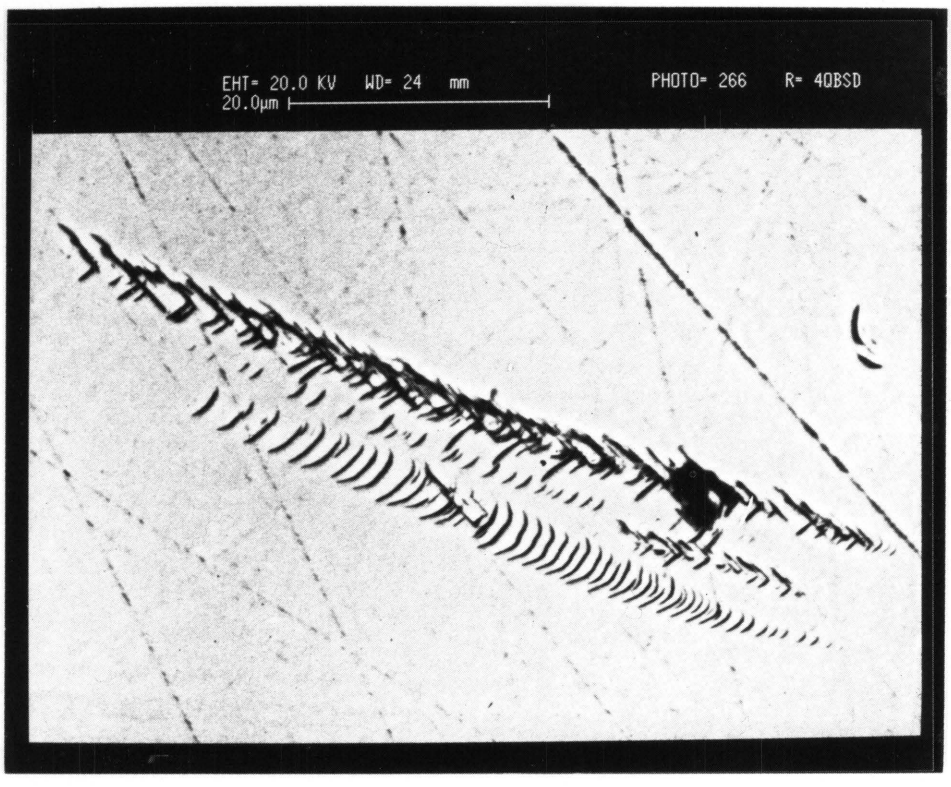

Figure 71: Unusual dissolution patterns developed occasionally on the pyrite leached surface. - RC 1024 (electron backscatter image)

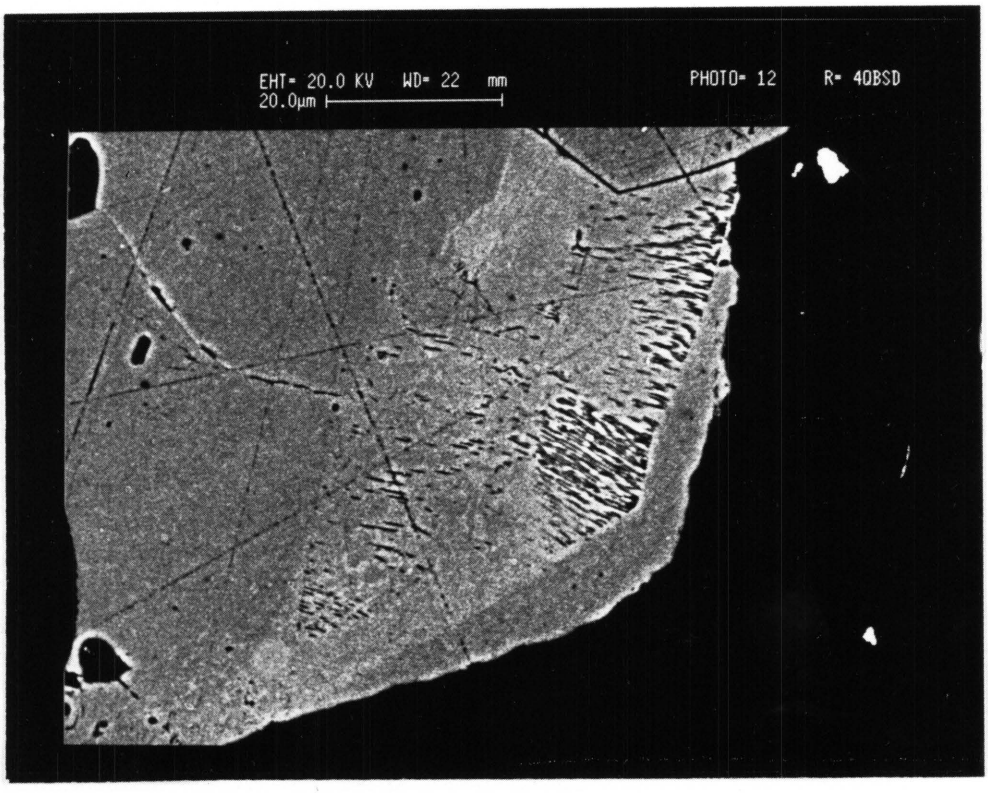

Figure 72: A leached pyrite crystal showing areas of different composition; an As-enriched area (light grey) contains numerous dissolution channels, while an As-poor region (grey) displays few dissolution features. - RC 1016 (electron backscatter image)

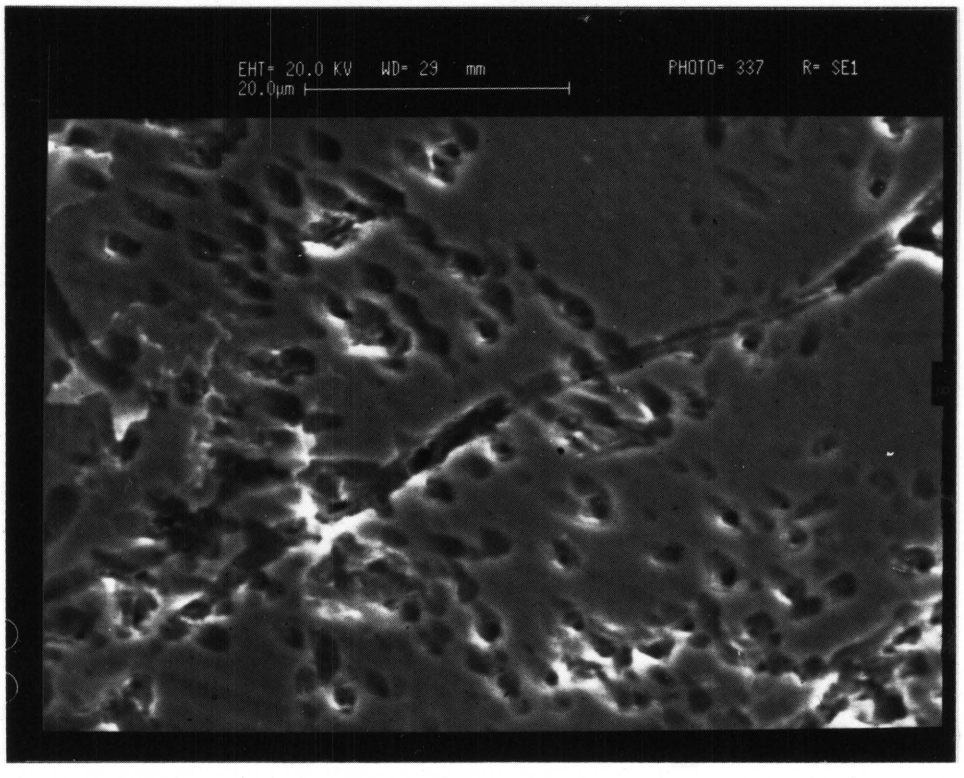

Figure 73: A leached pyrite crystal surface, exhibiting the nature of dissolution pits within an As-rich area. - RC 1024 (secondary electron image)

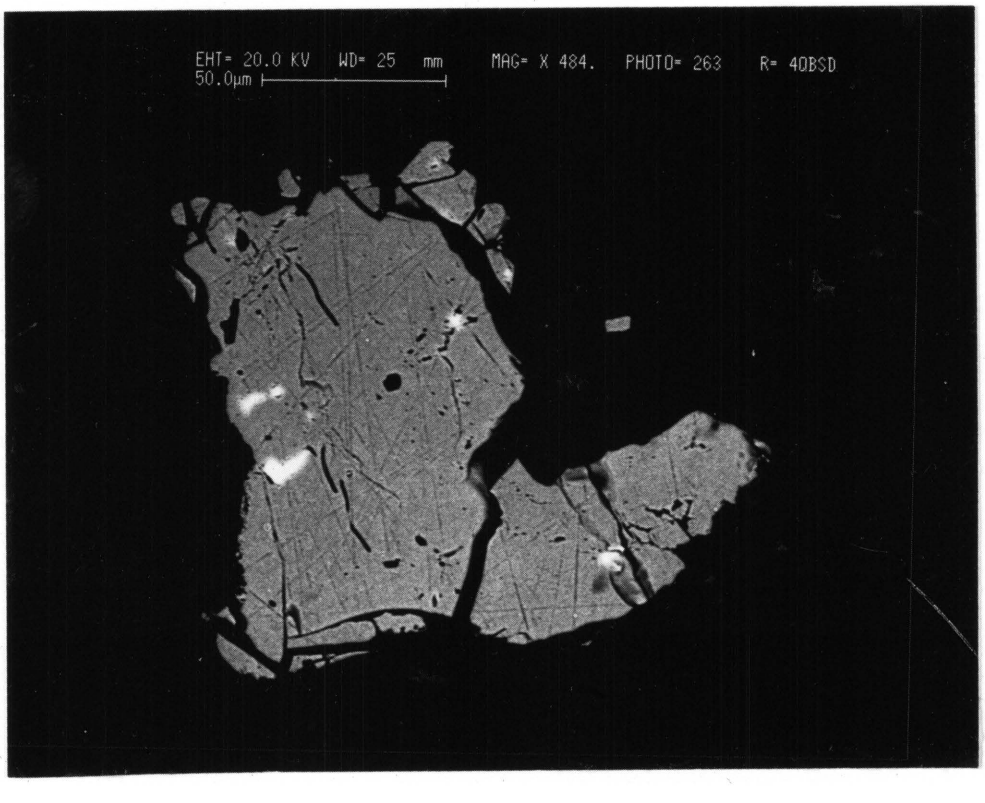

Figure 74: A pyrite crystal after 96 hours of bacterial leaching, exhibits fracturing, due to extensive leaching along former cracks - RC 1024 (electron backscatter image)

6.2.4 Agnes Pyrite

The various types of Agnes pyrite crystals behaved differently during microbiological oxidation tests. Only after the pyrite crystals had been leached for more than 10 hours, did any leaching features develop on their surfaces.

The initial bacterial activity on the *massive intergrown pyrite* crystals occurred along the grain boundaries. In addition compositional zoning within the pyrite is revealed by variations in the intensity of leaching (Figures 75, 76 and 77). With an increase in leaching time the formation of individual pits in the centres of the crystals took place, in addition to a further development of dissolution channels along grain boundaries, cracks and other lineations. These dissolution effects on the massive intergrown pyrite crystals are displayed in Figure 78.

The dissolution channels, which developed during bacterial leaching of the intergrown pyrite crystals, consist of individual square-shaped pits, orientated in the same direction. These dissolution pits coalesce to form both pearl-string-like structures and channels that cut across the pyrite crystals (Figure 79). The square pits are on average 1 μm in diameter. The orientation of the dissolution pits remains constant even when these merge to form leaching channels.

During bacterial oxidation the zoned individual pyrite crystals from the Agnes ore developed leaching effects similar to the massive intergrown crystals. Leaching took place along the different compositional zones within the first pyrite generation, whereas no or few dissolution features developed within the second pyrite generation (Figure 80). Dissolution channels also formed along contacts between areas that differ in composition and along former cracks within these single crystals (Figure 81).

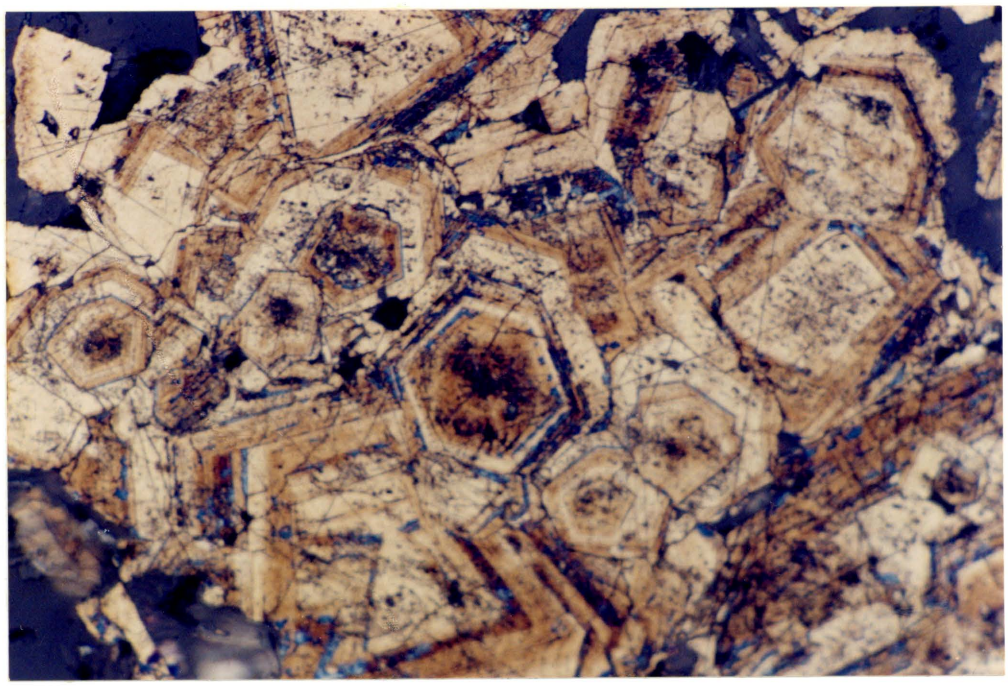

Figure 75: A mass of intergrown pyrite crystals after 10 hours of bioleaching - concentric compositional zoning is revealed within individual crystals due to a difference in intensity of bacterial activity on the individual zones. Leaching has also occurred along grain boundaries. - RC 1072 (photomicrograph under reflected light)

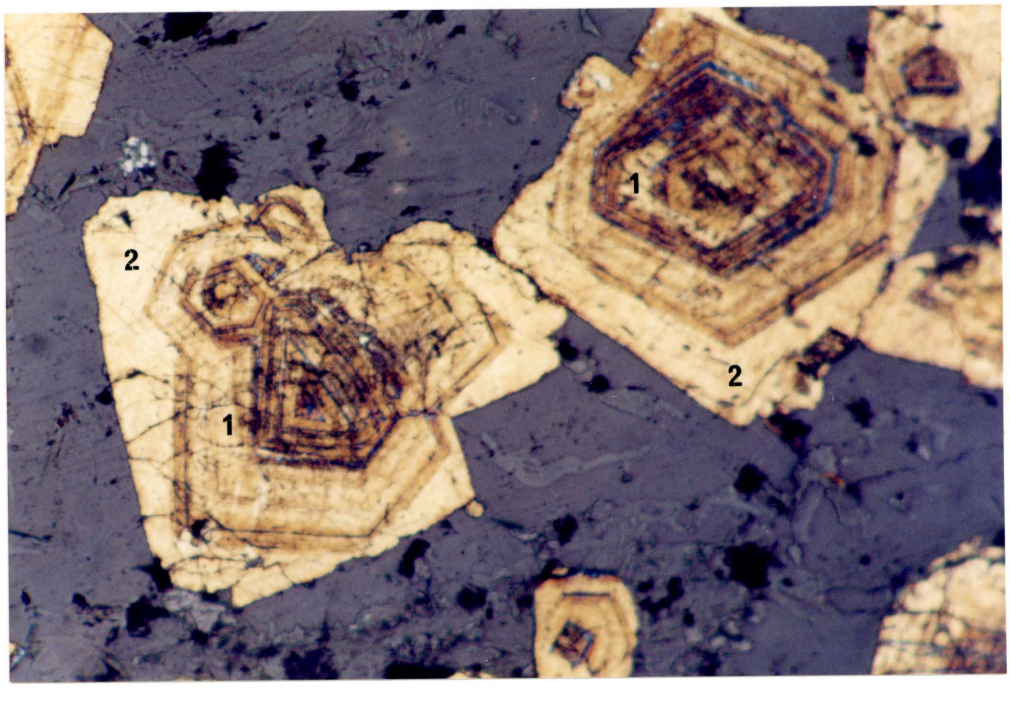

Figure 76: Bacterially leached pyrite particle (after 10 hours): leaching in the first generation pyrite (1) is concentrated along the concentric zoning present in the pyrite. The second generation (2) displays few leaching effects - RC 1072 (photomicrograph under reflected light)

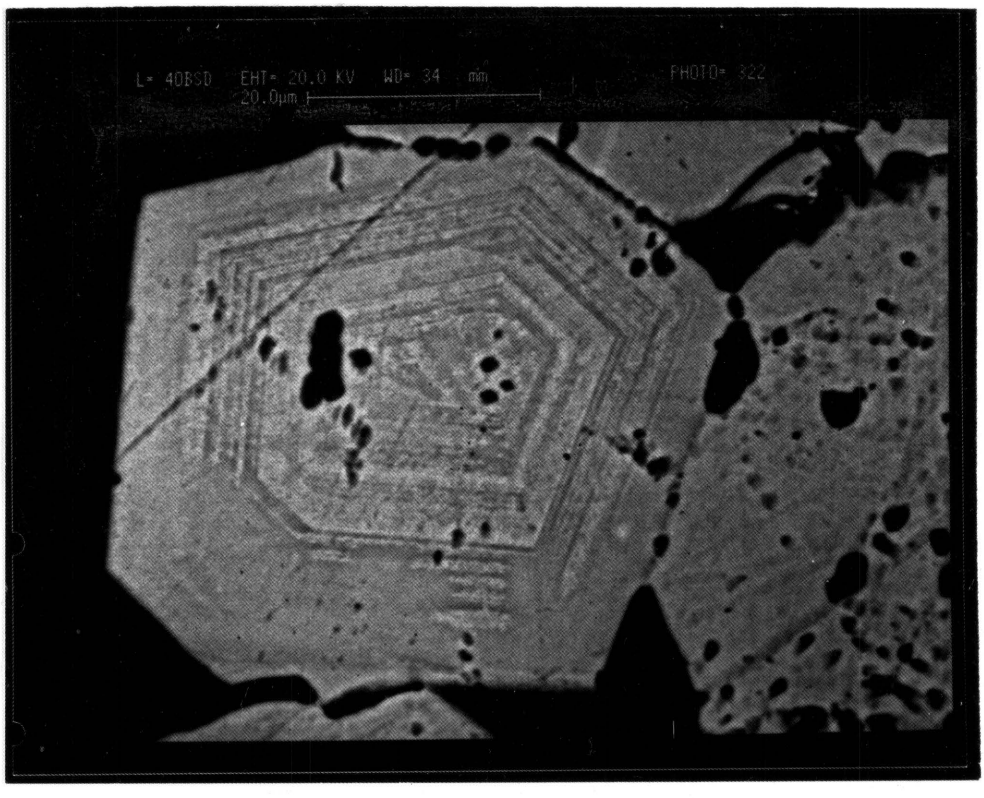

Figure 77: Pyrite crystal after 10 hours of leaching: preferential oxidation of the As-rich zones in the pyrite reveals fine compositional zoning within the crystal - RC 1056 (electron backscatter image)

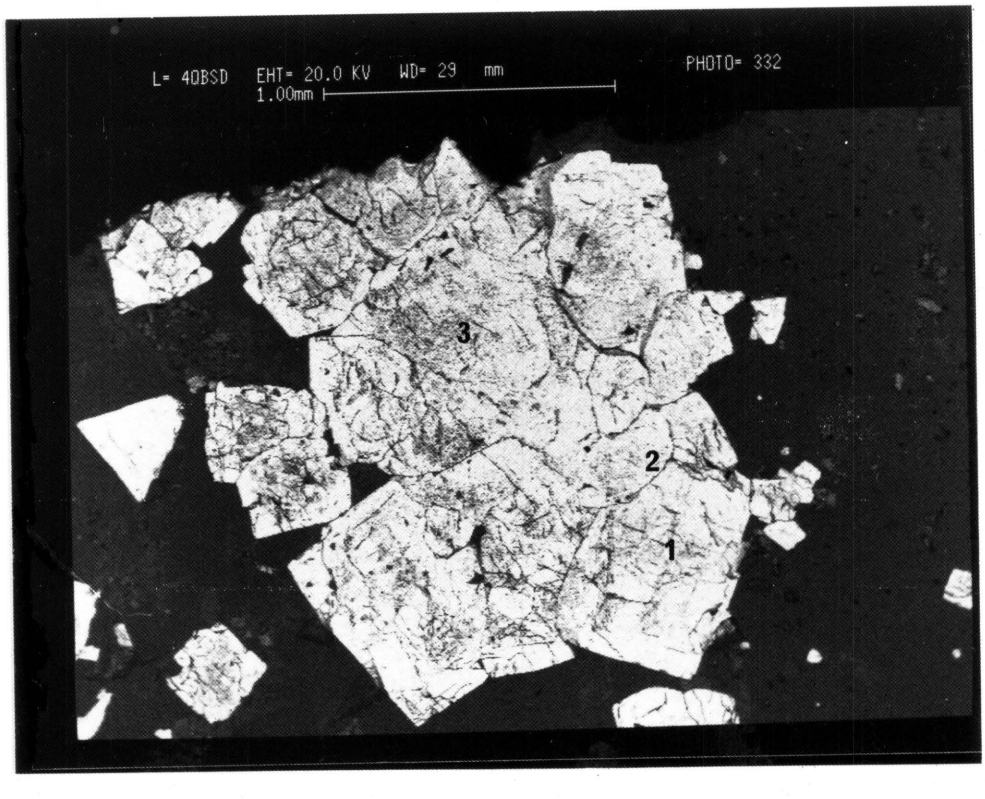

Figure 78: Intergrown pyrite crystals after 20 hours of bioleaching: leaching effects include the following: (1) dissolution channels that have developed along former cracks, (2) channels along the grain boundaries and (3) pit formation in the crystal centres along As-rich zones - RC 1072 (electron backscatter image)

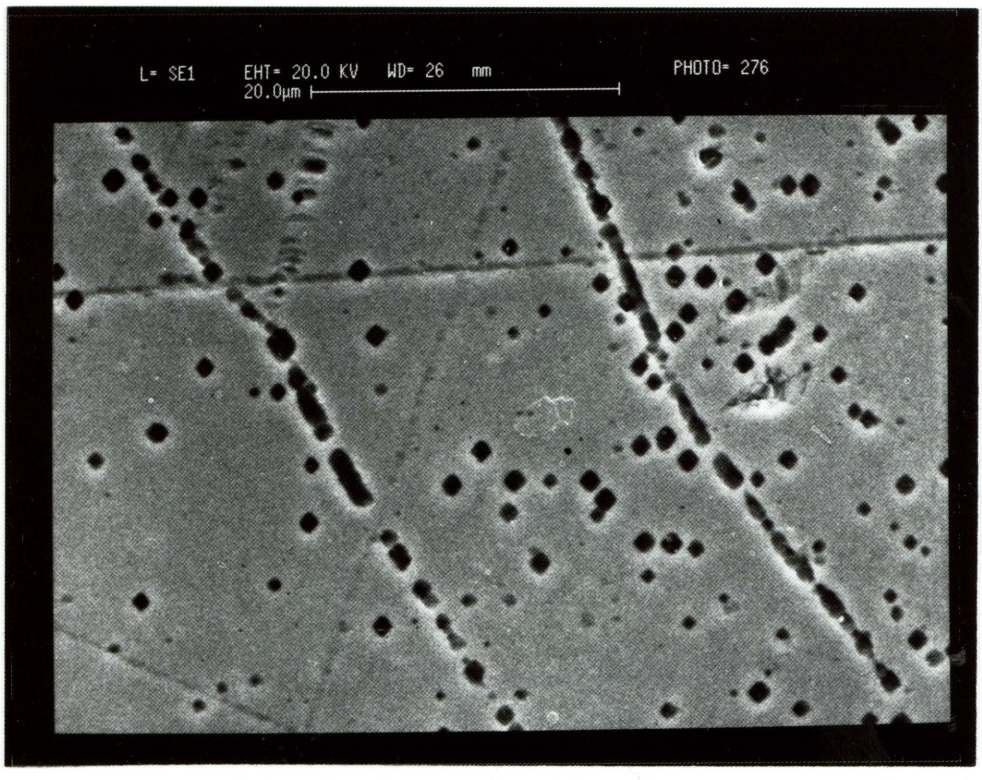

Figure 79: A pyrite crystal, after 20 hours of leaching, illustrating the development of dissolution channels by coalescence of closely-spaced square pits along former cracks - RC 1024 (electron backscatter image)

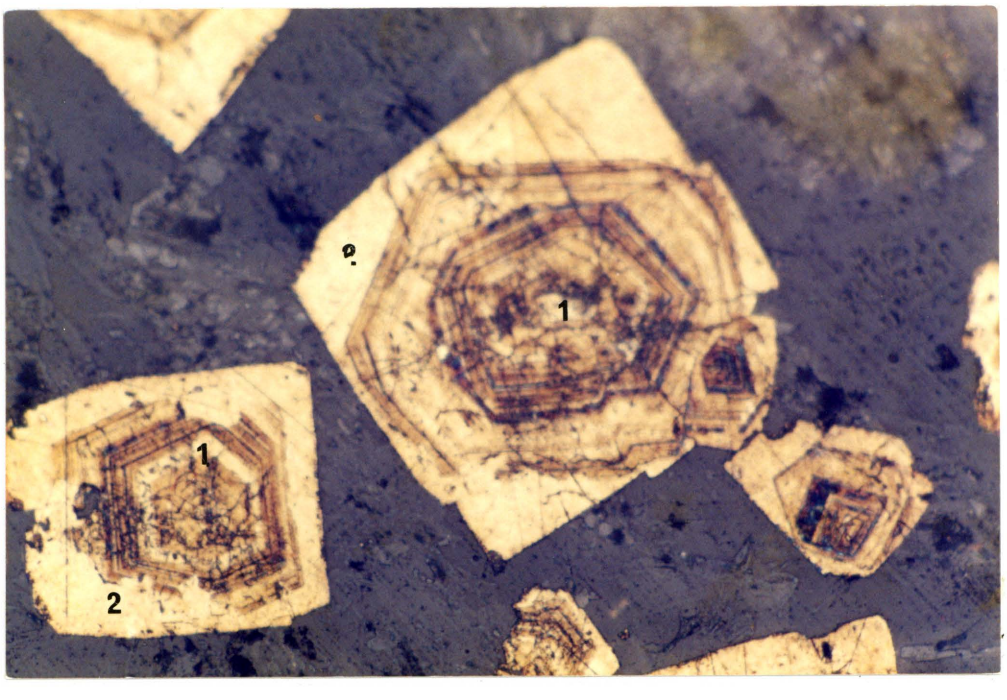

Figure 80: Bacterially leached pyrite crystal after 10 hours: the first generation pyrite (1) reveals leaching along concentric zones, while the second generation (2) displays few dissolution features - RC 1072 (Photomicrogaph in air, reflected light - X 250)

A)

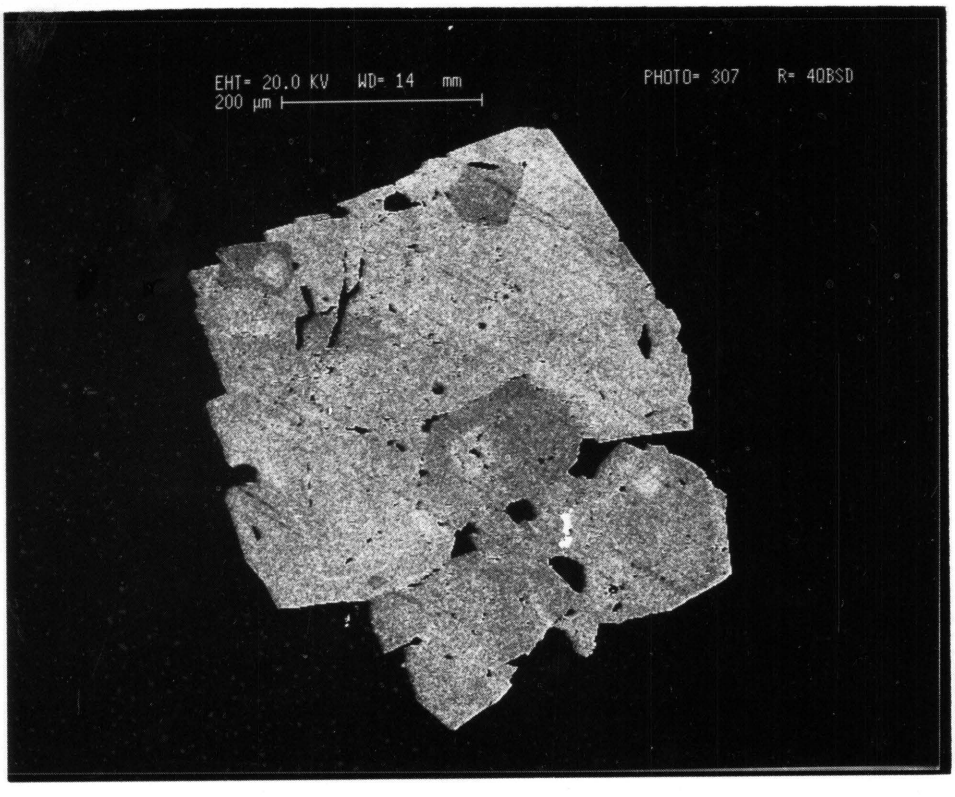

B)

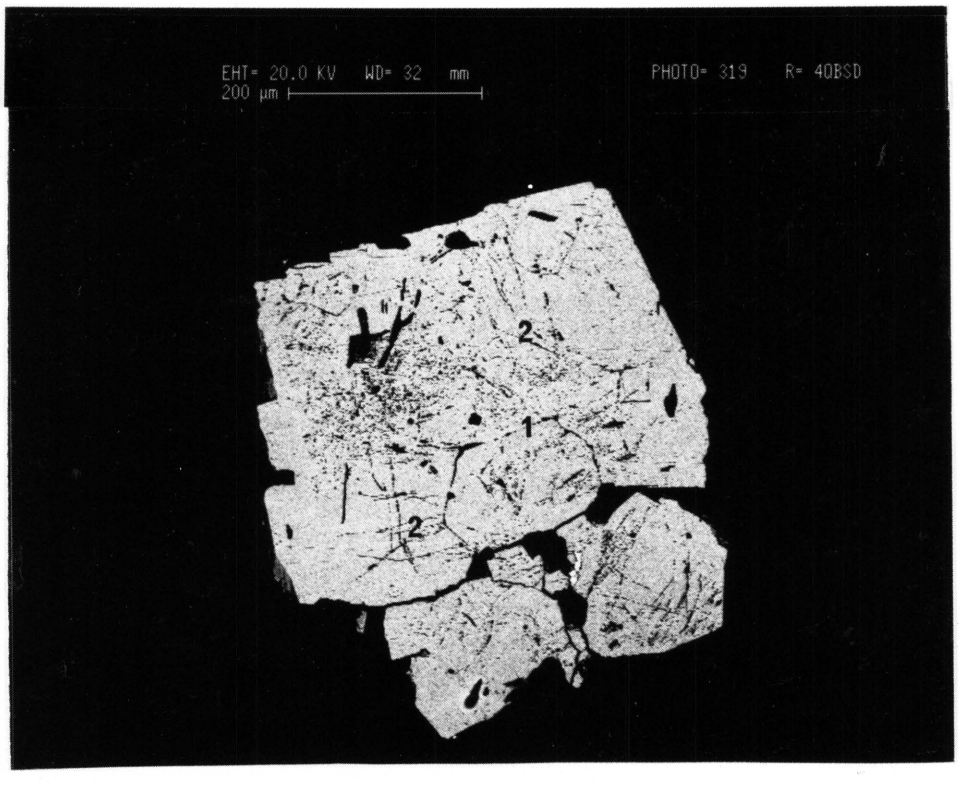

Figure 81: A single pyrite crystal: A) - before leaching and B) - after bioleaching of 10 hours - dissolution channels are visible (1) along the contacts between compositionally diverse regions and (2) along former cracks - RC 1056 (electron backscatter image)

After 24 hours of bacterial oxidation the first generation of pyrite exhibited extensive pit formation (Figure 82). These pits have dimensions of approximately 2μm. Few dissolution pits were present in the secondary overgrowth. After 36 hours of bacterial leaching this preferential leaching of the first generation pyrite continued (Figure 83). The second generation pyrite overgrowths exhibit the formation of dissolution channels only, with few pits. The contacts between extensively leached areas and unleached areas are distinct, defined by an abrupt change in the concentration of dissolution pits, as is evident from Figure 84. The shape of the pits in the centres of the pyrite crystals is shown in Figure 85. The pits are square-shaped with average diameters smaller than 1 μm, and have identical orientations.

The peripheries of the pyrite particles were oxidized by bacteria only after extended leaching times. Thus, after 4 days of bacterial leaching, evidence of dissolution (pit formation) occurred in these secondary overgrowths. The leaching pits that developed, however, were elongated in one direction and were rectangular in outline. This is in contrast to the square leaching pits that formed in the centres of the crystals. In Figure 86 both square and rectangular pits can be seen on opposite sides of the contact between the two generations of pyrite. The parallel orientation of the elongated rectangular pits, is illustrated in Figure 87. Further bacterial oxidation led to the development of crude hexagonal dissolution pits within unleached areas, as is evident from Figure 88.

Variations in the shape of the dissolution pits are generally correlated with different pyrite generations, but it appears that the orientation of a certain part of the crystal will determine the shape of dissolution pit that will be developed. This variation in the form of the dissolution pits, therefore, indicates that the different pyrite generations differ in their crystallographic direction.

Pyrite crystals, which had already undergone one cycle of leaching, were bacterially oxidized for additional periods. During this further cycle of leaching, small dissolution pits (1 μm in diameter) formed within the pre-existing deeper and larger (5μm) dissolution pits, as is evident from Figure 89. This indicates that during bacterial oxidation pits increase in size, in both a lateral and vertical direction. Although the rate of oxidation may not be the same in all the crystallographic directions, leaching still continues in all directions. This is in contrast to the proposals of Southwood and Southwood (1985), who concluded that leaching is confined to the leading face (closed end) of dissolution pores within the pyrite, while no oxidation of the walls take place.

Figure 82: The effects of bacterial leaching on massively intergrown pyrite crystals: after 24 hours extensive pitting and dissolution channels are visible in the centres of individual crystals, while the margins of the crystals are relatively free of leaching effects - RC 1005 (electron backscatter image)

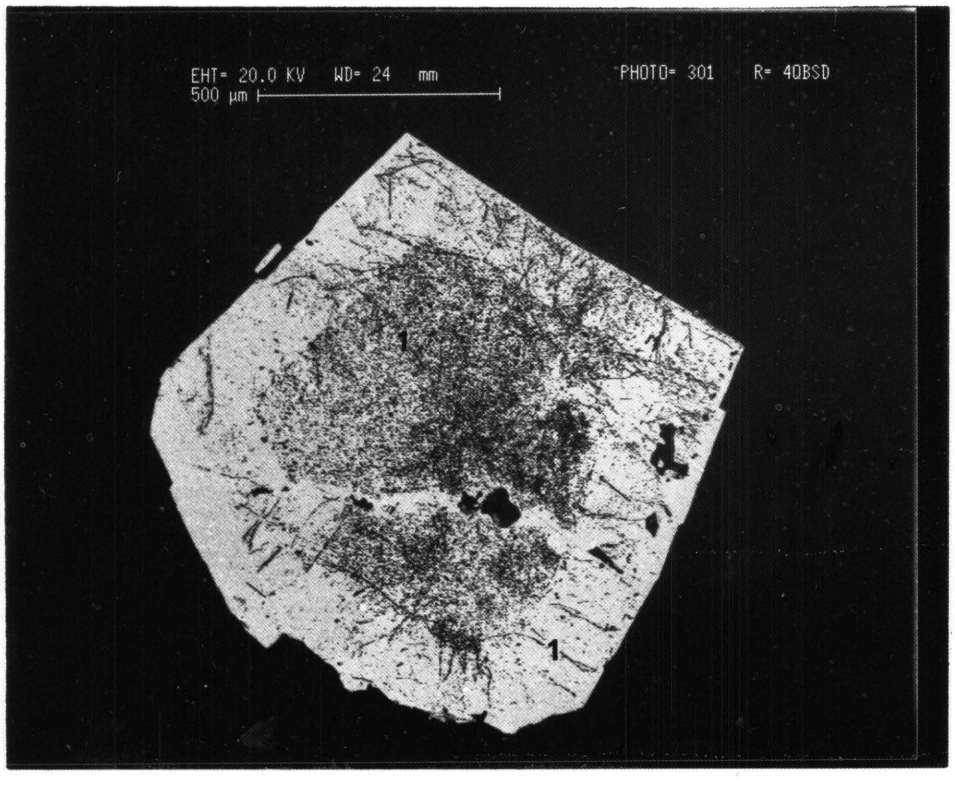

Figure 83: A bacterially leached pyrite crystal (after 36 hours) exhibits the following leaching features: (1) dissolution channels along former cracks throughout the crystal and extensive pit development in the centre of the crystal only - RC 1005 (electron backscatter image)

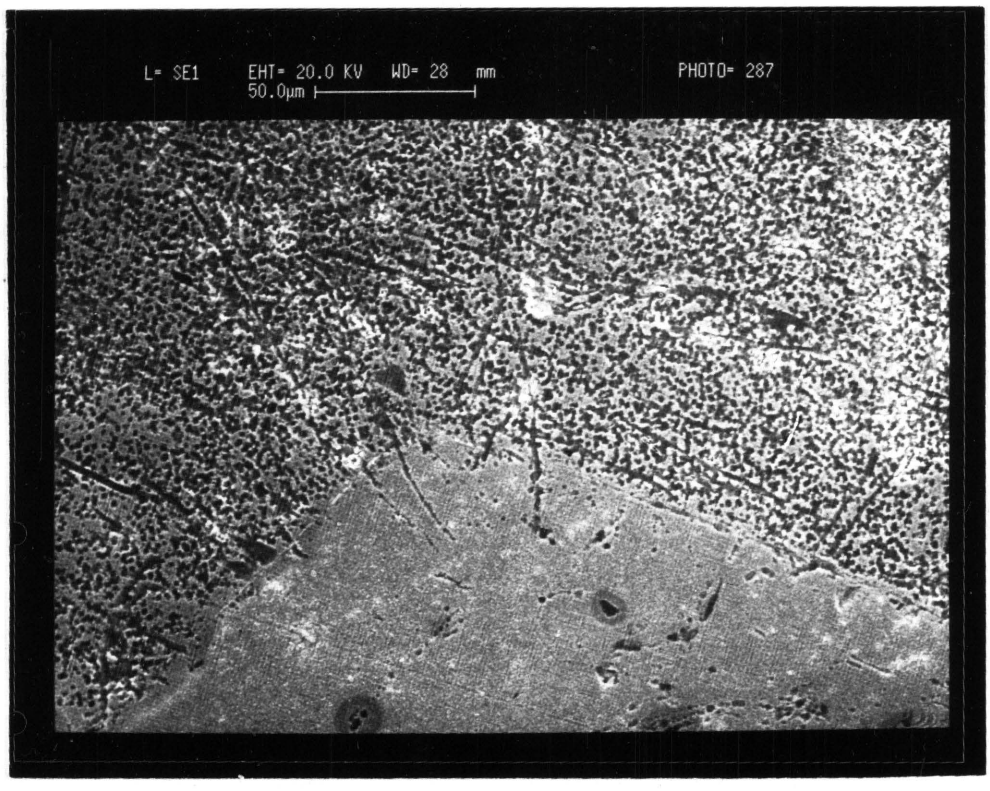

Figure 84: A leached pyrite crystal (after 48 hours), displaying the contact between an extensively leached area (pitted) and an unleached region: the difference in leaching behaviour appears to be due to the crystallographic orientation of the pyrite in the two areas - RC 1005 (electron backscatter image)

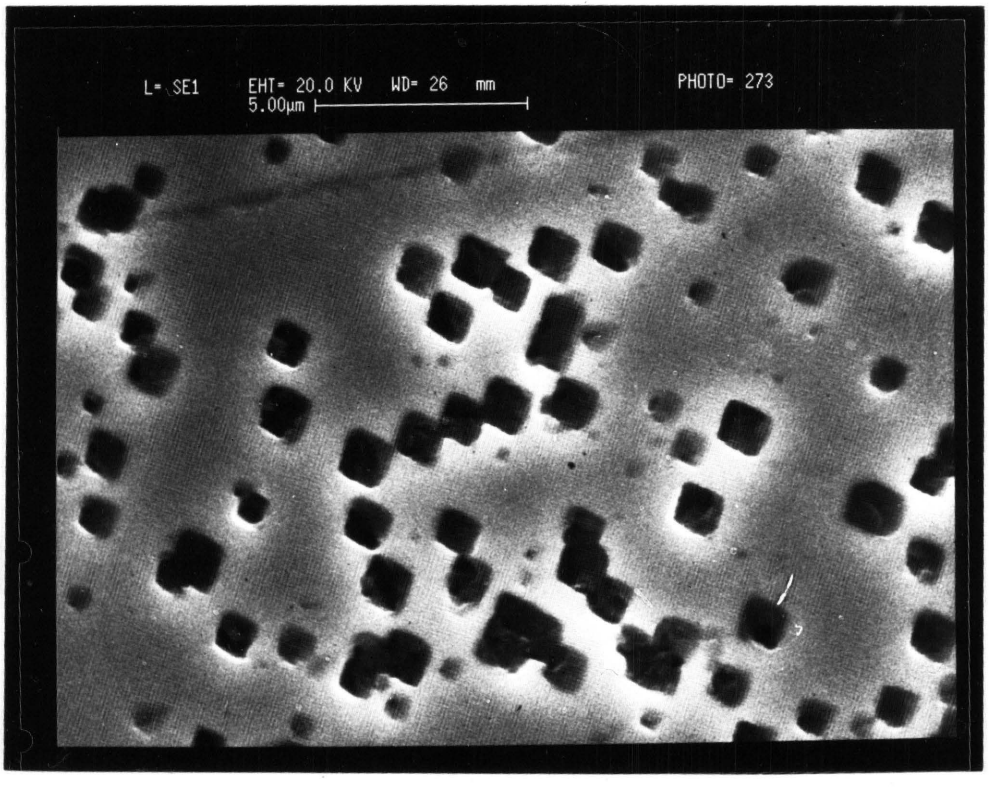

Figure 85: A pyrite crystal, after 3 days of leaching: the square nature and parallel axial orientation of dissolution pits are apparent. - RC 1005 (electron backscatter image)

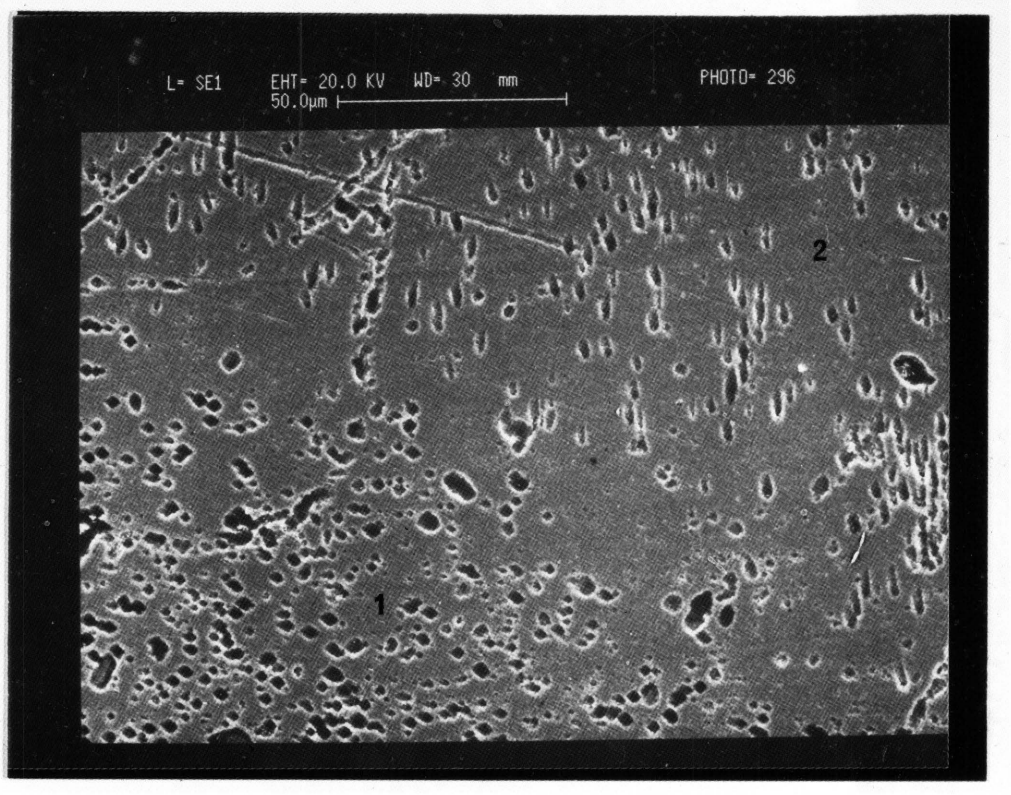

Figure 86: A leached pyrite crystal (after 4 days): two distinct orientation directions are apparent. They are defined (1) by square pits and (2) by elongated pits - RC 1056 (secondary electron image)

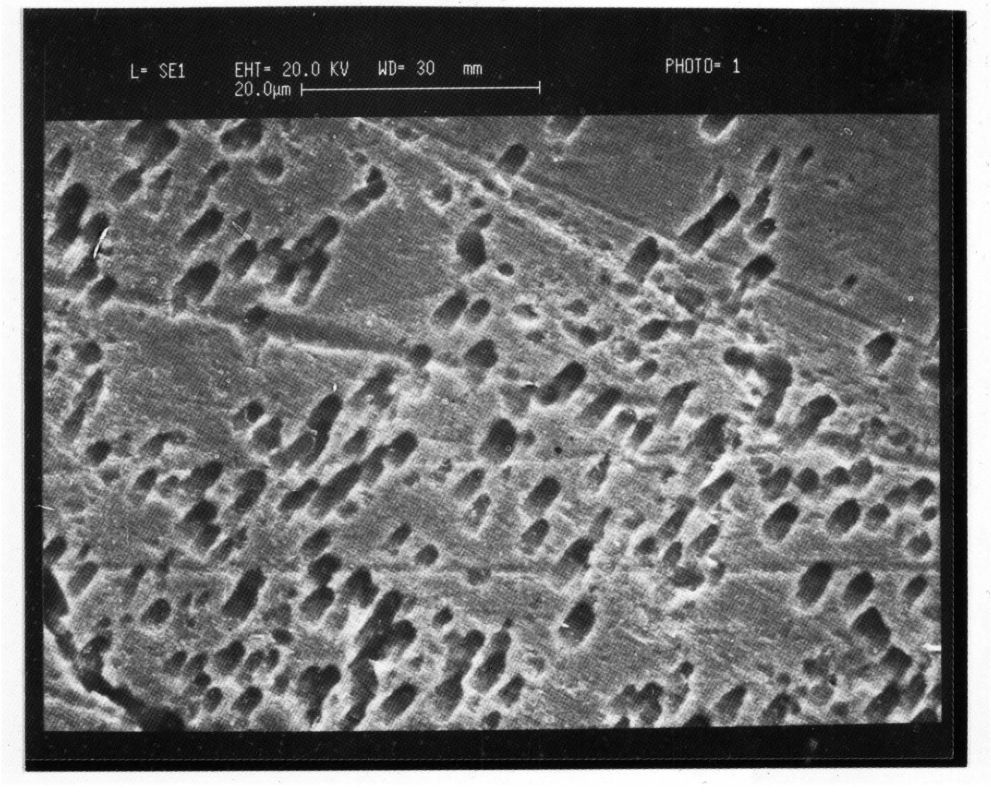

Figure 87: A leached pyrite crystal surface, exhibiting the rectangular nature and parallel axial orientation of the dissolution pits - RC 1056 (secondary electron image)

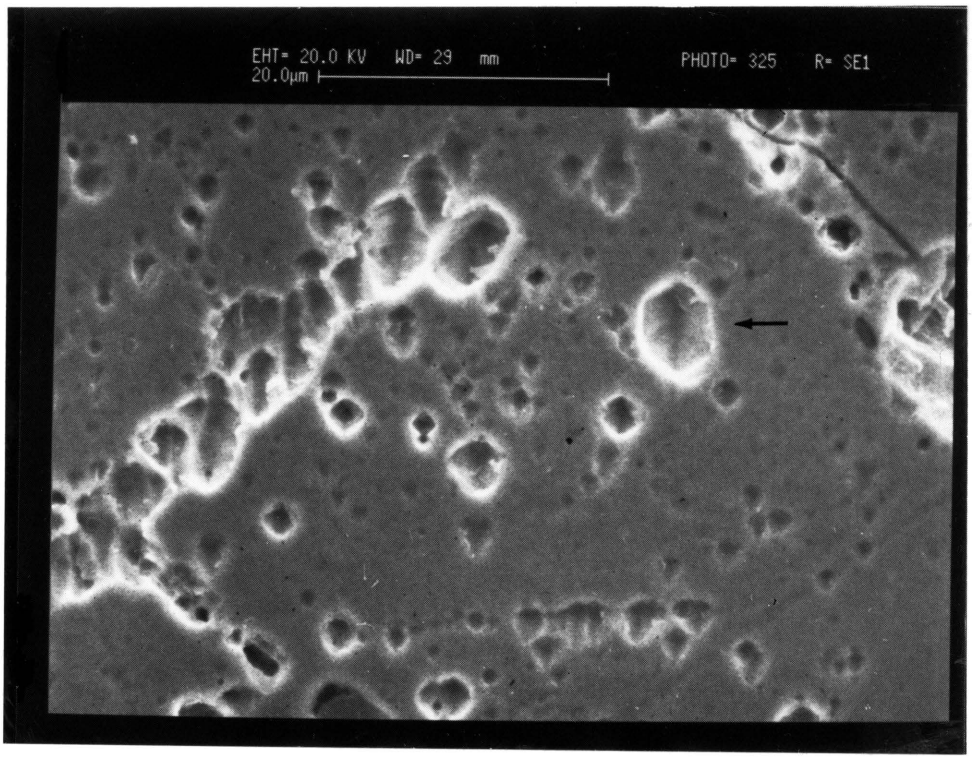

Figure 88: A pyrite crystal after 9 days of leaching, shows an approximately hexagonal leaching pit (arrow - RC 1056 (secondary electron image)

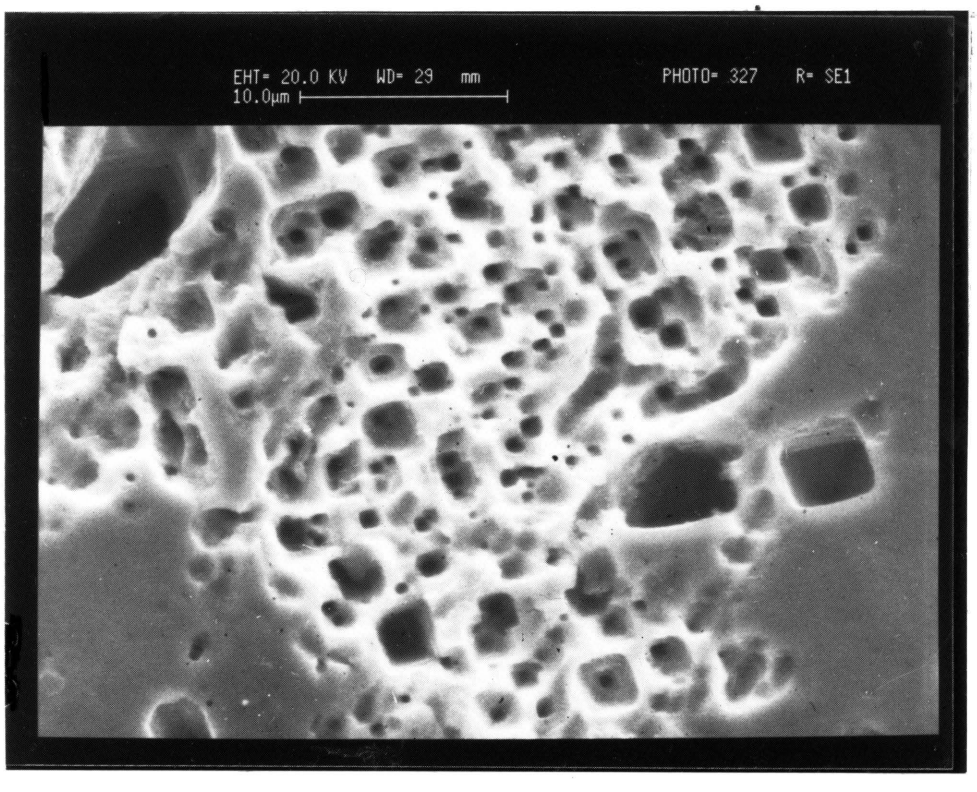

Figure 89: A pyrite crystal after 9 days of leaching (more than one cycle): lateral growth of the pits is illustrated by the presence of small incipient pits, within larger pre-existing dissolution pits - RC 1005 (secondary electron image)

It is not only the orientation that plays a role during bacterial leaching of Agnes pyrite crystals. Figure 90 shows unequivocally that the composition of the pyrite has a direct influence on the rate of bacterial oxidation. From the high concentration of dissolution pits in the As-rich regions, and low concentration in the As-poor regions, it is evident that the As-rich areas are leached at a higher rate than the As-poor regions. The variation in pit-concentration between As-rich and As-poor zones, is also evident from Figure 91.

The effect of compositional zoning on the bacterial leaching of the pyrite crystals, is also illustrated in Figure 92. A variation in the pit- concentrations renders the zoning discernible. It is important to note that the orientation of the pits is the same in all the zones. Thus, the leaching of certain zones at a higher rate than the others is in this case due to the effect of composition, and not to the effect of crystallographic direction.

The liberation of gold particles from the pyrite crystals during bacterial leaching, took place during the early stages of pyrite oxidation, when dissolution channels formed along pre-existing cracks, which cut randomly across the crystal faces, at the contact between pyrite domains of different composition or of different generations, and around inclusions, thereby liberating gold inclusions. The preferential oxidation of the As-rich (Au-rich) zones in the zoned pyrite during bacterial leaching resulted in an enhanced recovery of submicroscopic gold, while later stage oxidation of the As-poor zones resulted in a drop in gold recovery. Thus, during the early stages of sulphide oxidation, the liberation of gold was enhanced, but further liberation of gold took place more or less proportionately to the degree of oxidation of the pyrite.

The presence of dissolution pits is the most significant leaching characteristic observed on the pyrite crystal surfaces. Bennet and Tributsch (1978) and Hansford (1986) also observed dissolution pits on the surface of pyrite crystals.

To explain the various dissolution figures, the crystallographic features of the pyrite crystal should be considered. Pyrite crystallizes in the cubic system and belongs to the class $\frac{2}{m}3$. This class contains three diad axes perpendicular to three mutually perpendicular planes of symmetry, four triad axes and a symmetry centre.

A)

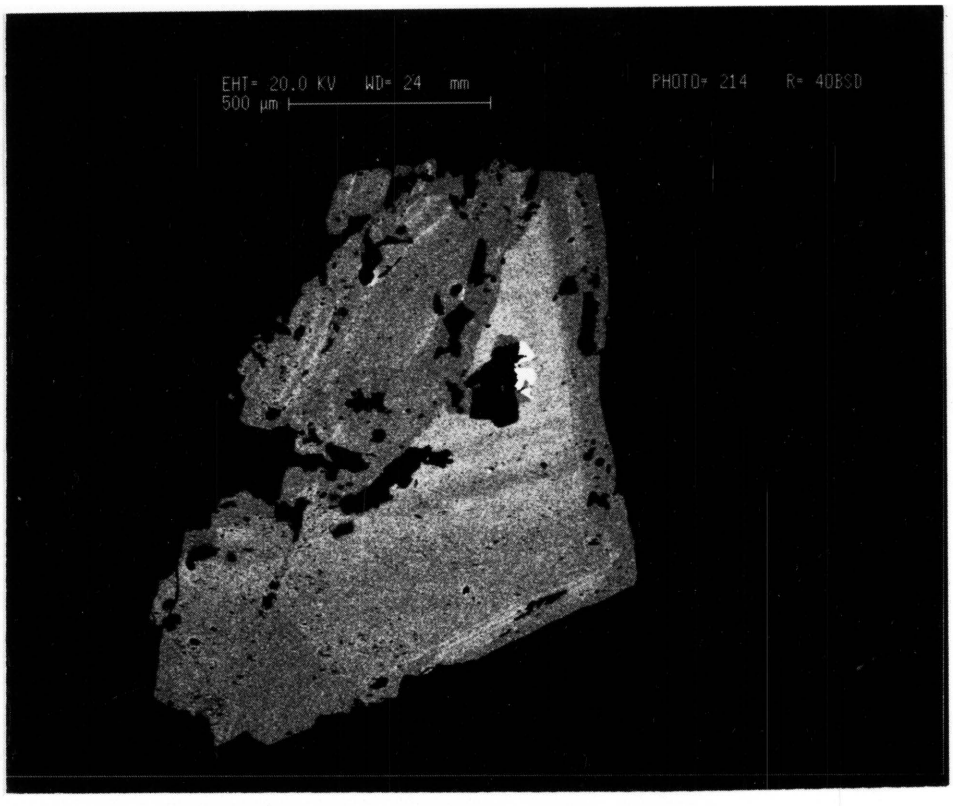

B)

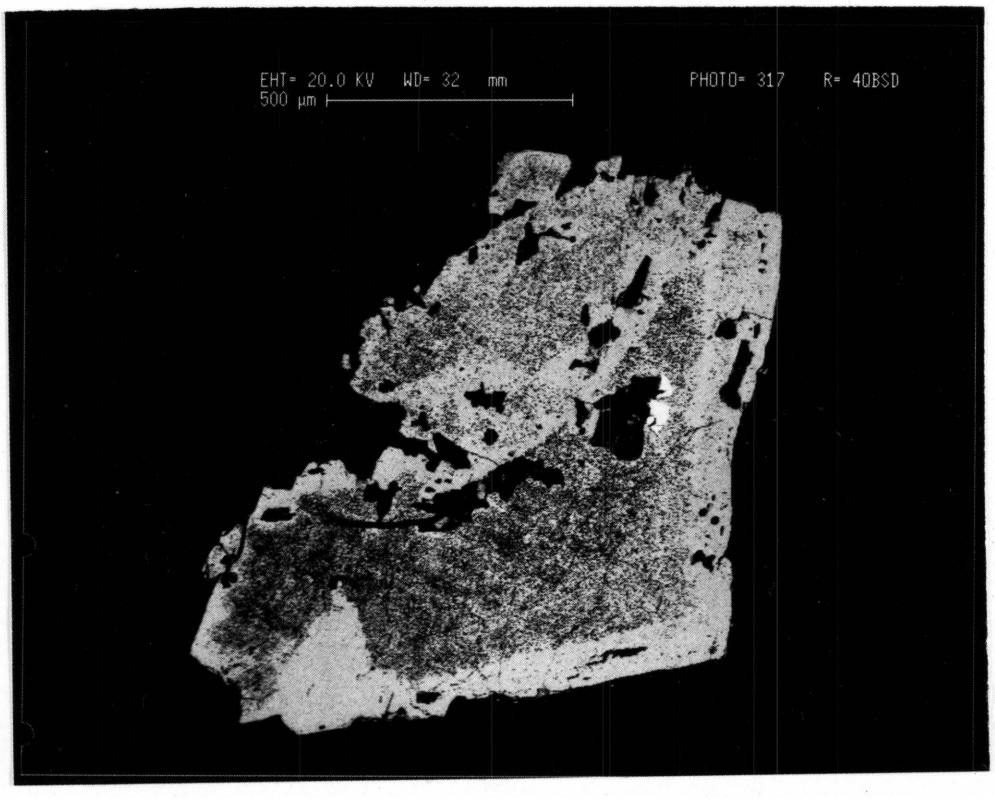

Figure 90: An individual pyrite crystal: (A) before leaching and (B) after bacterial leaching for two days: the influence of composition is shown by extensive pitting within the As-rich areas - RC 1056 (electron backscatter image)

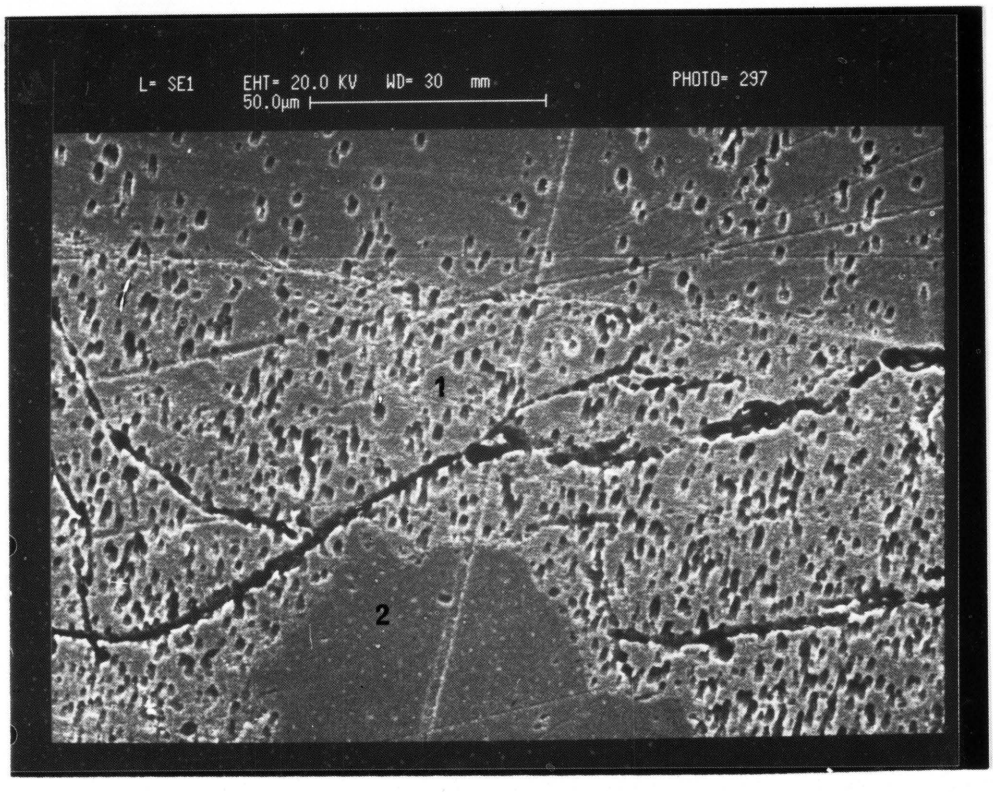

Figure 91: A bacterially leached pyrite crystal, showing abundant pit development within the As-rich first generation pyrite (1), while few dissolution features are present in the second generation (2) - RC 1005 (secondary electron image)

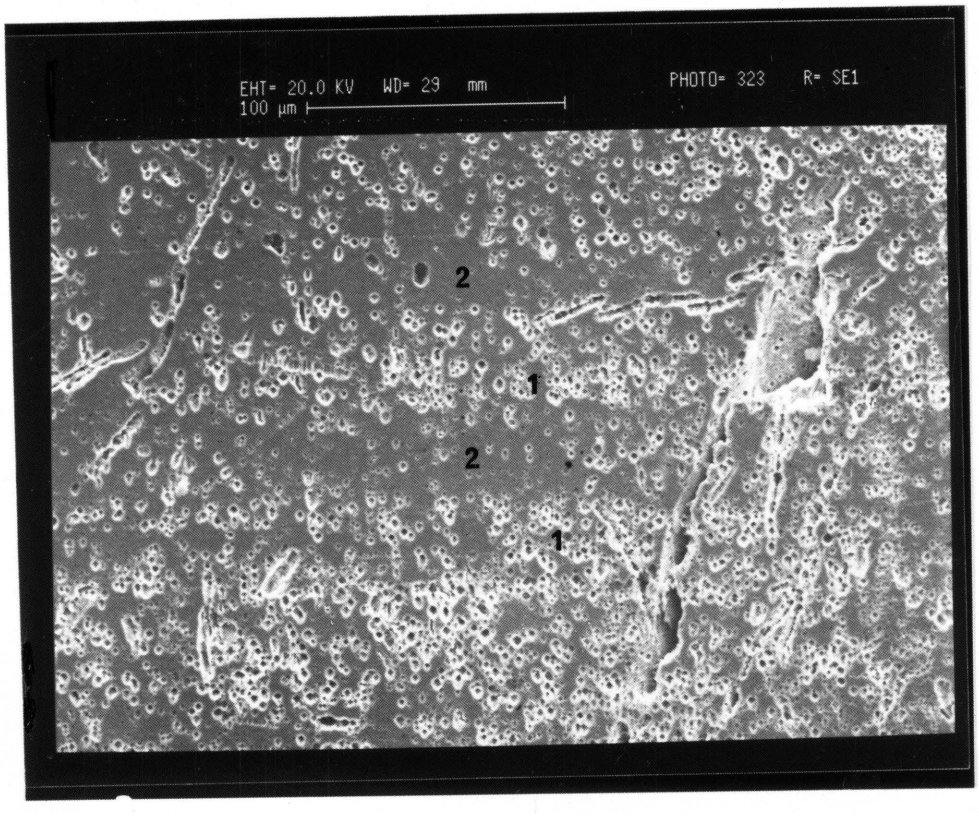

Figure 92: A leached pyrite crystal, exhibiting dissolution channels along former cracks, as well as pitting. Zoning is displayed by a variation in pit-intensities: the As-rich zones (1) containing more pits than the As-poor zones (2) - RC 1056 (secondary electron image)

According to Phillips (1963), when a crystal is attacked by a suitable solvent the initial dissolution often takes place in a manner which is visibly related to the underlying structure, thus forming etch pits. The particular shapes of the pits are partly dependent on such factors as the nature of the solvent and its concentration, but their symmetry and their attitude on different crystal faces may be considered an indication of the symmetry of the underlying structure (Phillips, 1963). However, the nature of the solvent used by the bacteria to dissolve the sulphides is still not adequately established, but the symmetry of the underlying structure can be considered in an attempt to explain the pit outlines and patterns.

Square pits probably resulted from dissolution restricted by planes of the cube {100}. However, the face symmetry of a cube in pyrite only contains a diad axis and two planes of symmetry. Therefore, theoretically these dissolution pits cannot be square and should rather be termed *pseudo-square.* Rectangular and slightly distorted pits possibly developed on the surfaces which cut the cube planes obliquely. The hexagonal pits most probably formed on the octahedron {111} faces which are perpendicular to the triad axes. These pits will therefore probably be bounded by planes of the rhombic dodecahedron {110} and the icositetrahedron {*hll*} (possibly {311}) (Phillips, 1963).

As shown already, square-shaped pits were initially formed during the bacterial oxidation of the pyrite crystals. Only after longer leaching time, did rectangular leaching pits develop, indicating that dissolution occurs more easily along the crystallographic direction parallel to the {100} planes. It is anticipated that leaching perpendicular to the (111) planes, i.e. closed-packed array in the cubic system, is much more difficult, and that explains why prolonged residence times are required to form hexagonal dissolution pits. Thus, the orientation of the exposed pyrite crystals seems to play a role in the distribution and the nature of the bacterial leaching features. However, further detailed work using orientated crystals should be performed to determine the role of crystallographic direction with respect to the rate of bacterial activity.

The distribution pattern and form of bacterial dissolution pits on the surface of the pyrite crystals are important indicators of the factors controlling the bioleaching of pyrite. The As-rich areas, in general, contain more leaching features per unit area than the As-poor regions, as a result of a more rapid rate of oxidation. Thus, selective and preferential leaching of the As-rich areas took place. Grain boundaries, contacts between domains of diverse composition, cracks, etc. were also preferential sites of bacterial attack. Dissolution pits vary in shape from square, rectangular, hexagonal to inclined elongated pits. These different forms of pits, suggest that the crystal face being attacked, is important.

These results indicate that the bacterial leaching rates are affected by crystal and chemical deviations from the ideal sulphide crystal structure.

6.3 RESULTS OF ACID FERRIC SULPHATE LEACHING

6.3.1 New Consort Arsenopyrite

The loellingite inclusions within New Consort arsenopyrite reacted rapidly during the initial stages of acidic leaching. After only 3 hours of oxidation (at 15 g/l [FeIII]), the loellingite inclusions were extensively leached. Figure 93 (A) shows loellingite inclusions within arsenopyrite before leaching, and Figure 93 (B) displays the same crystal after 3 hours of acid leaching. Extensive dissolution pits (< 1 μm in diameter) are visible on the surface of the loellingite particle. The arsenopyrite enclosing the loellingite inclusion however, displays no evidence of leaching.

After increased leaching times, the arsenopyrite still did not exhibit any chemical leaching features, but additional dissolution of the loellingite inclusions had occurred. After 36 hours of sterile acid leaching the loellingite were leached extensively.

A sterile leaching test, at a ferric iron concentration of 45 g/l, was also performed. After 10 days, the arsenopyrite itself exhibited effects of ferric iron dissolution along former cracks (Figure 94).

It is clear from the above results that loellingite is selectively and rapidly dissolved by this sterile ferric sulphate acid solution. However, for any dissolution of arsenopyrite to take place, a much higher ferric iron concentration, and a longer leaching time, are needed.

The above results indicate that during bacterial leaching tests the leaching of loellingite is considered to be due to the action of the ferric sulphate, which is also present in the bacterial leach solution, and not to direct bacterial activity. However, the bacteria do have an indirect influence by oxidizing ferrous iron to ferric iron, which goes into the bacterial leach solution as ferric sulphate. It is this oxidizing agent which is responsible for the loellingite dissolution. Thus, the leaching of loellingite during bacterial oxidation is indirectly dependent on the presence of bacteria.

A)

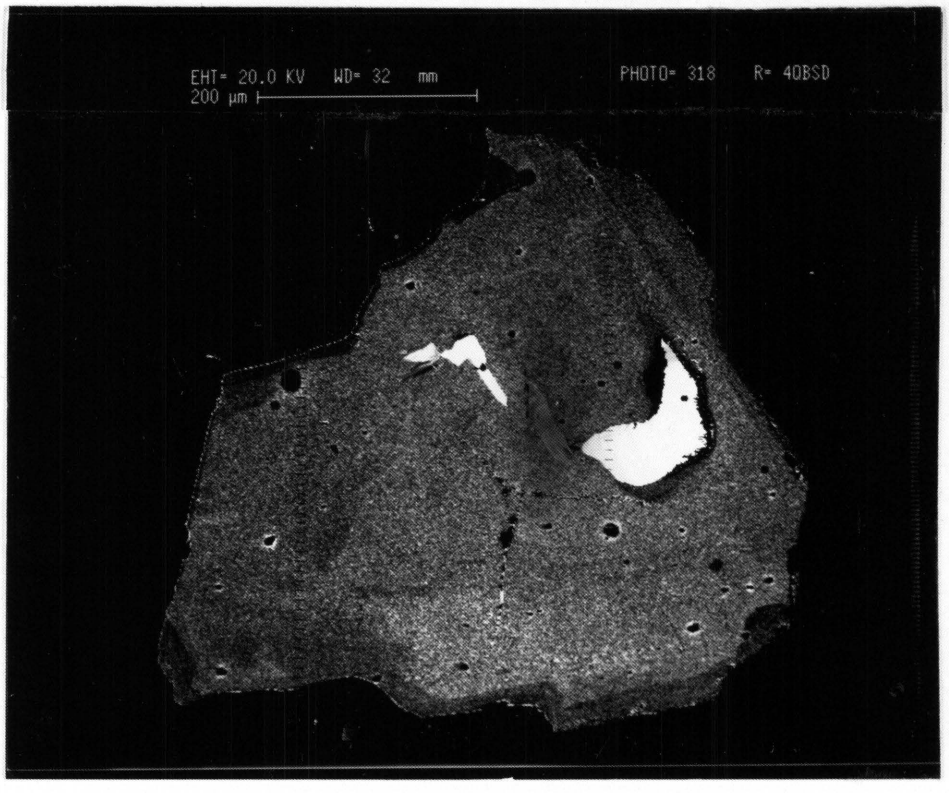

B)

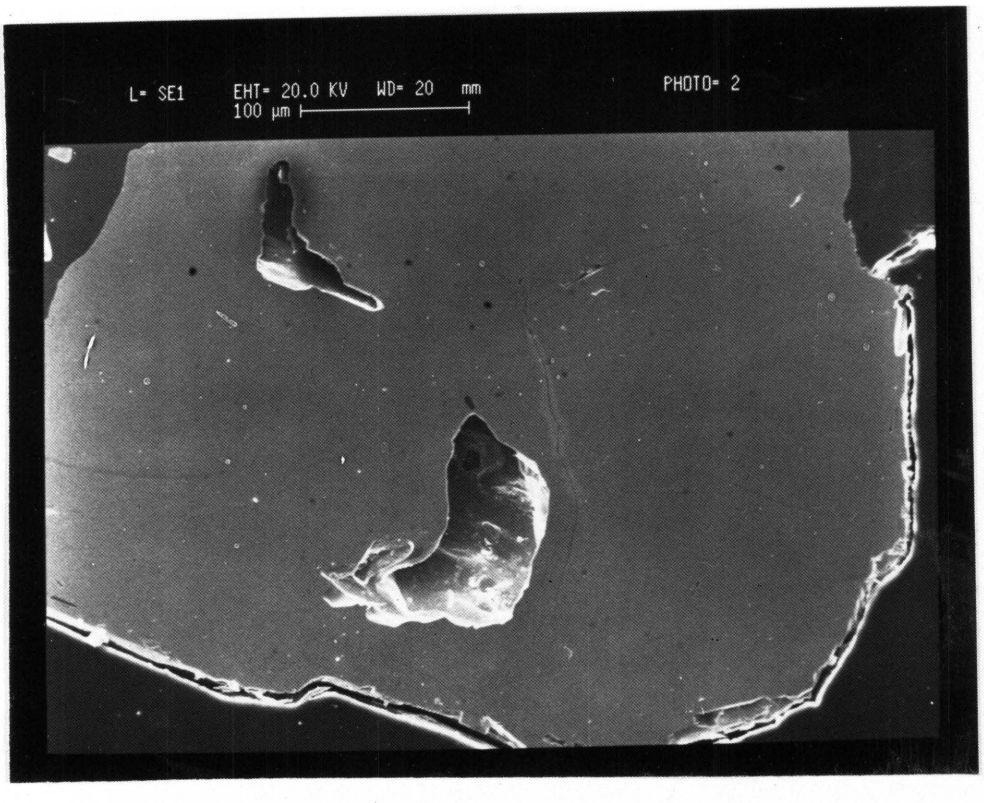

Figure 93: An arsenopyrite crystal: (A) before leaching, containing loellingite inclusions (white) (electron backscatter image), and (B) after three hours of ferric sulphate acid leaching: the preferential dissolution of the loellingite inclusions is apparent - RC 1057 (secondary electron image)

A)

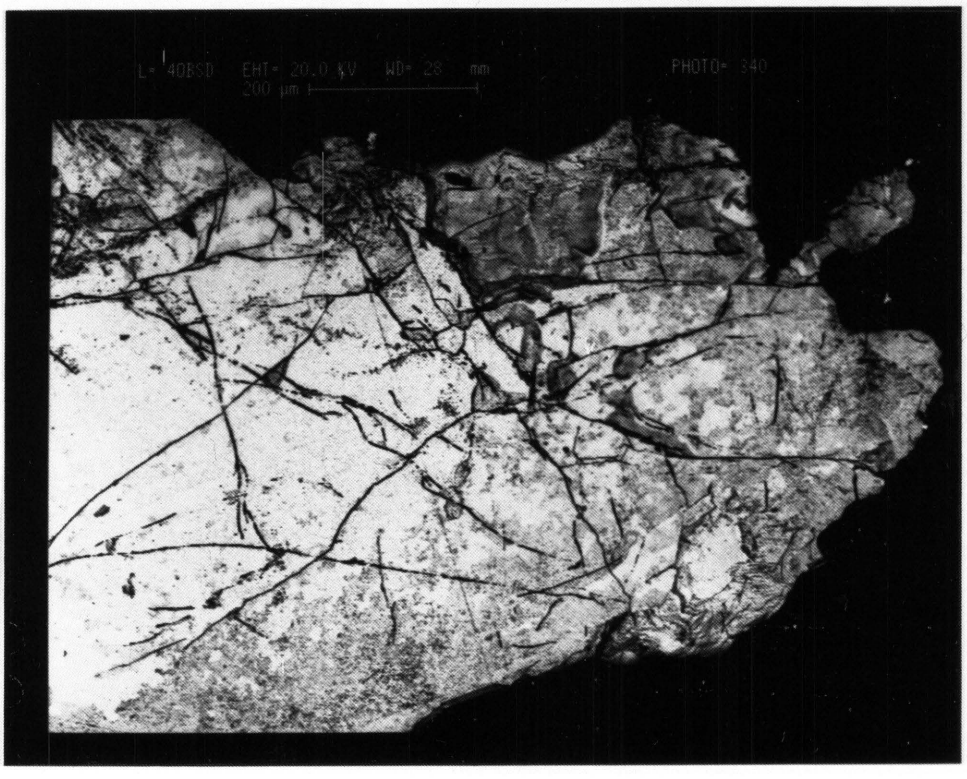

B)

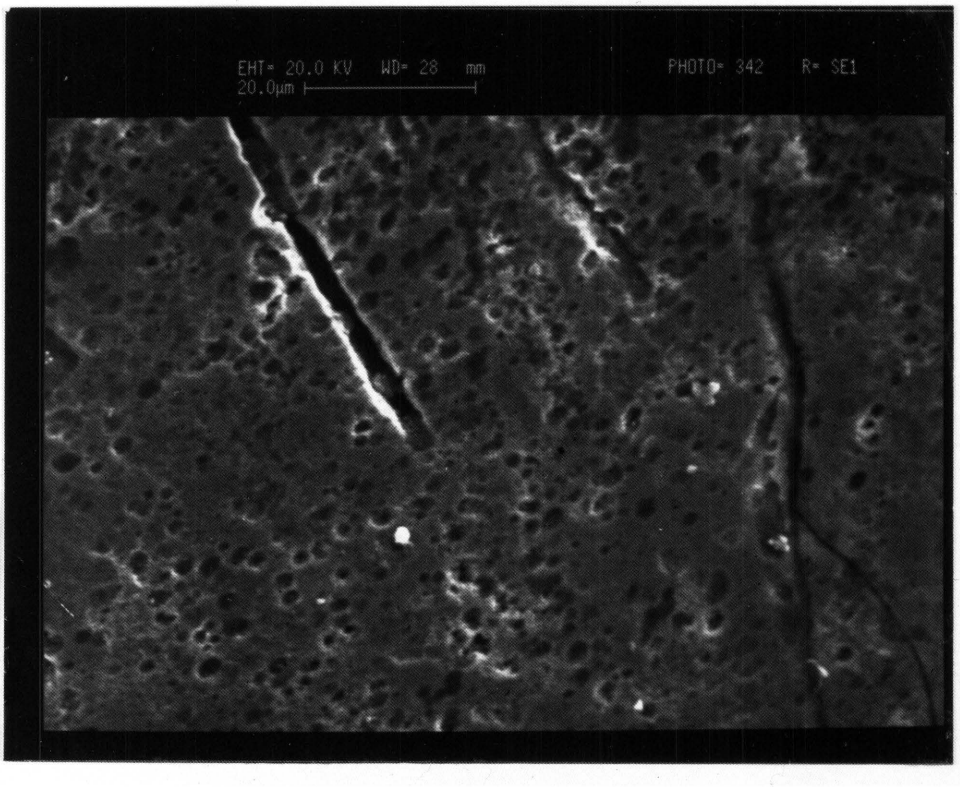

Figure 94: An acid leached arsenopyrite (after 10 days): (A) extensive dissolution has occurred along former cracks, while etch pits have formed along the edges of the particle (electron backscatter image); (B) at higher magnification the nature of the pits and leached channels are visible - RC 1048 (secondary electron image)

6.3.2 Sheba Arsenopyrite

After the initial leaching period of 3 hours no reaction between the zoned arsenopyrite and the ferric sulphate solution (15 g/l [FeIII]) had occurred. With increased leaching time the crystals still remained passive. Even after 24 hours of leaching, the crystals did not exhibit any chemical leaching features.

Due to the inert nature of the arsenopyrite, additional tests were conducted with ferric iron concentrations increased to 30, 45 and finally 60 g/l. This increase in ferric iron concentration resulted in an increase in the acidity of the solution, as is evident from Table III, (previous section).

Only after the crystals were subjected to a sterile solution with a ferric iron concentration of 60 g/l for 10 hours, could the effects of chemical dissolution be observed. Figure 95 (a) shows an arsenopyrite crystal before leaching, and Figure 95 (b) after leaching. Chemical etching can be observed across the entire crystal surface as small etch pits, randomly distributed. The edges of the crystals were also chemically attacked. This resulted in jagged crystal peripheries (Figure 96). Leaching also occurred along former cracks within the crystals. It is significant and important that no selective chemical dissolution of compositionally different zones occurred.

Thus, the ferric sulphate leaching had no significant effect on Sheba arsenopyrite, under conditions similar to those that prevailed during bacterial oxidation.

6.3.3 Sheba Pyrite

The Sheba pyrite crystals were relatively inert during the ferric sulphate sterile dissolution tests. Only at 45 g/l ferric iron concentration after 10 days, did any dissolution effects develop. In these crystals dissolution occurred mainly along former cracks in the pyrite (Figure 97).

With enhanced leaching times, dissolution continued along the cracks, while the surfaces of the pyrite crystals were unaffected.

A)

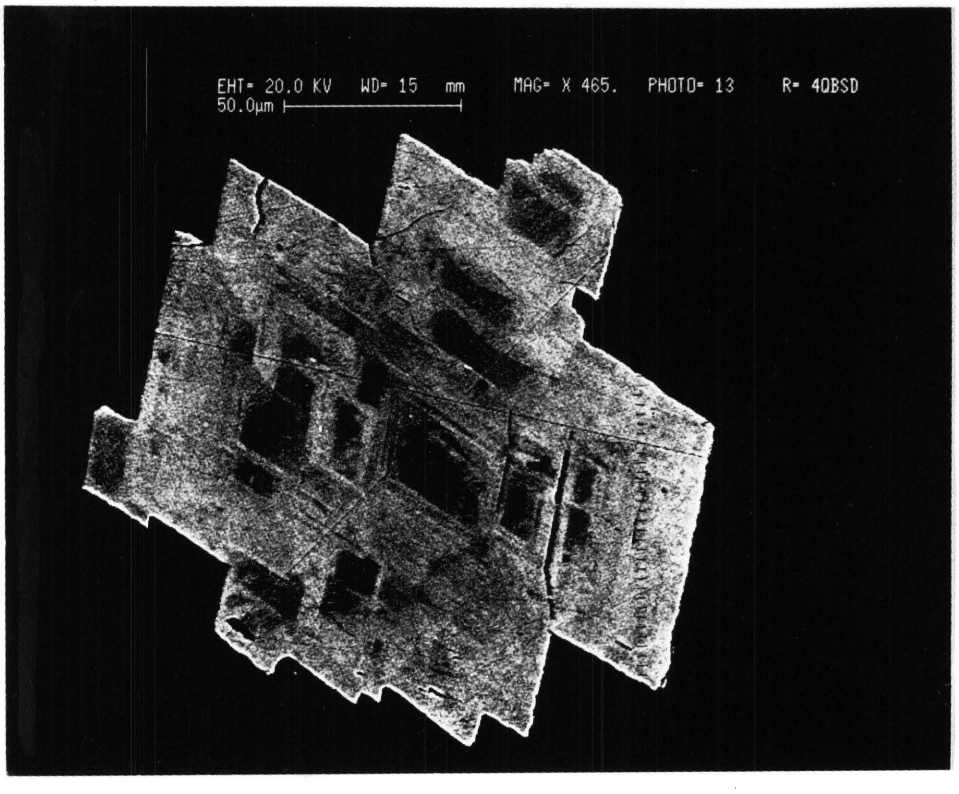

B)

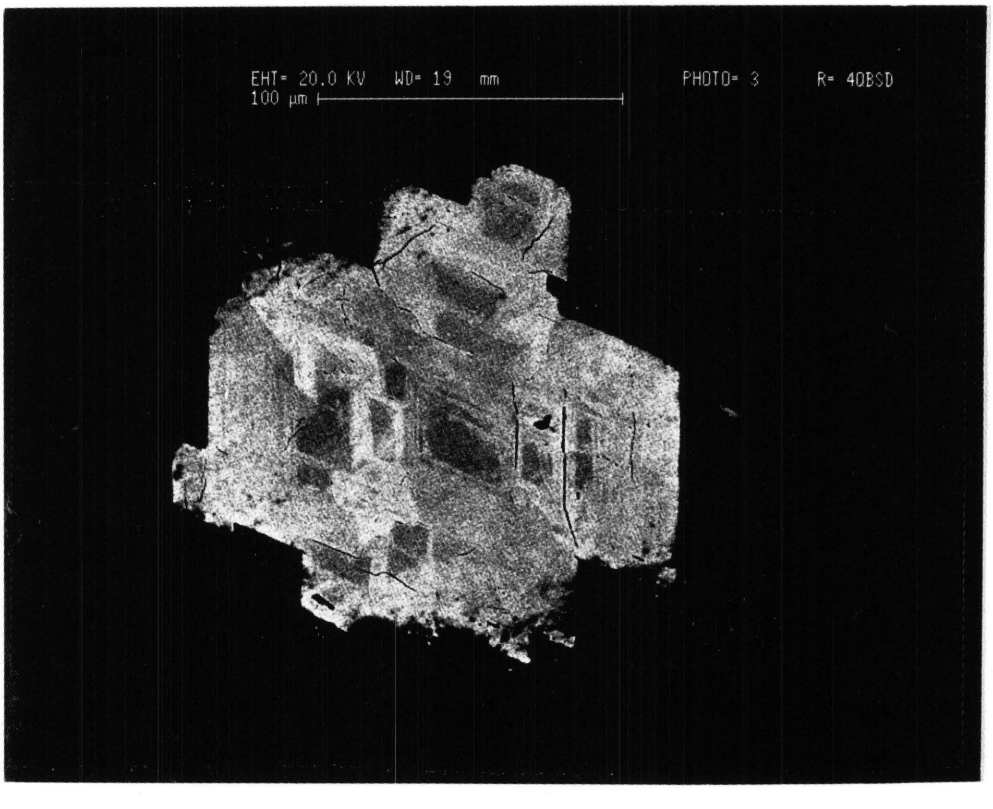

Figure 95: A zoned Sheba arsenopyrite crystal: (A) - before and (B) - after 10 hours of leaching in a 60 g/l sterile ferric sulphate solution: jagged edges of the leached crystal are visible - RC 1009 (electron backscatter image)

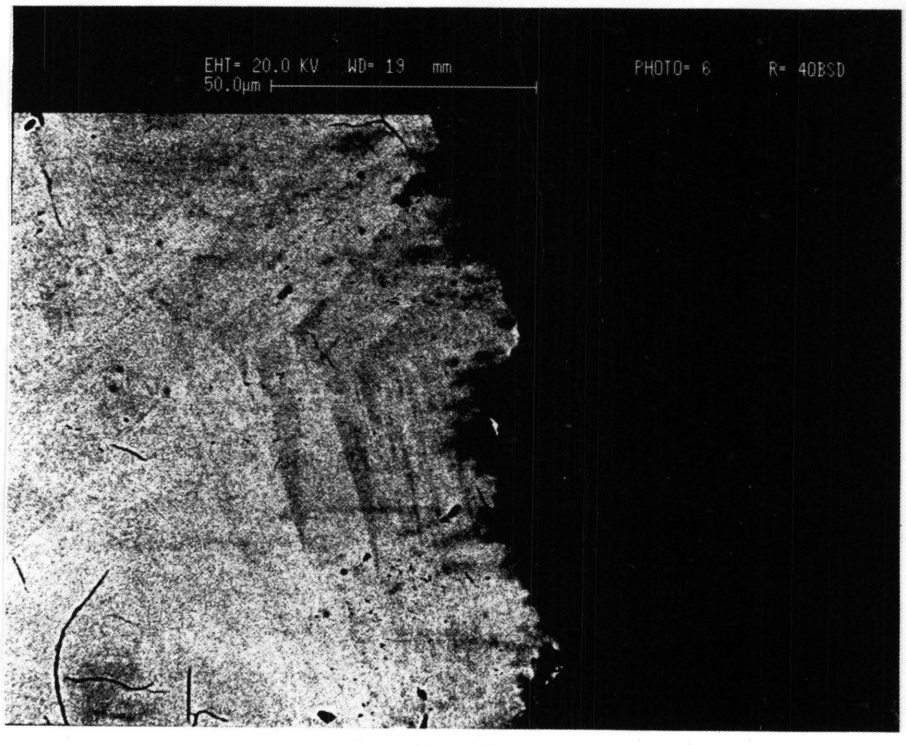

Figure 96: Details of the jagged edge of the arsenopyrite crystal shown in Figure 96 - RC 1009 (electron backscatter image)

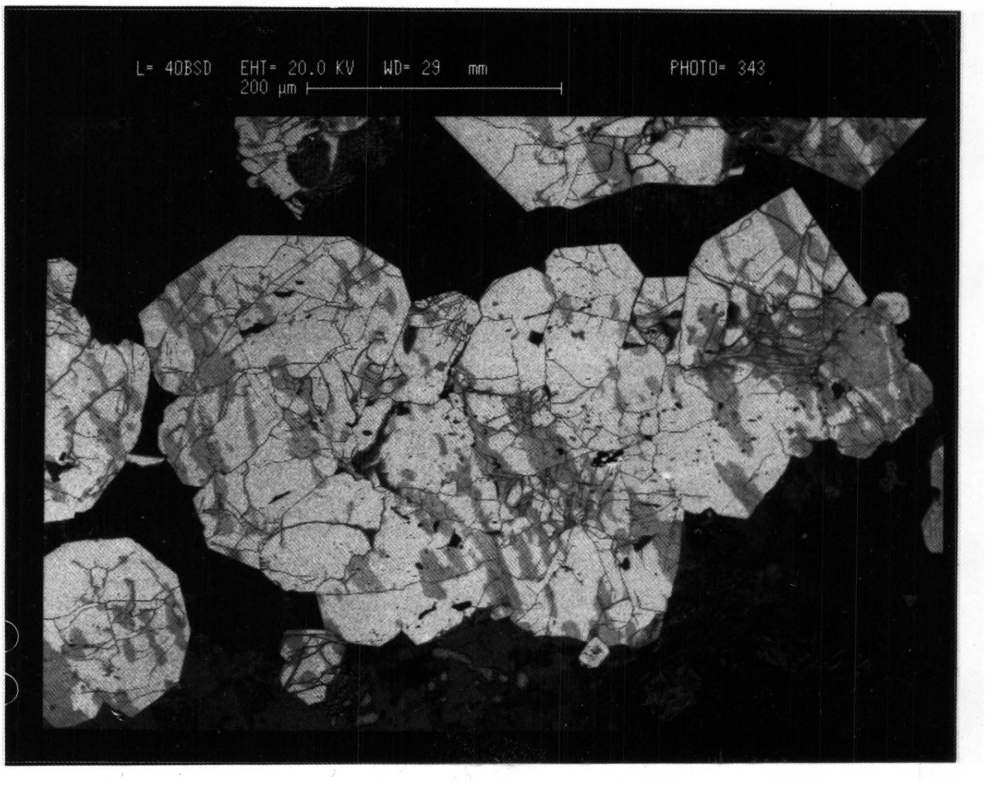

Figure 97: An acid leached pyrite crystal, exhibiting dissolution mainly associated with cracks - RC 1040 (electron backscatter image)

6.3.4 Agnes Pyrite

The pyrite crystals from the Agnes mine were not chemically leached during the initial (15 g/l [FeIII]) sterile control ferric sulphate tests. However, at higher ferric iron concentrations of 45 g/l and a dissolution time of 10 days, some dissolution effects developed (Figure 98). The core of the crystal displayed pitting, due to the development of square-shaped etch pits. The intermediate zone showed sporadic occurrence of elongated etch pits (Figure 99), while the edge of the crystal is extensively dissolved (Figure 100).

It is interesting to note that the etch pits that formed had a similar shape and distribution to those that developed during bacterial leaching .

With an increase in sterile leaching, enhanced dissolution occurred along the edges of the crystals. Additional etch pits developed within the centre of the crystals. However, the main effect in the sterile solution was along the former cracks and on the rims of the crystals.

In summary, under the normal conditions that prevail during bacterial leaching, ferric sulphate leaching had no effect on the pyrite crystals. Only with extended leaching periods and highly concentrated leach solution, did ferric sulphate dissolution features develop on the Agnes pyrite surfaces.

A)

B)

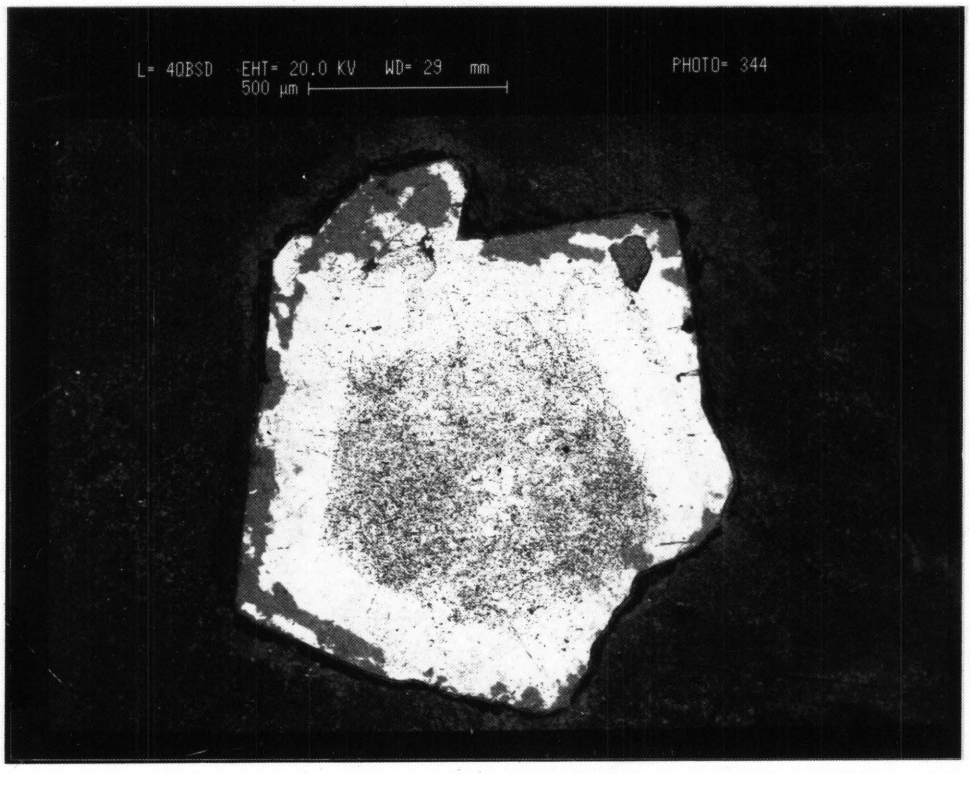

Figure 98: (A) - A pyrite crystal consisting of an As-rich core (1), an As-poor intermediate zone (2) and an As-rich rim (3) (B) - After 10 days of sterile acid leaching: the core shows the development of abundant square etch pits, sparse elongated etch figures occur in the intermediate zone, and the rim is extensively leached - RC 1004 (electron backscatter image)

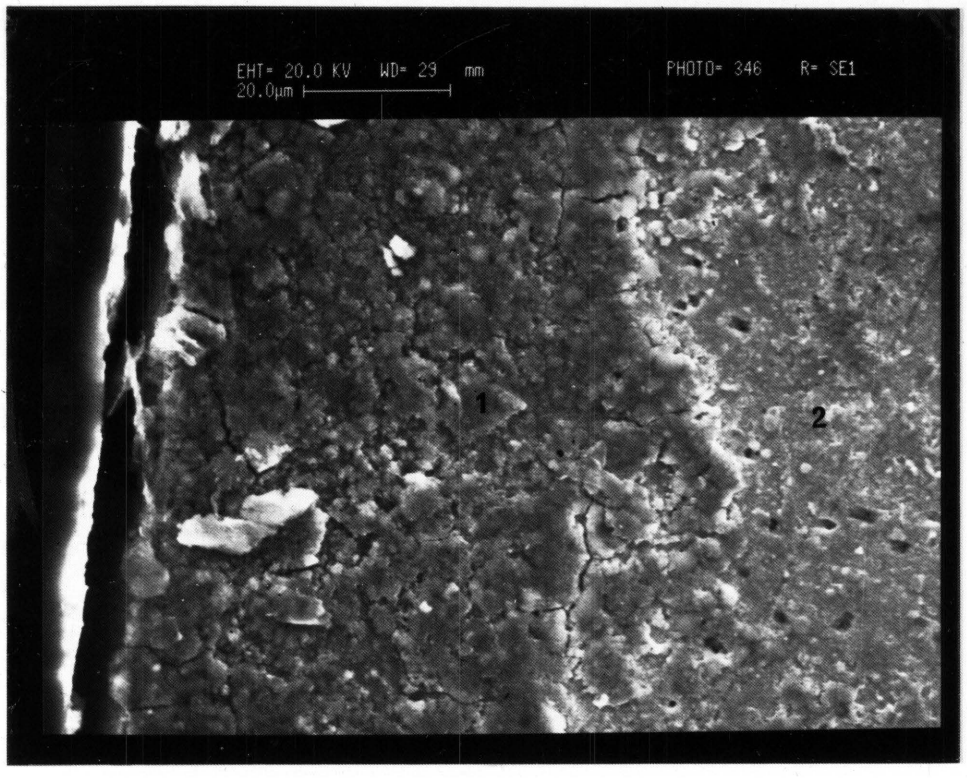

Figure 99: The edge of the crystal shown in Fig. 98: extensive dissolution and disintegration within the crystal edge (1) is visible, while only pit formation is observed in the adjacent intermediate zone (2) - RC 1004 (secondary electron image)·

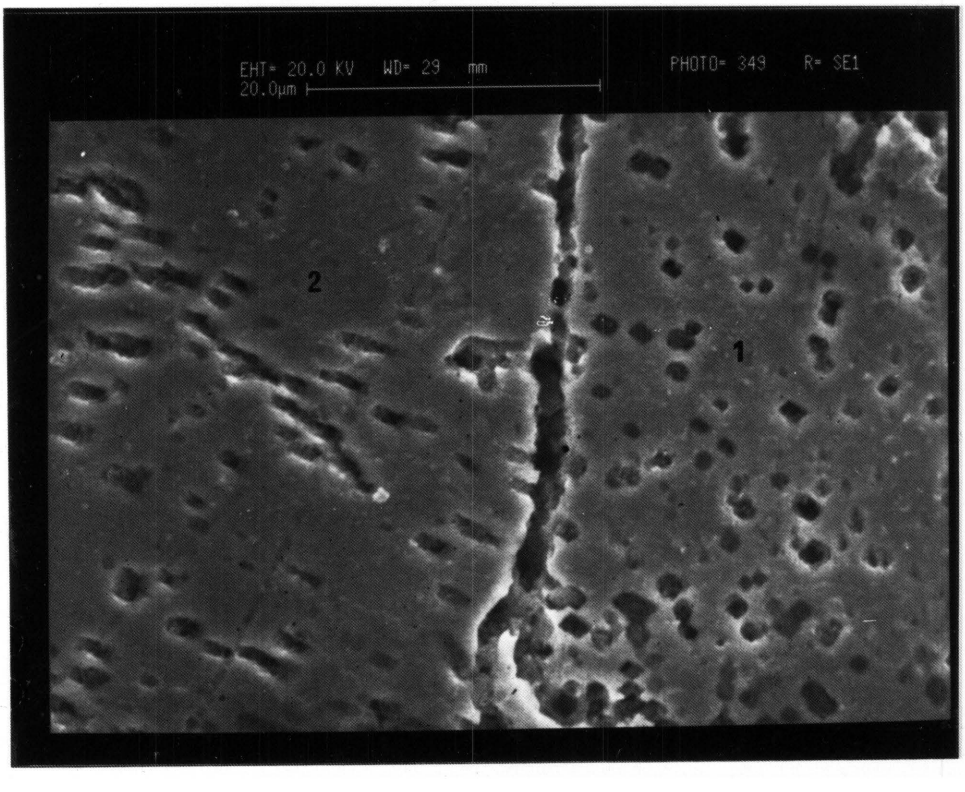

Figure 100: A sterile acid leached pyrite crystal (after 10 days): two distinct orientation directions are apparent. They are characterized by (1) by square etch pits and (2) by elongated etch pits. RC 1004 (secondary electron image)

6.3.5 Discussion of acid ferric sulphate leaching

The investigation of the ferric sulphate leaching of sulphides was conducted to establish whether the oxidation of sulphides during bio-leaching is a result of direct attack by bacteria, or wether it is merely due to leaching by ferric sulphate, which is present in the bacterial solution.

During ferric sulphate leaching tests, the New Consort arsenopyrite exhibited dissolution features, only at very high ferric iron concentrations (60 g/ℓ), much higher than those present in the bacterial leaching tests (15 g/ℓ). This indicates that the leaching of the New Consort arsenopyrite during biooxidation is predominantly the result of direct bacterial activity.

Similarly, no chemical leaching of the Sheba arsenopyrite, Sheba pyrite and Agnes pyrite occurred under sterile conditions. This is contrary to the proposals of several scientists, such as Karavaiko *et al.* (1977), Bennett and Tributsch (1978) and others who suggested the chemical oxidation of sulphides during the bacterial oxidation process

The independent acid leaching tests, using sterile ferric sulphate at the same concentration as is present during bacterial leaching, failed to show any oxidation of the sulphides. Therefore, the leaching of arsenopyrite during bacterial oxidation by *Thiobacillus ferrooxidans* at 30 °C, cannot occur to any great extent as a result of ferric sulphate leaching. This point of view is shared by several other scientists who concluded that ferric sulphate leaching of pyrite (Keller & Murr, 1982; Taylor, *et al.,* 1984; Bärtels, *et al.*,1989) and of pyrite-arsenopyrite mixtures (Norman & Snyman, 1988) during bacterial oxidation is negligible. The results obtained indicate that the concentration of the ferric iron in the bacterial solution is too low to promote a chemical attack on the arsenopyrite or pyrite.

7 DISCUSSION

The results from the previous section will be discussed by a comparison of the different minerals present in the samples and their response to bacterial oxidation tests. However, other important mineralogical factors concerning the bacterial activity were established during the present investigation and will also be dealt with.

7.1 Mineralogical Factors Affecting Bacterial Oxidation

The present investigation demonstrated that a number of mineralogical factors have a significant influence on the mode and rate of bacterial activity. In order to assess their relative importance in controlling the rate of bacterial leaching these mineralogical factors are discussed below.

7.1.1 *Composition*

During bacterial oxidation tests arsenopyrite, in comparison to pyrite, is more rapidly oxidized by bacteria. It is evident from the literature that the sequence of mineral oxidation is determined by their electrode potentials. Arsenopyrite has a lower electrode potential than pyrite Karavaiko, *et al.*, (1986). Therefore, arsenopyrite, being anodic, is preferentially leached above pyrite, being cathodic.

The composition of the arsenopyrite crystals plays a fundamental role in the mode of bacterial oxidation. This is unequivocally demonstrated by a comparison in leaching behaviour between firstly, the New Consort and Sheba arsenopyrite, and secondly, between the various compositional zones within the Sheba arsenopyrite. The As-rich New Consort arsenopyrite leached very slowly in comparison to the Sheba arsenopyrite. Furthermore, the relatively As-rich zones in the S-rich Sheba arsenopyrite were preferentially oxidized by the bacteria, rather than the As-poor zones.

In the bacterial oxidation of both Sheba and Agnes pyrite crystals compositional differences, due to zoning and generation differences, were also important. The As-rich zones were preferentially attacked during the initial stages of leaching. During further periods of oxidation, these As-rich zones continued to be leached at a higher rate than the As-poor areas. Thus, selective and preferential leaching of the As-rich areas took place in the pyrite crystals.

From the above, it appears evident that compositional differences are important during bacterial oxidation. However, it appears that the As-content of the arsenopyrite alone cannot be the controlling factor. This is evident since the As-rich arsenopyrite from New Consort were not as rapidly oxidized as the As-rich zones in the Sheba arsenopyrite, which contain lower amounts of As. Therefore, additional factors must play a role in the bacterial oxidation of arsenopyrite and pyrite.

7.1.2 *Preferential attack along crystallographic directions in sulphides*

Evidence on the effects of orientation of the exposed surface of the sulphide crystal includes the different shapes of the dissolution pits that formed during bacterial oxidation of the arsenopyrite from New Consort, and pyrite from Sheba and Agnes. The shapes of the dissolution pits in pyrite range from square, rectangular, elongated to hexagonal. The different pit outlines correlate with different generations of pyrite. The variation in the distribution of the pits suggests that the rate of bacterial attack differs along various crystallographic directions. However, during the present investigation this effect was not quantified.

7.1.3 *Mechanical deviations*

From the results obtained in this investigation, the initial bacterial activity on the sulphide minerals occurred along former cracks, lineations, grain boundaries, zone contacts, contacts along different generations or composition, etc. These are all mechanical imperfections and deviations in the sulphide crystal structures.

7.1.4 *Defects*

As outlined above, mineralogical factors such as composition, crystallographic direction and structural differences, indicate that imperfections and deviations in the crystal structure determine the sites and rate of bacterial activity. Such deviations and imperfections are known as "*defects*". The following discussion of various types of defects is based on the work by Barret & Massalski (1966) and Poirier (1985).

A perfect crystal is one whose lattice periodicity would be nowhere disturbed and the crystal energy at a surface will be identical throughout the whole surface area. However, there is no such thing as a *perfect* crystal: real crystals contain defects where periodicity is locally broken. Due to the

defects in a crystal, the atoms within the crystal structure will change their relative position. This change in relative position of the atoms is known as strain. The quantity of strain energy at the surface of a crystal can be determined by considering the type of defect and their concentration.

The following types of defects occur in crystals:

1) POINT DEFECTS:

Point defects are disturbances in a crystal, which extend for no more than a few interatomic distances in any direction. These point defects produce strain in the crystal, and are therefore points of higher strain energy. Two types occur within sulphides:

A) Vacancy defect - it consists of an atomic lattice site from which the atom is missing. Two types can be distinguished:

i) constitutional vacancies - these are sites which are necessarily empty in a given structure and

ii) extrinsic vacancies - these are created to preserve electrical neutrality

B) Interstitial defects - these consist of small domains in a crystal which contain an extra atom or impurities (such as the presence of metallic gold within the crystal structure of arsenopyrite or pyrite)

2) LINE DEFECTS:

These dislocations are linear defects which distort the atomic planes in the crystal
Two main types of dislocation occur:

i) Edge dislocation - this type of dislocation has the effect of introducing additional planes of atoms into the regular atomic array. The edge of the extra plane coincides with the dislocation.

ii) Screw dislocation - this type of dislocation has the effect of converting successive planes of atoms normal to the dislocation into a single screw surface or spiral ramp about the origin of the screw dislocation. In this case the displacement of atoms are parallel to the dislocation.

A considerable amount of strain energy is stored in the elastically distorted region around a dislocation line. An internal strain field is created which extends through the whole crystal, with an intensity that decreases directly with the distance from the dislocation. The free energy of a dislocated crystal is always greater than that of a perfect crystal.

3) TWO-DIMENSIONAL DEFECTS:

Dislocations are frequently arrayed closely together on planes and curved surfaces within a crystal, such an array is known as a two-dimensional defect. Grain boundaries, sub-grain

boundaries and twin boundaries are examples of such defects. Grain boundaries are two-dimensional high energy defects separating crystals of different lattice orientations. Twin boundaries also contain high strain energy.

4) THREE-DIMENSIONAL DEFECTS:
The following are classified under this type: clusters of point defects, voids, cracks and particles of different orientation or structure than the surrounding matrix. Interphase boundaries also contain high strain energies.

Any oxidation process could be considered as proceeding firstly, by means of the formation of some high-energy species, known as the activation complex or transition state, and secondly, by the breakdown of this complex to its products (Barrow, 1966). During the oxidation of pyrite (or arsenopyrite) by bacteria, electron transfer occurs at the pyrite surface, between FeS_2, the reducing agent (bacteria) and any oxidant species (Fe^{3+}). The mechanism whereby this electron transfer occurs, must thereby include the formation of an activation complex. Luther (1987) established that such a complex can be an initial formation of a persulfidobridge between pyrite and the oxidant (in this case Fe^{3+}).

The idea of an activated complex can be represented by a plot of the energy of the system as ordinate versus the reaction coordinate as abiscissa. The diagram that can be constructed to represent the bacterial oxidation reaction, is shown in Figure 101. The energy of the system is partially transformed from the reactants to the products. Enough energy must be available to permit the rearrangement to products, thereby surmounting the activated-complex-energy barrier. The rate of the reaction therefore depends on two factors: the energy require to form the activation complex and the rate with which the complex breaks up to give products.

It is evident then that bacterial leaching will take place initially where additional energy is available to decrease the required activation energy. It is therefore apparent that regions with a high strain, will be preferentially oxidized, since energy will be available when strain is released. This additional available energy will assist the reactants to form an activated complex. In other words, a lower activated-complex-barrier occurs in the strained regions. The rate of oxidation at these strained areas will thus be higher than in the unstrained regions.

From the previous discussion on defects, it should be evident that all defects suffer strain, and contains varying amounts of strain energy. This implies that regions, containing defects (and thus high strain energies), will be preferentially leached during bacterial oxidation. This explains the results obtained during this investigation, in which the initial bacterial activity occurred along chemical and mechanical deviations in the crystal structure.

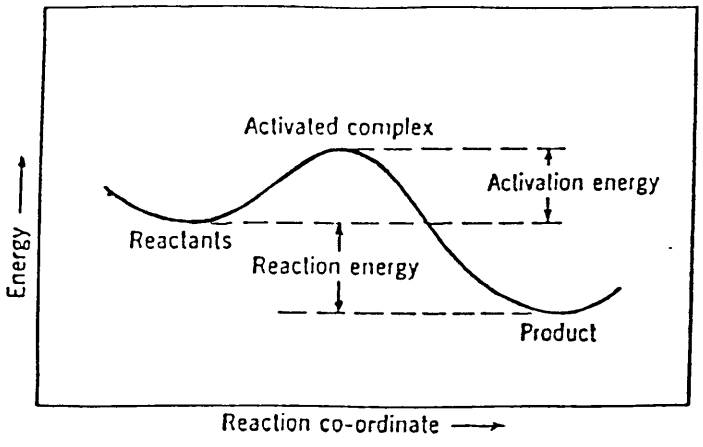

Figure 101: Schematic representation of potential energy along a reaction co-ordinate for a unit process (Kingery, 1959)

Within S-rich arsenopyrite, the higher amount of As atoms in the As-rich zones, in comparison with the As-poor zones, will create strain in the crystal, due to the larger size of the As^{3-} anion, substituting for the smaller S^{2-} anion. This will also be the case for gold. This substitution of Au^{3+} for the smaller Fe^{3+} or As^{3+} atoms, will create further strain within the arsenopyrite crystal. These substitutions will therefore increase the strain energy within the As-rich zones of S-rich arsenopyrites. Due to this higher amount of strain energy available, the rate of bacterial oxidation of these zones will therefore be faster than oxidation of S-rich zones, as observed during this investigation.

However, the New Consort arsenopyrite has a higher As-content than Sheba arsenopyrite, but is leached much more slowly than As-rich zones in Sheba arsenopyrites. This seems to contradict the above observations on the incorporation of As in the arsenopyrite, which it has been suggested, will create additional strain energies, resulting in rapid leaching.

However, Buerger (1936) established that the incorporation of As in the arsenopyrite crystal forms As-enriched arsenopyrite leading to a decrease in crystal symmetry. This substitution of As for S results in the destruction of glide planes and screw axes of the monoclinic space group, making the structure triclinic. The defects are therefore lost during the transition of the crystal from a

monoclinic to a triclinic structure. These triclinic As-rich arsenopyrites will thus be stable with lower amounts of defects than the S-rich arsenopyrite, which usually has a monoclinic structure, with high amounts of defects (Fuess, *et al*., 1987).

From the above it is clear that the New Consort As-rich arsenopyrite would be expected to have a triclinic crystal structure, with small amounts of defects. During bacterial leaching these crystals will therefore leach more slowly than the S-rich monoclinic Sheba crystals. This modification in crystal structure and the accompanying change in the amounts of defects, are proposed as a reason for the slower rate of oxidation of the New Consort As-rich arsenopyrites, as observed during this investigation.

The incorporation of As within the pyrite also leads to additional strain energies within the As-rich regions of the crystal. The highest amount of submicroscopic gold also occurs in the As-rich domains within pyrite crystals. Furthermore, Narseev and Stravova (in Petrovskaya 1974; quoted in Boyle, 1979) suggested that dispersed gold in the pyrite lattice is coincident with point defects. The octahedral covalent radius of the gold ion (1.40 Å) and arsenic (1.39 Å) is much higher than the covalent radius of ferrous iron in pyrite (1.23 Å) (Marion, 1987). Thus, the incorporation of As and Au in the pyrite structure, will create additional strain within the crystal. It is thus evident that the As-rich areas and zones within the Agnes and Sheba pyrite crystals will be the preferred sites for bacterial attack. The pits and channels that formed on pyrite surfaces during bacterial leaching will therefore be due respectively to point defects and dislocations, which vary in abundance and nature in different crystallographic directions.

No evidence of bacterial attachment to the mineral surfaces was observed, although this was not directly investigated during this study. However, the initial dissolution pits have dimensions comparable to those of the *T. ferrooxidans* bacterium. This suggests that direct bacterial activity (either by enzyme secretion or cell attachment) occurred in very close proximity to the crystal. A micro-bacterium-mineral environment is considered to form, promoting chemical gradients whereby oxidation can occur.

Therefore, the bacteria will by their enzymatic attack, oxidize the sulphide at the point of attachment. If the point of attachment happens to be at a defect additional strain energy will be available for the use of the bacteria to oxidize the sulphide. Due to the high availability of energy, continuous and enhanced oxidation of the mineral substrate will occur at these sites. The pits, therefore, increase in dimensions in all the directions, both in width and in depth. This suggests a direct contact between the bacterium and the sulphide surfaces.

If the point of attachment by the bacteria does not coincide with any defects, the rate of oxidation at that point will be slow, due to high energy requirements. No dissolution pits will form initially. However, with an increase in leaching time, oxidation will also take place at these non-defective sites.

This direct bacterial attachment was also proposed by Karavaiko & Pivovarova (1977), Murr and Berry (1976), Bennet and Tributsch (1978) and Natarajan (1988). Thus, the mere presence of bacteria in the leach solution is not enough to oxidize sulphide minerals; direct bacterial attachment to the mineral surface is a prerequisite for solubilization of sulphides.

7.2 Liberation of Gold

NEW CONSORT ORE MINERALS:

The amount of particulate gold present in the New Consort arsenopyrite is well in excess of the amount of submicroscopic gold. These gold particles occur mainly in association with loellingite and along cracks and quartz veins in the arsenopyrite. These are also the sites of initial bacterial attack. During the early stages of bacterial oxidation, the regions which host particulate gold are preferentially attacked. Liberation of most of the particulate gold therefore occurs during the initial stages of bacterial leaching of the New Consort ore minerals.

The remaining gold is homogeneously distributed through the arsenopyrite as submicroscopic gold. The recovery of this remaining refractory gold from the arsenopyrite will therefore proceed at a rate more or less proportional to the rate of oxidation of the arsenopyrite.

SHEBA SULPHIDES:

The gold recovery-sulphide oxidation curve obtained for a Sheba flotation concentrate (Figure 2) can be explained from the results obtained during this investigation. During the initial stages of bacterial oxidation leaching occurred along the zone contacts. However, much of the gold present as inclusions in the Sheba arsenopyrite, occurs along the contacts between the relatively As-rich and As-poor zones. Therefore during these early stages of bacterial leaching (i.e. at a low percentage of sulphide oxidation) these gold particles were released. Furthermore, preferential dissolution of the As-rich zones, which contain large amounts of submicroscopic gold, occurred. During bacterial leaching of Sheba pyrite crystals, the As-rich (relative Au-rich) areas in the pyrite were preferentially leached by the bacteria. Thus, high amounts of gold were liberated from the arsenopyrite and pyrite during the very early stages of sulphide oxidation.

This selective leaching of the gold-bearing regions in arsenopyrite explains why a low percentage of sulphide dissolution will result in an accelerated release of gold. Therefore, this preferential oxidation accounts for the enhanced gold liberation observed during a low percentage of sulphide oxidation in Figure 2.

Further increased periods of bacterial oxidation resulted in the oxidation of the As-poor zones in the arsenopyrite and pyrite. These zones contain very low amounts of refractory gold. The recovery of refractory gold during later stages of sulphide oxidation, will therefore be low. This is in agreement with the trend obtained in the gold recovery plot in Figure 2. This also explains the efficiency of bacterial oxidation as a pre-treatment method for this Sheba-type of gold ore: only partial oxidation of the sulphides is necessary for a high percentage recovery of refractory gold.

AGNES SULPHIDES:

The gold recovery from an Agnes flotation concentrate during bacterial oxidation is shown in Figure 1. During bacterial oxidation the first generation As-rich zones, which contain the highest amount of submicroscopic gold, were leached preferentially. Particulate gold was also liberated during the initial bacterial activity. Therefore, during the early stages of sulphide oxidation, refractory gold was released at a rate higher than the rate of pyrite oxidation. In Figure 1 this slightly elevated rate of gold liberation at lower percentages of sulphide oxidation, is evident.

The remaining refractory gold within the Agnes pyrite crystals is distributed in the first and second generation As-poor zones. The recovery of this remaining refractory gold from the pyrite crystals will therefore proceed at a rate more or less proportional to the rate of oxidation of the pyrite. This would produce the second stage of sulphide oxidation as observed from Figure 1.

7.3 Models Proposed for Bacterial Leaching of Sulphides

A number of models have been proposed by previous investigators to predict the behaviour of sulphides during the microbiological oxidation process. These include: the propagating pore model proposed by Southwood and Southwood (1985), the mechanistic numerical model proposed by Lazer *et al.* (1986) and an oxidation model by Hansford (1986).

Southwood and Southwood (1985) observed the development of cylindrical pores, parallel to certain crystallographic directions of pyrite, during the bacterial leaching tests on Barberton-type ores. They concluded that the pores developed along dislocations and that dissolution was confined to the leading end (closed end) of the pores, and thus, no oxidation of the pore walls took place. A simple shrinking core model, whereby leaching occurs at an equal rate over the whole surface of the crystal, could however, not be applied directly to this type of leaching. From their observation on pyrite they postulated a *hybrid* between the shrinking particle and the propagating pore concept as a model for the bacterial oxidation process of sulphides and tested it by using a S-rich assemblage of pyrite and arsenopyrite.

The present study has shown that bacterial oxidation of pyrite occurred due to the presence of defects, by pitting and channeling. Further dissolution within these features were not confined to one direction only, as proposed by Southwood and Southwood (1985), but leaching continued in both lateral and vertical directions. Furthermore, preferential leaching of As-rich areas in pyrite took place. This preferential selective oxidation of As-rich zones is conspicuous within zoned arsenopyrites. However, Southwood and Southwood (1985) only investigated the effect of bacterial leaching on pyrite and extrapolated similar effects for the leaching of arsenopyrite. This present work indicated the significant difference in behaviour between pyrite and arsenopyrite during bacterial oxidation. In arsenopyrite the rate of oxidation is much higher for the As-rich zones, than for the S-rich zones. Clearly, the propagating pore concept cannot satisfy such an unequal rate of oxidation of certain compositional zones within the crystals. Therefore, the *propagating pore* model is unable to predict the gold release during bacterial oxidation of arsenopyrite and pyrite satisfactorily.

A flotation pyrite concentrate was used by Hansford (1986), during a study to derive a mathematical model describing bio-leaching kinetics. He applied the propagating pore model of Southwood and Southwood (1985) as a basis of the actual mechanism by which leaching took place. A reasonably good agreement was found between the model and the experimental data. Since the propagating pore model was derived using leached pyrite crystals and only pyrite was used during the study by Hansford, this satisfactory agreement can be understood. However, if the effects of zoning in pyrite on the bacterial oxidation process are taken into account, a more exact agreement would be obtained.

An attempt was made by Lazer, *et al.* (1986) to describe the relationship between sulphide oxidation and gold release during bacterial leaching of a refractory gold ore (arsenopyritic-pyritic) from Barberton, by means of a mathematical and mineralogical model. However, their mineralogical observations did not support their experimental data. Their model commences with an assumption that the gold liberation from sulphides is proportional to the amount of sulphide breakdown. However, this can only be assumed if the gold is evenly distributed in sulphides. This is generally not the case in Barberton type arsenopyrite-pyrite gold ores, where compositional zoning and a concurrent variation in gold content, within arsenopyrites and pyrite, is common and ubiquitous (as is evident from the present work). It is therefore not surprising that their experimental data did not correspond to their calculated

values. The results obtained during this investigation indicate that the accelerated release of gold will be the result of the preferred and rapid leaching of the As-rich-Au-rich zones within the arsenopyrite. Therefore, zoning within the arsenopyrite and the consequent preferential leaching of Au-rich zones, may explain the discrepancy that Lazer and his co-workers encountered.

Most of the refractory gold in arsenopyrite-pyrite gold ores is present within arsenopyrite, while pyrite contains comparatively low quantities. The importance of the preferential leaching of high gold-bearing zones (As-rich zones) within the arsenopyrite is evident. Any representative model for bacterial oxidation of arsenopyrite-pyrite gold ores, must therefore include the effect of zoning.

To fit a model of oxidation to the microbiological leaching process of sulphides, is difficult. In the case of microbiological oxidation, the role played by the mineralogy of the ore used, is of fundamental importance. Not only is it necessary to identify the major minerals constituting the ore, but detailed information on the mode of gold occurrence in the mineral phases is a prerequisite in an attempt to model the liberation of gold with respect to the sulphide oxidation. A thorough mineralogical study on the leach residues should also be conducted to establish the mode of bacterial activity on the different sulphide minerals. Due to this complicated combination of factors controlling the bacterial oxidation of sulphides, it would be impossible to create *one* model of oxidation to satisfy all gold ore types. Separate models, for specific gold ore types, should be developed to describe the relationship between the oxidation of sulphides and the recovery of gold satisfactorily.

8 CONCLUSIONS

It can be concluded from this study that there are mineralogical differences of fundamental importance to the bacterial leaching process in the three ore types investigated here. These include:

1) *Differences in the nature of the major sulphides comprising the ore types:*

The New Consort ore consists largely of arsenopyrite ($FeAs_{1.1}S_{0.9}$) and nickeliferous loellingite inclusions. The As-rich arsenopyrite is poorly zoned.

The Sheba arsenopyrite is S-rich ($FeAs_{0.9}S_{1.1}$) and is extensively zoned, with alternate enrichment and impoverishment in arsenic in the zones. Pyrite in the Sheba ore comprises crystals with different generations and with compositional zoning. The zoning is due to variations in the arsenic content of the zones.

Pyrite is the major ore mineral present in the Agnes gold ore. Two generations of pyrite are present, separated by a period of resorption. Rhythmic compositional zoning, due to alternate enrichments and impoverishments in the As-content, is present in the first generation of Agnes pyrite. The As-rich zones contain a maximum of 2 atomic per cent As in the pyrite structure.

2) *The gold content*

20 % of the gold in the New Consort ore is refractory. This refractory gold is associated with arsenopyrite and loellingite, with particulate gold being the major mode of gold occurrence. In contrast, 70 % of the gold in the Sheba ore is refractory. This gold occurs as inclusions and as submicroscopic gold in both arsenopyrite and pyrite crystals. 20 % of the gold in the Agnes ore is refractory, and is associated with pyrite as particulate and submicroscopic gold.

3) *Distribution of gold*

Most of the particulate gold in the New Consort ore, occurs in association with loellingite and arsenopyrite. The submicroscopic gold content of the As-rich arsenopyrite is low (average < 450 ppm).

In the Sheba arsenopyrite submicroscopic gold (maximum = 6 700 ppm) is concentrated in zones with a relatively moderate Fe-content, a high As-content and a low S- and Sb-content. Particulate gold occurs at the contacts between the relatively As-rich and S-rich zones. Enrichment in gold also occurs within the As-rich areas in the pyrite crystals (maximum = 1500 ppm). Gold particles in pyrite generally occur at the contacts between the relatively As-rich and As-poor areas.

Submicroscopic gold in the Agnes pyrite crystals is generally enriched (maximum 1 500 ppm) in the As-rich zones of the first pyrite generation. Gold particles occur at contacts between different zones and generations.

During the bacterial and ferric sulphate leaching tests it was found that the various ore types responded differently.

The loellingite inclusions in the New Consort arsenopyrite, leached rapidly. However, it appears likely that ferric sulphate, present in the bacterial leach solution, is responsible for the leaching of loellingite. The arsenopyrite crystals, however, show relatively slow rates of oxidation. The primary dissolution of this As-rich arsenopyrite was along channels, which developed along former cracks and lineations.

During microbiological oxidation the Sheba arsenopyrite was leached to a greater extend during the same period of time, than the New Consort arsenopyrite or the Agnes and Sheba pyrite. The zonal composition of the Sheba arsenopyrite appears to play a fundamental role in the mode of bacterial oxidation. The relatively As-rich zones in the arsenopyrite were more rapidly leached by bacteria than the As-poor zones. Thus, during the very early stages of bacterial leaching, high amounts of refractory gold were liberated.

The initial bacterial activity on the zoned and unzoned pyrite surfaces from both Sheba and Agnes crystals took the form of dissolution channels along pre-existing cracks, along grain boundaries, along the contacts of pyrite of different composition and around inclusions. Preferential leaching of the As-rich zones within the pyrite crystals also took place.

The presence of dissolution pits is the most remarkable leaching characteristic observed on the pyrite crystal surfaces. These pits occur as isolated pits, as *pearls* in a pearl-string-like structure and as entities constituting part of channel-like features. They can be square, rectangular, hexagonal and inclined elongated pits. The shape and distribution of these dissolution pits indicated that orientation of the crystal face during exposure to lixiviant does play a role during bacterial leaching. This is due to preferential oxidation by bacteria along certain crystallographic directions, possibly due to the presence of defects, and to the atomic packing in the crystal structure. To what extent it influences the leaching, was not determined.

The nature and distribution of these pits indicate that the oxidation of both arsenopyrite and pyrite during bacterial leaching is due to direct bacterial activity (enzymatic attack by creating a micro-mineral-bacterium environment). It was further established that arsenopyrite and pyrite oxidation by ferric sulphate during bacterial oxidation is negligible.

During this investigation it was found that the sites of preferential bacterial attack are in most cases determined by the presence of defects. The availability of additional energy (i.e. strain-energy) at sites of defects, leads to a higher rate of bacterial oxidation at these sites.

A complex combination of mineralogical factors provide the reasons for the differences observed in the rate of both sulphide oxidation and gold liberation, thus explaining the shape of the gold recovery curves. From a detailed mineralogical study of the ore a hypothetical estimation of the behaviour of that ore during the bacterial oxidation process can be made.

All the ores studied here are of hydrothermal origin from the Barberton Mountain land. However, the mineralogy of the three differs greatly, and consequently their behaviour during bacterial leaching process also varies. To apply one model of sulphide oxidation to all three of these ore types will not be possible. For each type of deposit, the mineralogical factors must be carefully considered in any attempt to develop an oxidation model. Previous models proposed for the leaching of the refractory gold ores have proved inadequate. The results of the present study suggest that the reason for this lies in the insufficient attention given to the complex mineralogical features of these gold ores.

The results of this study emphasised the necessity of a multi-disciplinary approach in the development of an understanding of bacterial leaching as a pre-treatment process. Microbiologists are required to maximize the genetical aspects of the bacterium used, whereas metallurgical engineers are required to optimize leaching conditions. Mineralogical information is necessary both on the broader aspects of ore mineralogy and at a more fundamental level on the detailed mode of occurrence and distribution of gold within the mineral phases. More importantly, it has been established that mineralogical information can provide an understanding of the behaviour of different ore types during the bacterial leaching process.

9 RECOMMENDATIONS

The following recommendations for further research, can be made:

Oxidation models for specific types of gold ore should be developed, after a thorough and detailed mineralogical investigation on both the feed material and the bacterial leach residues.

By combining information from various disciplines of science, the mechanism and the mode of bacterial activity should be determined.

The control of crystallographic directions on the leaching behaviour of the bacteria, should be unequivocally established.

Attempts to determine the mode of occurrence of submicroscopic gold, i.e. in a solid-solution state or as small inclusions, should continue. During this process, the oxidation state of the submicroscopic gold should also be determined.

The transformation from monoclinic crystal structure in S-rich arsenopyrite to a triclinic structure in As-rich arsenopyrite, should be a major research effort, requiring special equipment, i.e. a TEM.

10 ACKNOWLEDGEMENTS

The author wishes to express her sincere thanks and appreciation to the management of Mintek for the opportunity to engage in an investigation of this nature. Furthermore, I am indebted to the following persons: Dr. J.P.R. de Villiers who initiated this study, Mr. E.A. Viljoen and Mrs. J. Russel for assisting me in electron microprobe analyses; Dr. E. Oosthuizen and Mrs. I. Penberthy for respectively allowing me to use the SEM and assisting me; Mr. A. de Sousa for preparing the photographs. The assistance of the staff of the Mineralogy Division during sample preparation is also acknowledged. My appreciation also goes to my colleagues in the Minerals Engineering Division for their assistance during the bacterial oxidation experiments. I am grateful to Dr. A. Pinches for worthwhile discussions on bacterial oxidation, the interest he showed in my work and for allowing me to use the bacterial oxidation facilities. The author also wishes to thank Anglovaal Limited for permission to use some of the diagrams. I would also like to express my sincere gratitude to my co-promoter, Dr. C.T. Logan for his assistance and encouragement. Furthermore, I am deeply indebted to my promoter, Dr. C.P. Snyman for his advice and useful suggestions during the course of this study and his promt attention to this thesis when time was of the essence. Finally, my appreciation also goes to Louis Claassen for his support and encouragement throughout the duration of this thesis.

11 REFERENCES

Agate, A.D. (1988). Isolation and preservation of bacterial cultures with special reference to leaching of Indian copper ores. *Mineral. Metall. Process.* pp. 66-69.

Anhaeusser, C.R. (1984). The nature of archaean gold mineralization in the Barberton mountain land. *Abstracts and Guide book to Archaean Gold Barberton Centenary Symposium 1984.* 28 pp.

Atkins, A.S. (1978). Studies on the oxidation of sulphide minerals (pyrite) in the presence of bacteria. *Bioextractive Applications and Optimization*. pp. 403-425.

Bakken, B.M., M.F. Hochella, A.F. Marshall and A.F. Turner (1989). High resolution microscopy of gold in unoxidized ore from the Carlin mine, Nevada. *Econ. Geol.,* vol.84, pp. 171-179.

Balashova, V.V., I.Y. Vedenina, G.E. Markosyan and G.A. Zavarzin (1974). *Leptospirillum ferrooxidans* and peculiarities of its autotrophic growth. *Mikrobiol.,* vol. 43, pp. 581-585.

Barrett, C.S. and T.B. Massalski (Eds.) (1966). *Structure of Metals - crystallographic methods, principles and data.* McGraw-Hill, New York, 654 pp.

Barrow, G.M. (Ed.) (1966). *Physical Chemistry.* McGraw-Hill, New York, 843 pp.

Bärtels, C.-C., G. Chatzitheodorou, M. Rodriquez-Leiva and H. Tributsch (1989). Novel technique for investigation and quantification of bacterial leaching by *Thiobacillus ferrooxidans*. *Biotech. Bioengng.,* vol. 33, pp. 1196-1204.

Bennett, J.C. and H. Tributsch (1978). Bacterial leaching patterns on pyrite crystal surfaces. *J. Bact.,* vol. 134, pp. 310-317.

Berry, V.K. and L.E. Murr (1978). Direct observations of bacteria and quantitative studies of their catalytic role in the leaching of low-grade, copper-bearing waste. In: L.E. Murr, *et al.* (Eds.), *Metallurgical applications of bacterial leaching and related microbiological phenomena.* Academic Press, New York, 1978, pp.403-426.

Boiron, M.C., M. Cathelineau and J.J. Trescases (1989). Conditions of gold-bearing arsenopyrite crystallization in the Villeranges Basin, Marche-Combrailles shear zone, France: a mineralogical and fluid inclusion study. *Econ. Geol.*, vol. 84, pp. 1340-1362.

Boyle, R.W. (Ed.) (1979). *The geochemistry of gold and its deposits.* Geological Survey of Canada (Bulletin 280), Ottawa, 584 pp.

Bruynesteyn, A. (1988). Biotechnology for gold ores: the state of the art. In: *Proceedings of Perth International Gold Conference,* Perth, 1988, Randol International Ltd. pp. 141 - 143.

Buerger, M.J. (1936). The symmetry and crystal structure of minerals of the arsenopyrite group. *Z. kristallogr.,* vol. 95, pp.83-113.

Cabri, L.J., S.L. Chryssoulis, J.P.R. de Villiers, J.H. Gilles Laflamme and P.R. Buseck (1989). The nature of "invisible" gold in arsenopyrite. *Can. Mineral.*, vol. 27, pp. 353-362.

Cabri, L.J., S.L. Chryssoulis, J.L. Campbell and W.J. Teesdale (1991). Comparison of *in-situ* analyses in arsenian pyrite. *Appl. Geochem.,* vol. 6, pp. 225-230.

Carter, A.J. (1991). Economic comparison of the alternative methods for the recovery of gold from refractory gold ores. *Proceedings of Colloquium on Bacterial Oxidation,* SAIMM, Johannesburg, June 18, 1991.

Cathelineau, M., M.C. Boiron, P. Holliger and M. Denis, (1989). Gold in arsenopyrites: crystal chemistry, location and state, physical and chemical condition of deposition. *Econ. Geol.*, pp.328-340.

Chryssoulis, S.L. and L.J. Cabri (1990). Significance of gold mineralogical balances in mineral processing. *Trans. Inst. Min. Metall. Sect. C.,* vol. 99, pp. C1-C10.

Clark, A.L.(1960) Arsenopyrite As:S -ratio as a possible geobarometer. *Geol. Soc. Amer. Bull.,* vol.71, pp 1844-1855.

Clark, A.L. (1960). The Fe-As-S system: Phase relations and applications. Part I and II. *Econ. Geol.*, vol. 55, pp.1345-1651.

Colmer, A.R. and M.E. Hinkle (1947). The role of microorganisms in mine drainage: a preliminary report. *SCI.*, vol. 1066, pp. 253-255.

Cook, N.J. and S. L. Chryssoulis (1990). Concentrations of invisible gold in the common sulphides. *Can. Mineral.,* vol.28, part 1, pp. 1-16.

Corrans, I.J., B. Harris and B.J. Ralph (1972). Bacterial leaching: an introduction to its application and theory and a study on its mechanism of operation. *J. S. Afr. Inst. Min. Metall.,* March, pp. 221-230.

Duncan, D.W. and A.D. Drummond (1973). Microbiological leaching of porphyry copper type mineralization: Post-leaching observations. *Can. J. Earth Sci.* vol. 10, pp. 476-483.

Ehrlich, H.L. (1988). Recent advances in microbial leaching of ores. *Miner. Metall. Process.*, pp. 57-60.

Fleet, M.E., P.J. MacLean and J. Barier (1989). Oscillatory-zoned As-bearing pyrite from strata-bound and stratiform gold deposits: An indicator of ore-fluid evolution. *Econ. Geol. Mon.,* vol. 6, pp. 356-362.

Foo, K.A., M.D. Bath, A. Ismay and J.H. Canterford (1989). New gold processing technologies: an engineer's perspective. *Gold Forum on Technology - World Gold '89,* pp. 233-250.

Fuess,H, T.Kratz, J.Topel-Schädt and G.Miehe (1987). Crystal structure refinement and electronmicroscopy of arsenopyrite. *Z. Kristallogr.,* vol. 179, pp. 335-346.

Gibbs, H.E., M. Errington, and F.D. Pooley (1985). Economics of bacterial leaching. *Can. Metall. Q.*, vol. 24, no. 2, pp. 121-125.

Graham, J., B.W. Robinson and R.K. Walker (1989). Gold in arsenopyrite. *Proceedings of Mineralogy-Petrology Symposium, Aust. Inst. Min. Metall., Sydney Branch,* pp. 55-57.

Hansford, G.S. (1986). Bacterial leaching of gold bearing pyrite concentrate. *Mintek, Tech. Memo., No.15239,* 77 pp.

Henley, K.J. (1975). Gold-ore mineralogy and its relation to metallurgical treatment. *Mineral. Sci. Eng.,* vol. 7, no. 4, pp. 289 - 321.

Hiltunen, P., A. Vuorinen, P. Rehtijärvi and O.H. Tuovinen (1981). Bacterial pyrite oxidation: release of iron and scanning electron microscopic observations. *Hydrometall.,* vol. 7, pp. 147-157.

Hutchins, S.R., J.A. Brierley and C.L. Brierley (1988). Microbial pretreatment of refractory sulphide and carbonaceous ores improves the economics of gold recovery. *Min. Eng.*, April 1988, pp.249-254.

Ingledew, W.J. (1986). Ferrous iron oxidation by *Thiobacillus Ferrooxidans*. *Biotechnology and Bioengineering Symposium,* pp.22-32.

Johan, Z., E. Marcoux and M. Bonnemaison (1989). Arsenopyrite aurifere: mode de substitution de Au dans la structure de Fe As S. *C.R. Acad. Sci. (Paris) Ser. II Mec. Phys. Chim. Sci., t. 308, pp.185-191.*

Karaivko, G.I., S.I. Kuznetsov and A.I. Golonizjk (Eds.) (1977). *The bacterial leaching of metals from ores.* Translator: W. Burns. Technicopy Ltd., England, 205 pp.

Karavaiko, G.I. and T.A.Pivovarova (1977). Mechanism of oxidation of reduced sulphur compounds by *Thiobacilli. In:* W. Schwartz (Ed.), *Conference on Bacterial Leaching.* Verslag Chemie, New York, pp. 37-46.

Karavaiko, G I, Chuchalin, L K, Pivovarova, T A, B A Yemel'yanov and A G Dorofeyev (1986). Microbiological leaching of metals from arsenopyrite containing concentrates. *In*: R.W. Lawrence, R.M.R. Branion and H.G. Ebner (Eds.), *Fundamental and Applied Biohydrometallurgy,* Elsevier Sci. Pub., Amsterdam, pp. 115-126.

Keller, L. and L.E. Murr (1982). Acid-bacterial and ferric sulphate leaching of pyrite single crystals. *Biotech. Bioengng,* vol. 24, pp. 83-96.

Kingery, W.D. (Ed.) (1959). *Kinetics of high-temperature processes*. Published jointly by The Technology Press of Massachusetts Institute of Technology and John Wiley & Sons, Inc., New york.

Komnitsas, C. and F.D. Pooley (1989). Mineralogical characteristics and treatment of refractory gold ores. *Mineral. Eng.*, vol. 2, no. 4, pp. 449-457.

Komnitsas, C. and Pooley, F.D. (1990). Bacterial oxidation of arsenical gold sulphide concentrate from Olympias,Greece. *Mineral. Eng.*, vol 3, pp.295-306.

Kretchmar, U. and S.D. Scott (1976). Phase relations involving arsenopyrite in the system Fe-As-S and their application. *Can. Mineral.*, vol. 141, pp. 364-386.

Kuznetsov, S.I., M.V. Ivanov and N.N. Lyalikova (Eds.) (1963). *Introduction to geological microbiology.* translator P. Broneer. International Series in Earth Sciences. McGraw-Hill, New York. 249 pp.

Lacey, D.T. and F. Lawson (1970). Kinetics of the liquid phase oxidation of acid ferrous sulphate by the bacterium *Thiobacillus ferrooxidans*. *Bioetech. Bioengng.,* vol. 12, pp. 373-408.

Lawrence, R.W. and A. Bruynesteyn (1983). Biological pre-oxidation to enhance gold and silver recovery from refractory pyritic ores and concentrates. *CIM Bulletin*, Sept. 1983, pp. 107-110.

Lazer, M.T., M.I. Southwood and A.J. Southwood (1986). The release of refractory gold from sulphide minerals during bacterial leaching. In: *Gold 100, Proceedings of the International Conference on Gold, vol2, Extractive Metallurgy of Gold,* S.A.I.M.M., Johannesburg, pp. 235-237.

Livesey-Goldblatt, E. (1986). Bacterial leaching of gold, uranium, pyrite bearing compacted mine tailing slimes. *In*: R.W. Lawrence, R.M.R. Branion and H.G. Ebner (Eds.), *Fundamental and Applied Biohydrometallurgy,* Elsevier Sci. Pub., Amsterdam, pp. 89-96.

Luther, G.W. (1987). Pyrite oxidation and reduction : Molecular orbital theory considerations. *Geoch. Cos. A.,* vol. 51, pp.3193-3199.

Marcoux, E., M. Bonnemaison, C. Braux and J. Zdenek (1989). Distribution de Au, Sb, et Fe dans i'arsenopyrite aurifere du Chatelet et de Villeranges. *C.R. Acad. Sci.* pp 293-300.

Marion, P., J-R.Regard and E. Wagner (1986). Etude de l'etat chimique de l'or dans seulfures auriferes par spectroscopie Mössbauer de ^{197}Au: premiers resultats. *C.R. Acad. Sci. (Paris) Ser II Mec. Phys. Chim. Sci., t. 302,* no 8, pp.571-574.

McPheat, I.W., J.E.A. Gooden and R. Toenend (1969). Submicroscopic gold in a pyrite concentrate. *Proc. Aust. Inst. Min. Metall.,* no. 231, Sept., pp. 19-25.

Mironov, A.G., S.M. Zhmodik and E.A. Maksimova (1981). An experimental investigation of the sorption of gold by pyrite with different thermoelectric properties. *Geokhim.,* no. 4, pp. 553-561.

Murr, L.E. and V.K. Berry (1976). Direct observation of selective attachment of bacteria on low-grade sulphide ores and other mineral surfaces. *Hydrometall.,* vol. 2, pp. 11-24.

Natarajan, K.A. (1988). Electrochemical aspects of bioleaching multisulphide minerals. *Miner. Metall. Process.*, May 1988, pp.61-65.

Neuerburg, G.J. (1975). A procedure, using Hydrofluoric acid, for quantitative mineral separations from silicate rocks. *J. Res. U.S. Geol. Surv.,* vol. 3, no.3, pp. 377-378.

Nicolaides, A.A (1987). Microbial mineral processing: the opportunities for genetic manipulation. *J. Chem. Technol. and Biotechnol.,* vol. 38, pp. 167-185.

Norman, P.F. and C.P. Snyman (1988). The biological and chemical leaching of an auriferous pyrite/arsenopyrite flotation concentrate: a microscopic examination. *Geomicrobiology Journal,* vol.6, pp. 1-10.

Panin, V.V., G.I. Karavaiko and S.I. Polkin (1977). Mechanism and kinetics of bacterial oxidation of sulphide minerals. In: *Biotechnology of Metals,* G.I. Karavainko, S.N. Groudev (Eds.), Moscow Centre of International Projects GKNT/UNEP, pp. 197-225.

Petrovskaya, N.V. (Ed.) (1974). Mineralogy and geochemistry of gold. *Tezizy Dok. Simp. Mineral. GeoKhim Zolota,* vols. 1 & 2. Akad. Nauk. SSR Dal'Nevost Nauch. Tsent., Vladivostok, USSR

Petruk, W. (1989). Recent progress in mineralogical investigations related to gold recovery. *CIM Bulletin, Nov. 1989.* pp.37-39.

Phillips, F.C. (Ed.) (1963). *An introduction to Crystallography.* John Wiley & Sons Inc, New York, 338 pp.

Pinches, A. (1990). Personal communication

Poirier, J.-P. (Ed.) (1985). *Creep of Crystals - High temperature processes in metals, ceramics and minerals.* Cambridge University Press, Cambridge, Great Britain, 260 pp.

Pooley, F.D. (1987). Use of bacterium to enhance recovery of gold from refractory ores. *Minprep 87, International Symposium on Innovative Plant and Processes for Mineral Engineering,* Doncaster, pp. 23-41.

Schouwstra, R.P. and J.P.R. de Villiers (1989). Gold mineralization and associated wallrock alteration in Main Reef Complex at Sheba mine, South Africa. *Trans. Inst. Min. Metall. Sect. B: Appl. Earth Sci.,* vol. 97, pp. B158-B170.

Schweigart, H. (1965). Solid solution of gold in sulphides. *Econ. Geol.,* vol. 60, pp. 1540-1542.

Schweigart, H. and W.R. Liebenberg (1966). Mineralogy and chemical behaviour of some refractory gold ores from Barberton Mountain Land. *Report. Nat. Inst. Metall., Johannesburg,* vol. 8, 97 pp.

Silverman, M. and L.H. Ehrlich (1964). Microbiological formation and degradation of minerals. *Adv. Appl. Microbiol.,* vol. 6, pp. 153-206.

Silverman, M.P. and D.G. Lundgren. (1959). Studies on the chemo-autotrophic iron bacterium *Ferrobacillus ferrooxidans:* An improved medium and harvesting procedure for securing high cell yields. *J. Bact.* vol. 77, no. 5, 742 pp.

Southwood, M.J. and A.J. Southwood (1985). Mineralogical observations on the bacterial leaching of auriferous pyrite: a new mathematical model and implications for release of gold. *In:* Lawrence, R.W., R.M.R. Branion and H.G. Ebner (Eds.), *Fundamental and Applied Biohydrometallurgy,* Elsevier Sci. Publ., Amsterdam, pp. 98-113.

Spisak, J.F. (1986). Biotechnology and the extractive metallurgical industries: perspectives for success. *Biotech. Bioeng. Symp.* no.16, pp.331-341.

Stillwell, F.L. and A.B. Edwards (1946). An occurrence of sub-microscopic gold in the Dolphin East Lode, Fiji. *Proc. Aus. Inst. Min. Metall.,* No. 141, pp. 31-47.

Taylor, B.E., M.C. Wheeler and D.K. Nordstrom (1984). Stable isotpe geochemistry of acid mine drainage: Experimental oxidation of pyrite. *Geoch. Cos. A.,* vol. 48, pp. 29-278.

Tributsch, H. (1976). The oxidation disintegration of sulphide crystals by *Thiobacillus ferrooxidans. Naturwissen.*, vol 663, pp. 88.

Wagener, J.H.F. and J. Wiegand (1986). The Sheba gold mine, Barberton greenstone belt. *In:* Annhaeusser, C.R. and S. Maske (Eds.) *Mineral Deposits of Southern Africa.* vol 1, pp. 155-161.

Wagner, F.E., P.H. Marion and J.R. Regnard (1986). Mössbauer study of the chemical state of gold in gold ores. In: *GOLD 100* - Proceeding of the International Conference on Gold, vol. 2: *Extractive Metallurgy of Gold.* pp. 435-443.

Wagner, F.E., P.H. Marion and J.R. Regnard (1988). ^{197}Au Mössbauer study of gold ores, mattes, roaster products, and gold minerals. *Hyperfine Interact.*, vol. 41, pp. 851-854.

Wells, J.D. and Mullens, T.E. (1973). Gold-bearing arsenian pyrite determined by microprobe analysis, Cortez and Carlin gold mines, Nevada. *Econ. Geol.,* vol.68, pp. 187-201.

Wu, X., and F. Delbove (1989). Hydrothermal synthesis of gold bearing arsenopyrite. *Econ. Geol.*, vol. 84, pp. 2029-2032.

Wuensch, B.J. (1974). Sulphide crystal Chemistry. *In: Sulphide Mineralogy*, Mineralogical Society of America - Short Course Notes, vol.1, pp. W21- 43.

APPENDICES

APPENDIX 1. MICROPROBE ANALYSES OF NEW CONSORT ARSENOPYRITES

Sample no.	Fe (at %)	As (at %)	S (at %)	Au (ppm)	Ni (ppm)	Co (ppm)	As/S
1.1	32.76	36.13	30.67	511	2596	554	1.18
1.2	33.09	35.02	31.68	662	993	687	1.10
1.3	32.95	35.90	30.61	358	2447	1078	1.17
1.4	32.87	35.85	30.76	1011	2266	818	1.16
1.5	33.21	35.99	30.47	0	2299	818	1.18
1.6	32.86	35.57	31.25	303	2038	889	1.14
1.7	33.04	36.04	30.54	0	2845	798	1.18
1.8	33.57	34.94	31.32	0	872	660	1.12
1.9	33.02	36.08	30.54	307	2274	544	1.18
10.1	32.67	35.20	31.92	200	643	426	1.10
2.1	31.91	35.81	31.15	0	9000	1907	1.15
2.5	32.27	35.62	30.99	0	8245	1745	1.15
2.6	32.07	35.73	31.33	508	6897	1143	1.14
7.1	33.98	34.69	30.72	293	4333	1576	1.13
7.2	34.11	34.11	31.46	732	1732	544	1.08
7.3	33.18	35.80	29.98	540	8756	1252	1.19
8.1	33.95	35.23	29.89	49	7177	1898	1.18
8.2	33.65	35.15	30.22	1660	7463	1819	1.16
8.26	32.53	34.81	32.10	0	4127	1105	1.08
8.21	31.95	35.57	31.49	489	8202	1172	1.13

APPENDIX 2. MICROPROBE ANALYSES OF SHEBA ARSENOPYRITE CRYSTALS

AS-RICH ZONES						AS-POOR ZONES					
Fe (at %)	As (at %)	S (at %)	Sb (ppm)	Au (ppm)	As/S	Fe (at %)	As (at %)	S (at %)	Sb (ppm)	Au (ppm)	As/S
33.5	31.67	34.66	49	2064	0.91	32.80	29.47	37.51	2278	447	0.79
33.38	30.24	36.15	1703	254	0.84	33.99	28.82	36.95	2790	0	0.78
33.35	32.32	33.63	574	64	0.96	34.03	28.07	37.67	3241	0	0.75
33.79	31.48	34.47	486	1652	0.91	34.56	27.91	37.25	3653	317	0.75
33.96	31.12	34.64	331	1080	0.90	34.15	27.72	37.95	2589	0	0.73
32.05	32.29	35.53	107	1299	0.91	33.82	28.11	37.85	1199	855	0.74
31.98	32.01	35.80	194	2502	0.89	32.37	30.15	37.18	2757	401	0.81
32.9	31.64	35.30	0	1774	0.90	32.77	28.66	38.29	3595	0	0.75
32.77	31.50	35.57	232	1109	0.89	32.70	28.90	38.17	2200	493	0.76
33.11	30.96	35.76	1578	0	0.87	31.90	29.18	38.52	473	2933	0.76
32.25	31.39	36.06	0	1212	0.87	32.49	28.42	38.85	1549	1203	0.73
32.78	30.88	36.17	645	0	0.85	32.33	27.99	39.50	2644	0	0.71
32.60	31.96	35.25	0	2169	0.91	32.85	28.26	38.65	3202	31	0.73
32.73	30.52	36.49	596	1914	0.84	33.42	28.07	38.25	3287	494	0.73
32.63	32.30	34.90	0	447	0.93	33.26	29.62	36.82	3133	0	0.80
32.85	31.31	35.50	332	1818	0.88	33.50	29.67	36.55	2539	191	0.81
32.28	31.58	35.80	342	2552	0.88	34.05	29.81	35.88	3172	603	0.83
32.86	31.17	35.72	0	702	0.87	32.96	29.41	37.37	2314	0	0.79
32.77	31.92	35.15	332	542	0.91	32.70	28.68	38.37	3689	253	0.75
33.02	31.23	35.46	293	1939	0.88	32.67	30.00	37.13	1598	348	0.81
33.51	30.30	35.88	1503	1299	0.84	32.95	29.22	37.53	2779	222	0.78
32.83	31.74	35.22	128	3199	0.90	32.96	28.59	38.12	2591	128	0.75
32.36	31.58	35.83	267	816	0.88	32.40	30.59	36.55	606	287	0.84
32.45	31.84	35.52	109	2822	0.90	32.58	29.74	36.48	1662	351	0.82
32.16	32.37	35.29	189	1837	0.92	33.41	28.55	37.67	4351	97	0.76
32.18	32.23	35.07	302	62	0.92	33.56	29.90	36.28	2669	0	0.82

32.30	31.26	36.00	567	525	0.87	33.26	28.68	37.79	3735	420	0.76
33.16	31.50	35.08	681	826	0.90	33.50	30.54	35.77	1454	325	0.85
32.95	31.16	35.19	418	3494	0.89	33.25	29.28	37.07	3341	650	0.79
33.84	32.24	33.73	374	1932	0.96	32.52	29.45	37.89	336	425	0.78
33.51	32.18	34.11	316	2217	0.94	32.14	28.73	38.85	2673	1	0.74
33.65	31.43	34.64	259	3136	0.91	32.61	30.50	36.60	2275	1235	0.83
34.09	31.04	34.65	508	1837	0.90	33.38	29.96	36.38	716	1016	0.82
34.60	31.02	34.27	499	1204	0.91						
34.32	31.50	33.98	470	2407	0.93						
32.47	31.20	36.09	443	2861	0.86						
32.17	31.10	36.48	311	1664	0.85						
32.19	31.14	36.37	312	1819	0.86						
32.02	32.13	35.63	0	1140	0.90						
32.55	31.31	35.94	76	2437	0.87						
32.29	31.05	36.37	368	3085	0.85						
32.78	31.45	35.55	57	2806	0.88						
33.48	31.75	34.58	350	1635	0.92						
32.61	31.19	35.87	246	2840	0.87						
32.57	31.46	35.69	161	2160	0.88						
33.13	30.28	36.41	255	1727	0.83						
33.40	31.20	35.01	566	3079	0.89						
33.47	30.58	35.68	396	3207	0.86						
33.61	31.28	34.81	273	3509	0.90						
32.40	31.17	36.25	2014	538	0.86						

APPENDIX 3. RECALCULATED CRYSTAL-CHEMICAL FORMULAE OF SHEBA ARSENOPYRITE CRYSTALS

Sample Number: RC 1016

Sample Number		Fe Sites		At %		As Sites		S Sites	
		Fe	As	Au	Sb	As	S	S	As
1016	b.9	0.9739	0.0064	0.0680	0.0403	0.9167	0.0833	1	0
	b10.1	0.9665	0.0081	0.0875	0.0023	0.9056	0.0944	1	0
	b10.2	0.9234	0.0320	0.0105	0.0800	0.8046	0.1954	1	0
	b10.18	0.9917	0.0016	0.0027	0.0271	0.9595	0.0405	1	0
	10.7	0.9803	0.0082	0.0689	0.0228	0.9050	0.0950	1	0
	11	0.9804	0.0115	0.0448	0.0155	0.8869	0.1131	1	0
	b13.1	0.9021	0.0092	0.0580	0.0054	0.8997	0.1003	1	0
	b13.2	0.8933	0.0125	0.1109	0.0097	0.8816	0.1184	1	0
	b13.3	0.8938	0.0228	0.0237	0.1002	0.8370	0.1630	1	0
	b13.8	0.8910	0.0333	0.0534	0.1117	0.8000	0.2000	1	0
	b13.10	0.9320	0.0120	0.0767	0.0000	0.8843	0.1157	1	0
	b13.11	0.9213	0.0148	0.0477	0.0113	0.8708	0.1292	1	0
	a.9	0.9033	0.0475	0.0000	0.1456	0.7569	0.2431	1	0
	b10.3	0.9166	0.0436	0.0079	0.1195	0.7681	0.2319	1	0
	b10.6	0.9490	0.0344	0.0247	0.1475	0.7964	0.2036	1	0
	b13.4	0.8820	0.0577	0.0000	0.1126	0.7293	0.2707	1	0
	b13.6	0.8522	0.0853	0.0107	0.1781	0.6621	0.3379	1	0
	b13.9	0.8799	0.0456	0.0149	0.0775	0.7623	0.2377	1	0
	b13.13	0.8780	0.0630	0.0093	0.1333	0.7156	0.2844	1	0
	b13.14	0.9259	0.0208	0.0000	0.0761	0.8450	0.1550	1	0

Sample Number: RC 1008

Sample Number		Fe Sites		At %		As Sites		S Sites	
		Fe	As	Au	Sb	As	S	S	As
1008	20.1	0.8943	0.0193	0.0571	0.0000	0.8512	0.1488	1	0
	20.2	0.9063	0.0251	0.0000	0.0307	0.8287	0.1713	1	0
	20.3	0.9248	0.0096	0.0928	0.0000	0.8971	0.1029	1	0
	20.5	0.8970	0.0320	0.0804	0.0284	0.8044	0.1956	1	0
	20.6	0.9350	0.0060	0.0190	0.0000	0.9195	0.0805	1	0
	20.7	0.9254	0.0158	0.0761	0.0157	0.8662	0.1338	1	0
	11.1	0.9017	0.0158	0.1083	0.0164	0.8664	0.1336	1	0
	11.4	0.9199	0.0186	0.0296	0.0000	0.8540	0.1460	1	0
	21.2	0.9323	0.0093	0.0228	0.0157	0.8988	0.1012	1	0
	9.2	0.9312	0.0162	0.0808	0.0138	0.8646	0.1354	1	0
	9.5	0.9339	0.0286	0.0544	0.0713	0.8158	0.1842	1	0
	9.8	0.9321	0.0108	0.1360	0.0061	0.8904	0.1096	1	0
	7.2	0.9032	0.0160	0.0348	0.0128	0.8654	0.1346	1	0
	7.1	0.9136	0.0120	0.1223	0.0053	0.8844	0.1156	1	0
	77.2	0.9113	0.0075	0.0840	0.0093	0.9098	0.0902	1	0
	20.4	0.8744	0.0585	0.0184	0.1071	0.7272	0.2728	1	0
	11.3	0.8646	0.0833	0.0052	0.1199	0.6667	0.3333	1	0
	11.5	0.8865	0.0318	0.0119	0.0285	0.8052	0.1948	1	0
	0.1	0.8931	0.0419	0.0144	0.0000	0.7734	0.2266	1	0
	9.1	0.8869	0.0773	0.0039	0.2020	0.6806	0.3194	1	0
	9.3	0.9250	0.0375	0.0000	0.1250	0.7866	0.2134	1	0
	9.4	0.8801	0.0766	0.0172	0.1747	0.6824	0.3176	1	0
	9.4	0.9365	0.0250	0.0136	0.0689	0.8287	0.1713	1	0
	9.7	0.8970	0.0559	0.0268	0.1570	0.7339	0.2661	1	0
	7.3	0.8583	0.0638	0.0178	0.0161	0.7134	0.2866	1	0
	77.3	0.8273	0.0918	0.0000	0.1290	0.6478	0.3522	1	0
	8.17	0.9453	0.0116	0.0346	0.0322	0.8863	0.1137	1	0

Sample Number: RC 1007

1007	8.101	0.9363	0.0148	0.1484	0.0201	0.8707	0.1293	1	0
	9.1	1.0033	0.0020	0.0828	0.0179	0.9538	0.0462	1	0
	9.2	0.9824	0.0034	0.1020	0.0151	0.9400	0.0600	1	0
	9.3	0.9714	0.0095	0.1325	0.0123	0.8979	0.1021	1	0
	9.5	0.9838	0.0121	0.0767	0.0239	0.8837	0.1163	1	0
	9.15	1.0096	0.0099	0.0501	0.0234	0.8952	0.1048	1	0
	9.16	1.0100	0.0057	0.1008	0.0221	0.9213	0.0787	1	0
	8.101	0.8997	0.0212	0.1267	0.0222	0.8433	0.1567	1	0
	8.12	0.8819	0.0255	0.0711	0.0151	0.8270	0.1730	1	0
	8.14	0.8851	0.0242	0.0777	0.0151	0.8320	0.1680	1	0
	8.16	0.8987	0.0107	0.0495	0.0000	0.8911	0.1089	1	0
	8.3	0.9057	0.0191	0.1047	0.0037	0.8521	0.1479	1	0
	3.5	0.8878	0.0251	0.1327	0.0180	0.8287	0.1713	1	0
	3.16	0.9221	0.0150	0.1203	0.0027	0.8696	0.1304	1	0
	3.17	0.9682	0.0073	0.0698	0.0168	0.9109	0.0891	1	0
	3.201	0.9091	0.0196	0.1206	0.0118	0.8500	0.1500	1	0
	2.1	0.9126	0.0159	0.0921	0.0077	0.8655	0.1345	1	0
	2.2	0.9099	0.0341	0.0721	0.0121	0.7976	0.2024	1	0
	1.1	0.9540	0.0133	0.1291	0.0268	0.8779	0.1221	1	0
	1.2	0.9381	0.0238	0.1350	0.0187	0.8332	0.1668	1	0
	1.3	0.9175	0.0378	0.0418	0.0334	0.7857	0.2143	1	0
	1.22	0.9655	0.0114	0.1465	0.0129	0.8871	0.1129	1	0
	9.7	0.9199	0.0621	0.0000	0.1299	0.7179	0.2821	1	0
	9.11	0.9034	0.0872	0.0000	0.1494	0.6580	0.3420	1	0
	9.14	0.9278	0.0839	0.0128	0.1688	0.6654	0.3346	1	0
	9.19	0.8999	0.0995	0.0000	0.1196	0.6310	0.3690	1	0
	8.11	0.8706	0.0441	0.0169	0.1324	0.7668	0.2332	1	0
	8.13	0.8558	0.0845	0.0000	0.1732	0.6640	0.3360	1	0
	8.15	0.8567	0.0779	0.0206	0.1050	0.6792	0.3208	1	0
	3.4	0.8185	0.1198	0.0000	0.1261	0.5888	0.4112	1	0
	3.18	0.8499	0.0988	0.0013	0.1502	0.6323	0.3677	1	0
	2.3	0.8737	0.0965	0.0201	0.1535	0.6373	0.3627	1	0
	8.1	0.9176	0.0071	0.0027	0.0148	0.9119	0.0881	1	0
	3.1	0.8972	0.0200	0.0255	0.0275	0.8484	0.1516	1	0

APPENDIX 4. ELECTRON MICROPROBE ANALYSES OF SHEBA PYRITE CRYSTALS (AS, FE, S = WT %; OTHERS = PPM)

Sample	Nr.	As	Ag	Bi	Pb	S	Sb	Sn	Au	Zn	Cu	Ni	Co	Fe	Total
RC 1039	1.1	0.21	281	438	660	53.21	0	433	381	0	257	0	924	46.85	100.61
	a.2	0.38	0	0	667	54.03	168	0	1025	0	0	0	615	46.45	101.12
	a.3	0.23	95	0	0	54.07	301	146	0	1014	1998	39	521	46.12	100.66
	c.1	0.57	762	2003	1158	53.22	145	0	0	8994	0	222	653	46.01	100.39
	c.2	0.52	1051	0	0	53.81	997	0	0	0	163	783	990	47.44	101.92
	c.3	0.99	0	0	430	53.4	267	0	0	0	0	3637	5378	46.16	101.13
	c.4	0.21	0	0	0	53.62	0	0	821	0	150	14166	692	47.37	101.51
RC 1038	1.1	0.11	0	0	821	53.42	513	0	356	416	0	110	887	47.67	101.50
	1.2	2.79	296	0	0	52.58	0	0	91	0	0	0	468	46.41	101.88
	1.3	0.79	399	0	320	53.66	379	354	3662	81	0	0	174	46.89	101.56
	1.4	3.33	797	0	0	51.12	240	261	0	0	5999	0	361	46.21	100.90
	1.5	4.12	0	0	0	50.64	191	171	518	1995	710	0	427	46.17	101.17
	c	0.21	281	438	660	53.21	0	433	381	0	257	0	924	46.85	100.54
	10.5	4.29	0	0	0	54.81	180	84	421	395	0	0	429	39.23	98.51
	10.6	2.58	456	0	0	57.21	0	0	748	439	0	207	462	40.82	100.85
	10.7	0.18	1151	1053	298	59.07	0	0	0	385	0	0	466	39.33	98.94
	10.8	0.22	0	0	0	59.18	638	0	0	0	0	0	467	40.81	100.35
	11.1	0.9	225	355	1025	53.25	435	0	927	595	506	3333	847	46.95	101.93
	11.3	0	113	0	1502	53.72	134	0	628	625	0	609	688	47.33	101.49
	11.4	1.78	0	237	0	53.34	368	0	847	552	1107	830	621	46.38	101.97
	11.6	0.49	225	0	1144	53.04	123	265	841	383	121	1429	740	47.04	101.10
	11.7	2.76	0	0	0	52.11	278	0	810	0	168	10347	1829	45.97	100.20
	11.8	0.1	451	0	0	54.51	0	0	377	1108	0	323	570	47.26	101.98
	11.9	1.67	225	0	0	53.28	335	0	169	212	0	6235	632	46.44	101.57
	11.10	0	0	0	0	53.66	0	238	710	526	278	391	689	46.09	100.04

Sample	Nr.	As	Ag	Bi	Pb	S	Sb	Sn	Au	Zn	Cu	Ni	Co	Fe	Total
RC1040	3.1	0.204	0	0	184	53.68	0	0	171	0	0	207	560	46.54	100.54
	3.2	2.35	0	0	737	52.05	0	0	431	359	0	0	707	45.71	100.35
	3.3	3.22	229	0	309	51.64	0	0	828	0	0	0	0	46	101.02
	3.4	1.4	689	0	0	53.11	364	0	732	376	848	0	613	46.55	101.06
	3.5	1.82	459	0	0	52.41	307	0	216	0	172	0	437	46.18	100.57
	3.6	3.38	0	0	0	51.22	511	185	0	965	208	0	371	45.08	99.92
	3.7	2.04	0	0	0	52.28	0	0	0	0	0	0	164	45.87	100.23
	3.8	1.56	0	0	0	52.38	320	0	434	276	136	0	648	47.05	101.19
	3.9	2.64	460	0	0	51.57	285	0	0	0	0	212	559	46.73	101.11
	3.10	0.17	0	0	0	52.52	217	0	0	102	0	0	540	47.55	100.33
	4.1	1.94	112	0	0	51.94	0	153	595	0	0	7358	3145	46.31	100.73
	4.2	0.01	0	0	421	53.422	0	0	336	0	0	9057	978	47.1	101.73
RC 1024	2.1	0.059	339	0	0	53.79	0	0	627	0	314	0	344	46.3	100.34
	2.2	0.077	0	0	0	53.35	0	0	294	0	133	157	334	46.78	100.30
	2.3	0.19	0	0	483	53.09	315	0	0	228	534	0	757	45.55	99.07
	2.4	0.68	113	0	0	53.43	0	0	169	0	242	1478	237	46.84	101.19
	9.1	0.77	340	0	0	53.34	0	183	465	0	0	2732	389	46.47	101.00
	9.2	0.74	227	0	0	54.24	0	0	253	243	0	3556	551	46.1	101.57
	9.3	0.038	341	592	362	54.41	304	0	0	0	0	0	465	46.79	101.46
	9.4	0.23	0	0	0	54.3	315	169	0	628	753	1125	476	46.9	101.61
	9.5	1.34	0	0	121	51.3	371	0	466	0	327	5556	1253	46.78	100.24
	9.7	0.79	0	354	0	53.35	0	0	505	0	193	3061	225	46.94	101.53

APPENDIX 5. ELECTRON MICROPROBE ANALYSES OF SHEBA PYRITE (ATOMIC PERCENTAGES)

Sample	Number	As	Ag	Bi	Pb	S	Sb	Sn	Au	Zn	Cu	Ni	Co	Fe
1039	1.1	0.111	0.01	0.008	0.013	66.26	0	0.014	0.01	0	0.02	0	0.06	33.49
	a.2	0.203	0	0	0.013	66.76	0.01	0	0.0206	0	0	0	0.041	32.95
	a.3	0.123	0.003	0	0	66.95	0.01	0.004	0	0.06	0.01	0.002	0.035	32.79
	c.1	0.304	0.02	0.038	0.022	66.48	0.005	0	0	0.054	0	0.015	0.044	33.00
	c.2	0.273	0.038	0	0	66.09	0.003	0	0	0	0.01	0.052	0.0666	33.46
	c.3	0.525	0	0	0.01	66.06	0.008	0	0	0	0	0.245	0.036	32.78
	c.4	0.109	0	0	0	66.16	0	0	0.016	0	0.01	0.095	0.046	33.56
1038	1.1	0.058	0	0	0.015	66.40	0.016	0	0.007	0.024	0	0.007	0.058	33.40
	1.2	1.47	0.011	0	0	65.15	0	0	0.0018	0	0	0	0.031	33.32
	1.3	0.42	0.014	0	0.006	66.26	0.012	0.011	0.007	0.004	0	0	0.011	33.24
	1.4	1.8	0.029	0	0	64.57	0.0088	0.009	0	0	0.038	0	0.024	33.51
	1.5	2.236	0	0	0	64.09	0.0066	0.0058	0.011	0.012	0.04	0	0.029	33.55
	c	0.11	0.01	0.008	0.013	66.26	0	0.014	0.007	0	0.016	0	0.062	33.49
	11.1	0.46	0.008	0.007	0.019	65.83	0.013	0	0.018	0.035	0.031	0.22	0.055	33.29
	11.3	0	0.004	0	0.028	66.23	0.004	0	0.012	0.037	0	0.04	0.045	33.59
	11.4	0.94	0	0.0045	0	65.68	0.012	0	0.017	0.033	0.068	0.056	0.041	33.14
	11.6	0.26	0.008	0	0.022	65.88	0.004	0.009	0.017	0.023	0.007	0.095	0.049	33.62
	11.7	1.45	0	0	0	64.26	0.009	0	0.016	0	0.01	0.69	0.0122	32.43
	11.8	0.053	0.016	0	0	66.57	0	0	0.0074	0.065	0	0.021	0.037	33.22
	11.9	0.86	0.008	0	0	65.68	0.011	0	0.003	0.012	0	0.412	0.042	32.96
	11.10	0	0	0	0	66.70	0	0.007	0.014	0.03	0.017	0.025	0.045	33.10
RC1040	3.1	0.13	0	0	0.0035	66.65	0	0	0.0035	0	0	0.014	0.037	33.17
	3.2	1.27	0	0	0.014	65.57	0	0	0.0088	0.022	0	0	0.048	33.06
	3.3	1.76	0.0086	0	0.006	64.98	0	0	0.017	0	0	0	0	33.23
	3.4	0.74	0.025	0	0	65.91	0.012	0	0.015	0.023	0.053	0	0.041	33.17
	3.5	0.977	0.017	0	0	65.70	0.01	0	0.0044	0	0.011	0	0.029	33.24
	3.6	1.84	0	0	0	65.12	0.017	0.0063	0	0.06	0.013	0	0.025	32.91
	3.7	1.09	0	0	0	65.75	0	0	0	0	0	0	0.011	33.12
	3.8	0.833	0	0	0	65.36	0.01	0	0.0088	0.017	0.0085	0	0.044	33.71
	3.9	1.42	0.017	0	0	64.78	0.0094	0	0	0	0	0.014	0.038	33.71
	3.101	0	0	0	0	65.70	0.0072	0	0	0.0062	0	0	0.036	34.15
	4.1	1.04	0.0042	0	0	64.96	0	0.0052	0.012	0	0	0.5	0.0214	33.25
	4.2	0	0	0	0.008	65.84	0	0	0.0067	0	0	0.6055	0.065	33.01

RC 1024	*2.1*	*0*	*0.013*	*0*	*0*	*66.85*	*0*	*0*	*0.013*	*0*	*0.019*	*0*	*0.023*	*33.04*
	2.2	*0*	*0*	*0*	*0*	*66.45*	*0*	*0*	*0.006*	*0*	*0.0084*	*0.011*	*0.022*	*33.45*
	2.3	*0.104*	*0*	*0*	*0.0095*	*67.16*	*0.01*	*0*	*0*	*0.014*	*0.034*	*0*	*0.052*	*32.60*
	2.4	*0.35*	*0.004*	*0*	*0*	*66.13*	*0*	*0*	*0.0033*	*0*	*0.015*	*0.098*	*0.015*	*33.37*
	9.1	*0.405*	*0.012*	*0*	*0*	*66.17*	*0*	*0.006*	*0.009*	*0*	*0*	*0.182*	*0.0257*	*33.18*
	9.2	*0.38*	*0.008*	*0*	*0*	*66.67*	*0*	*0*	*0.005*	*0.014*	*0*	*0.234*	*0.036*	*32.64*
	9.3	*0*	*0.012*	*0.011*	*0.006*	*66.82*	*0.009*	*0*	*0*	*0*	*0*	*0*	*0.031*	*33.08*
	9.4	*0.118*	*0*	*0*	*0*	*66.67*	*0.01*	*0.005*	*0*	*0.037*	*0.046*	*0.074*	*0.031*	*32.99*
	9.7	*0.41*	*0*	*0.007*	*0*	*65.94*	*0*	*0*	*0.01*	*0*	*0.011*	*0.203*	*0.014*	*33.39*

APPENDIX 6. MICROPROBE ANALYSES OF AGNES PYRITE CRYSTALS (AS, S, FE = WT %; OTHERS = PPM)

Sample	Number	As	Ag	Bi	Pb	S	Sb	Sn	Au	Zn	Cu	Ni	Co	Fe	Total
1055	3.1	0.03	0	0	0	50.29	383	146	203	0	177	0	220	49.48	99.92
	3.2	0.01	1195	0	0	50.62	169	0	163	0	0	439	451	49.88	100.74
	3.3	0.01	0	1021	0	50.64	0	0	0	0	271	157	251	50.87	101.69
	3.4	1.94	596	114	0	49.35	0	0	0	0	130	226	586	49.18	100.65
	3.5	0.85	0	0	0	50.17	0	0	0	0	0	108	0	49.61	100.7
	3.6	0.87	0	0	0	50.28	124	0	163	0	0	0	586	49.62	100.86
	3.7	0.37	513	0	0	51.76	0	0	203	377	0	0	356	49.60	101.89
	3.7	0.21	281	438	660	53.21	0	433	381	0	257	0	924	46.85	100.61
	3.7	0.29	0	0	2152	50.77	553	0	0	0	0	0	692	48.03	99.43
1055	7.1	0.05	0	0	0	53.05	0	0	804	0	0	0	411	46.54	99.77
	18.1	0.09	0	0	1129	53.17	107	462	0	0	0	389	774	46.66	100.21
	18.2	0.52	0	0	0	53.11	131	0	585	0	0	0	475	47.02	100.77
	18.3	1.49	783	838	1136	51.10	202	391	0	594	396	0	275	46.91	99.97
	18.4	0.59	392	0	0	52.66	119	0	0	0	0	0	364	46.97	100.32
	18.5	1.68	588	0	0	51.98	594	0	295	0	384	0	848	46.39	100.36
	18.6	1.37	980	0	0	52.11	0	0	0	0	732	0	607	47.06	100.79
	18.7	2.29	784	0	0	51.94	0	0	0	283	0	0	375	47.07	101.45
	18.8	0.04	0	119	0	53.66	0	365	0	214	499	0	366	47.76	101.58
	18.9	2.45	888	0	298	54.25	0	0	458	114	0	0	676	46.91	101.45
	18.10	1.66	2164	0	0	52.19	0	0	934	0	248	0	309	46.37	101.4
	18.11	0.67	0	0	656	53.98	252	0	0	0	0	308	1022	46.66	100.87
	18.12	3.15	295	0	0	52.33	382	0	253	0.041	0	0	575	46.25	100.45
	11.1	0.55	0	0	1135	52.56	0	0	0	0	0	0	598	47.48	100.91
	11.2	0	0	0	0	50.89	0	0	556	113	0	233	718	46.51	100.72
	11.3	1.91	493	600	0	53.14	0	0	0	570	0	0	477	47.76	101.67
	12.1	0.82	0	0	239	53.48	216	0	710	0	212	0	255	47.22	100.87
	12.2	2.42	0	1683	0	51.36	0	225	0	525	0	566	155	45.87	99.46
	12.3	0.25	0	120	0	53.81	577	0	0	0	614	0	434	46.39	101.19
	12.4	1.31	888	0	301	53.01	395	0	0	299	0	0	721	47.12	102.82
	12.5	0.03	0	0	0	53.91	142	0	577	0	0	0	319	46.39	100.66
	12.6	1.71	487	474	296	52.53	0	0	415	0	0	0	558	45.57	99.65
	12.7	1.83	0	0	236	54.05	653	0	0	254	396	0	506	45.38	99.66
	12.8	0.79	0	0	1594	52.84	236	0	0	0	0	292	743	44.57	99.4
	12.9	1.93	389	1894	0	52.06	118	0	0	448	0	0	546	45.33	99.67
	12.101	0	0	0	0	53.09	249	0	495	450	0	0	110	45.16	99.2
	12.11	0	875	0	0	52.46	130	166	1084	0	0	0	197	45.92	100.57

L-RC10 72	1	2.03	0	0	296	51.61	282	180	586	0	257	0	578	46.90	100.75
	2	2.02	0	0	356	52.29	0	0	1507	196	258	0	601	46.72	101.3
	3	0.03	0	0	177	53.68	320	0	0	0	247	196	746	47.18	101.08
	4	2.13	0	0	0	52.31	0	516	833	197	209	0	329	43.45	98.11
	5	3.23	585	0	356	51.46	437	278	0	0	601	0	546	43.04	98.02
	6	0.05	0	0	118	53.89	0	0	1269	0	0	0	297	44.21	98.31
RC1068	1.2	0	0	0	794	53.21	0	0	765	0	237	0	264	46.60	100.03
	1.3	1.88	344	0	285	52.09	340	0	0	593	0	0	170	46.06	100.21
	2.1	0.08	293	0	0	54.63	0	0	616	0	271	684	1898	45.92	101
	2.2	2.25	0	0	0	52.68	200	291	626	546	0	8151	3962	44.40	100.72
	2.3	0.02	489	0	0	53.96	403	0	370	0	124	0	165	42.24	100.37
	2.4	1.08	0	0	0	52.97	0	166	0	0	0	5875	2473	45.78	100.69
	2.5	0.37	0	0	354	53.42	107	709	662	310	0	2548	406	46.38	100.69
RC1056	1.1	0.09	0	0	0	53.29	0	0	0	254	247	0	318	46.94	100.41
	1.2	0.12	0	0	472	53.75	0	195	0	592	0	201	307	47.05	101.09
	1.3	1.89	583	0	119	52.68	0	0	0	0	147	0	743	46.96	101.69
	1.4	0.56	0	0	1004	53.81	0	0	0	436	160	0	833	47.56	102.17
	1.5	0.49	0	0	0	53.56	201	0	373	0	0	0	1008	47.79	102.01
	14.1	0	0	0	736	52.29	0	0	0	256	390	528	788	47.59	100.16
	14.2	3.01	0	0	0	50.22	0	159	289	295	0	0	576	46.73	100.09
	14.3	0.96	0	0	284	51.97	226	0	0	377	130	108	787	47.31	100.45
	14.4	0.02	0	0	0	52.17	317	200	0	230	0	1723	778	46.76	99.36
	14.5	3.12	774	0	0	50.40	0	119	0	0	388	0	565	46.06	99.69
	14.6	0	0	0	0	53.04	0	0	0	0	285	238	348	46.35	99.48
	14.7	2.82	0	0	856	50.81	124	159	66	0	0	0	209	45.88	99.72
	5.1	0.06	0	0	737	52.67	0	147	323	0	0	376	516	47.47	100.41
	5.2	0.81	0	0	0	51.97	0	0	0	0	0	0	200	47.43	100.28
	5.3	1.35	258	0	0	51.80	407	0	285	0	590	0	598	47.16	100.58
	5.4	1.59	857	0	341	51.02	0	0	0	323	318	0	545	47.13	99.91
	5.5	0.17	0	568	0	52.01	238	0	283	0	568	0	0	47.94	100.31
	5.6	0	0	455	0	51.96	600	0	690	730	66	0	221	48.79	101.04
	8.1	0.03	0	0	0	51.28	192	0	0	0	379	123	610	48.69	100.16
	8.2	2.42	256	0	0	50.45	0	0	0	0	424	0	136	48.63	101.59
	8.3	1.64	0	0	0	50.87	304	159	736	215	283	0	670	48.25	101
	8.4	0.23	0	0	0	52.28	0	0	0	324	0	0	568	47.73	100.33
	8.5	1.68	0	0	0	51.08	598	0	0	0	0	0	670	47.35	100.23
	8.6	0.05	1463	0	0	52.47	182	0	0	0	0	0	316	48.02	100.74

APPENDIX 7. ATOMIC PERCENTAGES OF ELEMENTS PRESENT IN AGNES PYRITE CRYSTALS

Sample	Number	As	Bi	Ag	Pb	S	Sb	Sn	Au	Zn	Cu	Ni	Co	Fe	Fe/S
1055	3.1	0.015	0	0	0	63.86	0.013	0.005	0.004	0	0.011	0	0.015	36.08	0.56
	3.2	0.003	0	0.045	0	63.79	0.006	0	0.003	0	0	0.031	0.031	36.09	0.56
	3.3	0.005	0.02	0	0	63.37	0	0	0	0	0.017	0.011	0.017	36.55	0.57
	3.4	1.06	0.002	0.022	0	62.87	0	0	0	0	0.008	0.016	0.041	35.98	0.57
	3.5	0.46	0	0	0	63.47	0	0	0	0	0	0.008	0	36.04	0.56
	3.6	0.046	0	0	0	63.49	0.004	0	0.003	0	0	0	0.04	35.98	0.56
	3.7	0.2	0	0.019	0	64.33	0	0	0.004	0.023	0	0	0.024	35.39	0.55
	3.71	0.111	0.008	0.01	0.013	66.26	0	0.014	0.01	0	0.02	0	0.06	33.49	0.50
	3.72	0.159	0	0	0.0424	64.62	0.018	0	0	0	0	0	0.048	35.10	0.54
	7.1	0.025	0	0	0	66.45	0	0	0.016	0	0	0	0.028	33.47	0.50
1055	18.1	0.0476	0	0	0.0218	66.38	0.0035	0.015	0	0	0	0.026	0.052	33.45	0.50
	18.2	0.275	0	0	0	66.08	0.004	0	0.012	0	0	0	0.032	33.59	0.50
	18.3	0.811	0.016	0.0295	0.0223	64.84	0.0067	0.0134	0	0.0369	0.0254	0	0.019	34.17	0.52
	18.4	0.3176	0	0.0146	0	65.88	0.0039	0	0	0	0	0	0.0248	33.74	0.51
	18.5	0.907	0	0.022	0	65.42	0.0197	0	0.006	0	0.0244	0	0.058	33.52	0.51
	18.6	0.737	0	0.0355	0	65.28	0	0	0	0	0.0463	0	0.0414	33.85	0.51
	18.7	1.22	0	0.0251	0	64.92	0	0	0	0.017	0	0	0.025	33.78	0.52
	18.8	0	0.0023	0	0	66.12	0	0.0122	0	0.012	0.031	0	0.024	33.79	0.51
	18.9	0.028	0	0.0325	0.0057	66.74	0	0	0.0092	0.0069	0	0	0.045	33.13	0.49
	18.10	1.31	0	0.0804	0	65.25	0	0	0.019	0	0.015	0	0.02	33.29	0.51
	18.11	0	0	0	0.0126	66.75	0.0082	0	0	0	0	0.021	0.0688	33.12	0.49
	18.12	0.089	0	0.011	0	65.67	0.0126	0	0.005	0.025	0	0	0.0393	33.33	0.50
	11.1	0.368	0	0	0.022	65.56	0	0	0	0	0	0	0.04	34.01	0.51
	11.2	1.71	0	0	0	64.41	0	0	0.012	0.007	0	0.016	0.049	33.79	0.52
	11.3	0.292	0.011	0.018	0	65.71	0	0	0	0.034	0	0	0.032	33.90	0.51
	12.1	0	0	0	0.005	66.32	0.007	0	0.014	0	0.013	0	0.017	33.61	0.50
	12.2	1.04	0.032	0	0	65.33	0	0.008	0	0.0328	0	0.039	0.011	33.50	0.51
	12.3	0.43	0.002	0	0	66.53	0.019	0	0	0	0.038	0	0.029	32.93	0.49
	12.4	1.28	0	0.032	0.006	65.28	0.013	0	0	0.018	0	0	0.048	33.31	0.51
	12.5	0.13	0	0	0	66.81	0.005	0	0.012	0	0	0	0.022	33.01	0.49
	12.6	0.71	0.009	0.018	0.006	66.22	0	0	0.009	0	0	0	0.038	32.98	0.49
	12.7	0.015	0	0	0.005	67.39	0.021	0	0	0.016	0.025	0	0.034	32.48	0.48
	12.8	0.92	0	0	0.031	66.67	0.008	0	0	0	0	0.02	0.05	32.29	0.48
	12.9	0.99	0.036	0.014	0	65.92	0.004	0	0	0.027	0	0	0.037	32.95	0.49
	12.10	0.42	0	0	0	66.85	0.008	0	0.01	0.027	0	0	0.008	32.65	0.48
	12.11	1.04	0	0.032	0	65.80	0.004	0.006	0.022	0	0	0	0.013	33.07	0.50

L-RC10 72	1	1.09	0	0	0.006	64.93	0.009	0.006	0.012	0	0.016	0	0.039	33.88	0.52
	2	1.08	0	0	0.007	65.31	0	0	0.031	0.012	0.016	0	0.041	33.50	0.51
	3	0.018	0	0	0.003	66.38	0.01	0	0	0	0.015	0.013	0.05	33.50	0.50
	4	1.17	0	0	0	66.86	0	0.018	0.017	0.012	0.013	0	0.023	31.88	0.47
	5	1.78	0	0.22	0.007	66.26	0.014	0.01	0	0	0.039	0	0.038	31.82	0.48
	6	0.026	0	0	0.002	67.93	0	0	0.026	0	0	0	0.02	31.99	0.47
RC1068	1.2	0	0	0	0.015	66.49	0	0	0.015	0	0.015	0	0.018	33.43	0.50
	1.3	1.01	0	0.013	0.006	65.60	0.011	0	0	0.036	0	0	0.012	33.31	0.50
	2.1	0.043	0	0.011	0	67.28	0	0	0.012	0	0.017	0.046	0.127	32.46	0.48
	2.2	1.21	0	0	0	65.96	0.007	0.01	0.013	0.034	0	0.557	0.27	31.92	0.48
	2.3	0.01	0	0.018	0	66.97	0.013	0	0.007	0	0.008	0	0.01	32.95	0.49
	2.4	0.58	0	0	0	66.07	0	0.006	0	0	0	0.4	0.17	32.78	0.49
	2.5	0.19	0	0	0.007	66.42	0.004	0.023	0.013	0.019	0	0.17	0.027	33.11	0.49
RC1056	1.1	0.046	0	0	0	66.34	0	0	0	0.016	0.016	0	0.022	33.55	0.50
	1.2	0.062	0	0	0.009	66.45	0	0.007	0	0.036	0	0.013	0.021	33.39	0.50
	1.3	1.01	0	0.0215	0.002	65.42	0	0	0	0	0.009	0	0.05	33.48	0.51
	1.4	0.29	0	0	0.019	66.07	0	0	0	0.026	0.01	0	0.056	33.53	0.50
	1.5	0.26	0	0	0	65.89	0.007	0	0.007	0	0	0	0.067	33.76	0.51
	14.1	0	0	0	0.014	65.57	0	0	0	0.016	0.024	0.036	0.054	34.27	0.52
	14.2	1.64	0	0	0	64.06	0	0.005	0.006	0.018	0	0	0.04	34.22	0.53
	14.3	0.52	0	0	0.005	65.26	0.008	0	0	0.023	0.008	0.007	0.054	34.11	0.52
	14.4	0.01	0	0.029	0	65.86	0.01	0.007	0	0.014	0	0.12	0.053	33.89	0.51
	14.5	1.71	0	0	0	64.42	0	0.004	0	0	0.025	0	0.039	33.80	0.52
	14.6	0	0	0	0	66.55	0	0	0	0	0.018	0.016	0.023	33.39	0.50
	14.7	1.54	0	0	0.017	64.79	0.004	0.005	0.014	0	0	0	0.015	33.59	0.51
	5.1	0.031	0	0	0.014	65.82	0	0.005	0.006	0	0	0.026	0.035	34.06	0.51
	5.2	0.44	0	0.01	0	65.31	0	0	0	0	0	0	0.014	34.22	0.52
	5.3	0.72	0	0.032	0	65.11	0.014	0	0.006	0	0.037	0	0.041	34.04	0.52
	5.4	0.86	0	0	0.007	64.73	0	0	0	0.02	0.02	0	0.037	34.32	0.53
	5.5	0.089	0.011	0	0	65.28	0.008	0	0.006	0	0.036	0	0	34.54	0.52
	5.6	0	0.009	0	0	64.89	0.019	0	0.014	0.045	0.01	0	0.015	34.99	0.53
	8.1	0.018	0	0	0	64.65	0.006	0	0	0	0.024	0.008	0.042	35.24	0.54
	8.2	1.3	0	0.01	0	63.50	0	0	0	0	0.027	0	0.01	35.15	0.55
	8.3	0.088	0	0	0	64.10	0.01	0.005	0.015	0.013	0.018	0	0.046	34.90	0.54
	8.4	0.12	0	0	0	65.49	0	0	0	0.02	0	0	0.039	34.32	0.52
	8.5	0.91	0	0	0	64.63	0.02	0	0	0	0	0	0.046	34.39	0.53
	8.6	0.027	0	0.054	0	65.48	0.006	0	0	0	0	0	0.022	34.41	0.52